Fabrication of reliable, self-biased and nonlinear magnetoelectric composites and their applications

Menghui Li

Dissertation submitted to the faculty of the
Virginia Polytechnic Institute and State University
in partial fulfillment of the requirements for the degree of
Doctor of Philosophy
In
Materials Science and Engineering

Dwight D Viehland (Chair)
Jie-Fang Li
Louis J Guido
Levon V Asryan

September 05, 2014
Blacksburg, Virginia

Keywords: Magnetoelectric, piezoelectric, magnetostricive, magnetic sensors

Fabrication of Reliable, Self-biased and Nonlinear Magnetoelectric Composites and Their Applications

Menghui Li

ABSTRACT

The magnetoelectric (ME) effect—i.e., the induction of magnetization by an applied electric field (*E*) or a polarization by an applied magnetic field (*H*)—is of great interest to researchers due to its potential applications in magnetic sensors. Moreover, the ME effect in laminate composites is known to be much higher than in single phase and particulate composites due to combination of the magnetostrictive and piezoelectric effects in the individual layers. Given that the highest ME coefficient have been found in Metglas/piezo-fiber laminate composites, this study was designed to investigate and enhance the magnetoelectric (ME) effect in Metglas/piezo-fiber laminate composites, as well as develop their potential for magnetic sensor applications.

To initiate this investigation, a theoretical model was derived to analyze the thickness effect of the magnetostrictive, piezoelectric, epoxy and Kapton layers on the ME coefficient. As a result, the importance of the coupling effect by epoxy layers was revealed. I used spin-coating, vacuum bagging, hot pressing, and screen printing techniques to decrease the thickness of the epoxy layer in order to maintain homogeneity, and to obtain good repeatability of the 16 ME laminates fabricated at one time. This protocol resulted in a more efficient way to induce self-stress to Metglas/PZT laminates, which is essential for increasing the ME coefficient.

With an enhanced ME effect in the Metglas/piezo-fiber laminates, magnetic field sensitivity could then be increased. An ME sensor unit, which consisted of a Metglas/PMN-PT laminate and a low noise charge amplifier, had a magnetic field sensitivity of 10 pT/$Hz^{0.5}$ in a well-shielded environment. Stacking four of these ME laminates could further increase the signal-to-noise (SNR) ratio. I studied the optimized distance between a pair of Metglas/PZT ME laminates. A stack of up to four ME sensors was constructed to decrease the equivalent magnetic noise. The magnetic field sensitivity was effectively enhanced compared to a single laminate. Finally, a number of four Metglas/PZT sensor units array was constructed to further increase the sensitivity.

ME laminate composites operated in passive mode have typically required an external magnetic bias field in order to maximize the value of the piezomagnetic coefficient, which has many drawbacks. I studied the ME effect in an Ni/Metglas/PZT laminate at zero bias field by utilizing the remnant magnetization between the Ni and Metglas layers. To further enhance this effect, annealed Metglas was bonded on the Metglas/PZT laminate since it is known that hard-soft ferromagnetic bilayers generate built-in magnetic field in these Metglas layers. As a result, giant α_{ME} values could be achieved at a zero bias field at low frequency range or at electromechanical resonance (EMR). The sensor unit consisting of self-biased ME laminate arrays is considerably smaller compared to a unit that uses magnet-biased ME laminates.

Introducing the converse ME effect and nonlinear ME effect in Metglas/piezo-fiber laminates affords a variety of potential applications. Therefore, I theoretically and experimentally studied converse ME effects in laminates with longitudinally magnetized and longitudinally poled, or (L-L) mode. The optimum structure for producing the maximum effect was obtained for Metglas/PZT laminates. Additionally, the optimum structure and materials for

enhancing the nonlinear ME effect in Metglas/PZT laminates are reviewed herein. In particular, this study revealed that modulating the EMR in laminates with high-Q piezo-fibers could enhance the SNR. The stress effect on nonlinear ME effect is also discussed—namely that magnetic field sensitivities can be enhanced by this modulation-demodulation technique.

To my wife and family

ACKNOWLEDGEMENTS

First of all, I would like to express my infinite gratitude to my advisor, Professor Dwight Viehland, for his guidance and support. His professionalism, his many valuable suggestions on my research, his patience in revising my manuscripts, and his helpful advice with respect to this dissertation and presentations truly inspired me to achieve high-level research work.

Equally important, I would like to thank Dr. Jiefang Li for her great help in equipment setup and suggestions on experimental design. I could not have succeeded in many of my research areas without her help.

I would also like to thank my committee members, Dr. Levon Asryan and Dr. Louis Guido. Their insightful suggestions helped me to revise my research results and dissertation.

I would like to thank Dr. Guo-quan Lu, Dr. Shashank Priya and Dr. Kathy Lu for allowing me to use the equipment and facilities in their laboratories. Their input improved my research results and saved a great deal of time.

I also extend my thanks to Dr. Davresh Hasanyan and and Passive Sensors Unlimited (PSU) for their help in deriving the model for the ME effect, which afforded me a much deeper understanding of the fundamental effects of each material.

I am grateful to Dr. Jaydip Das, Dr. David Gray, Dr. Liangguo Shen and PSU for their help in circuit knowledge, magnetic field calculation, equipment setup (data logger) and experimental design. I would like to thank David Berry and PSU for their collaboration in processing improvement of fabricating ME laminates. I also would like to thank PSU for supply of piezo-fibers.

I also acknowledge the assistance of Dr. Yaojing Wang, Dr. Junqi Gao and Ying Shen for their valuable discussions on ME materials and applications. We worked together to develop a new generation of magnetic sensors, of which we are all proud!

I would like to thank the members of Prof. Viehland's group for their amazing support: Dr. Yan Li, Dr. Wenwen Ge, Dr. Yaodong Yang, Dr. Jianjun Yao, Dr Zhiguang Wang, Yanxi Li Chengtao Luo, and Yue Zhang. I will always have good memories of working with you all over the years.

Similarly, I thank Dr. Bo Chen, Dr. Wenle Li, Dr. Yuchang Wu, Yuan Zhou, and Zhipeng Tian—my fellow MSE graduate students at Virginia Tech. I received so much help and support from these guys! The research work and life in general at VT was a pleasure because of each of you.

I thank the publishers for their permissions to reprint figures in this dissertation: AIP, APS, IEEE, IOP and John Wiley and Sons.

Last, but certainly not least, I would like to thank my parents, Dr. Zengliang Li and Yongmei Liu, for their love, encouragement and support. I would also like to express my gratitude to Sunan Zhao for her support and love during my PhD study.

Table of Contents

LIST OF TABLES

LIST OF FIGURES

CHAPTER 1.

INTRODUCTION

1.1. Magnetoelectric Effect

Multiferroic materials that feature the coexistence of at least two ferroic orders (ferroelectic, ferromagnetic, or ferroelastic) have been of significant interest to researchers due to their potential applications in multifunctional devices.[1-3] The coupling interaction between the magnetic and electric orders is known as the magnetoelectric (ME) effect, as shown in Figure 1.1. This effect facilitates control of the ferroelectric polarization (P) by a magnetic field (H), or a change of magnetization (M) by an electric field (E). Typically, the ME voltage coefficient α_{ME} is used to evaluate the performance of an ME material. α_{ME} is defined by the electric field dE induced by an applied magnetic field dH (α_{ME} = dE/dH); or conversely, by the magnetic field induced by an applied electric field.

The ME effect was first observed in Cr_2O_3 single crystals in the early 1960s.[4-6] Single-phase materials display a linear ME effect, which is caused by a direct coupling between the dipole and spin moments. The largest α_{ME} value in Cr_2O_3 single crystals was reported to be in the range of 20 mV/cm·Oe. The ME effect in single-phase materials has always been found to be low and only at low temperatures, which hinder such materials from being widely used in multifunctional devices.[7]

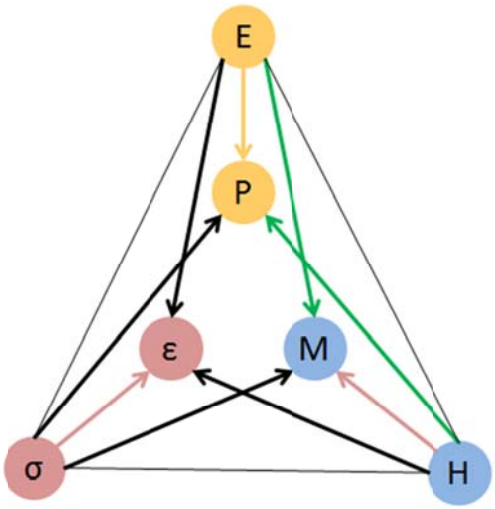

Figure 1.1. Phase control in ferroics and multiferroics. The green arrow indicates magnetoelectric multiferroic.

The development of a composite material provides valuable opportunities to tailor specific engineer properties, which would otherwise not be possible within any of its constituent phases. For example, the ME effect in composites is a result of elastically coupling the piezoelectric and piezomagnetic effects, whereby the piezomagnetic material is deformed under an applied magnetic field. This deformation results in the initiation of mechanical voltage that acts on the piezoelectric material, thereby inducing an electric polarization change.[8] The inverse process is known as the converse ME effect. Either directly or conversely, the ME effect refers to the net effect of piezoelectric and magnetostrictive materials.

ME thin films have generated a great deal of interest in recent years. Researchers have shown that epitaxial layers of ME thin films such as $BiFeO_3$ grown on $SrTiO_3$ are

able to enhance magnetization and produce a strong piezoelectric response.[9] Self-assembled multiferroic nanostructures such as $CoFe_2O_4$ nanopillars embedded in a $BaTiO_3$ matrix on $SrTiO_3$ substrates have shown a strong coupling of the ordered parameters through the heteroepitaxy of the two lattices.[10]

Other composites with different structures and materials have also been studied. For example, a composite of $Pb(Zr_{1-x}Ti_x)O_3$ (PZT) and $Td_{1-x}Dy_xFe_2$ (Terfenol-D) particles mixed together in a polymer matrix has been reported.[11] The Terfenol-D particles change their shapes under an applied magnetic field, and pass the resulting elastic force through the polymer matrix to the PZT particles, thereby inducing a charge. The ME voltage coefficient of ME particle composite materials is generally small. The theoretical value of α_{ME} is predicted to be ~ 100 mV/cm·Oe, with the highest experimental value reported to be ~10 mV/cm·Oe.

Since 2000, an enhancement in the value of α_{ME} by up to 10,000 times in comparison to previous ME materials has been achieved in ME laminated composites consisting of piezoelectric and magnetostrictive layers.[12-14] Such ME laminates can be fabricated by con-firing and by epoxy-bonding method. Co-firing of ME laminates is important because it affords compatibility with current industrial production processes. Laminates comprised of a variety of different materials—e.g., $Pb(Zr_{1-x}Ti_x)O_3$ (PZT) and $CoFe_2O_4$, PZT and $NiFe_2O_4$ (NFO), $(Zn_{1/3}Nb_{2/3})$–$0.8Pb(Zr_{0.5}Ti_{0.5})O_3$ (PZNT) and $(Ni_{0.6}Cu_{0.2}Zn_{0.2})Fe_2O_3$ (NCZF), and $Pb(Mg_{1/3}Nb_{2/3})O_3$-$PbTiO_3$ (PMN-PT) and NCZF—have been reported.[14-17] It should be noted that even though a value of ME voltage coefficient of 1.47 V/cm·Oe can be achieved in NCZF/PMN-PT/NCZF trilayer laminates,

the main drawback of these composites is that co-firing limits the choice of materials. Moreover, there are few ME laminates that can be co-fired below 600 ℃.

Another widely used method for fabricating ME laminates is via the bonding of the magnetostrictive layer (such as Terfenol-D, Galfenol or Metglas layers) and the piezoelectric layer (such as PZT, PMN-PT) using an epoxy resin.[18-20] Figure 1.2 shows a schematic of one ME laminate of Terfenol-D and PMN-PT epoxied together. Important to note is that epoxied ME laminates are unable to maintain their structural integrity at high temperatures. Specifically, at temperatures above 200 ℃ the epoxy will soften, thereby reducing the mechanical coupling between the piezoelectric and magnetostrictive layers. To data, ME voltage coefficient values of laminate composites have been reported to be as high as 22 V/cm·Oe at quasi-static frequencies.[21,22]

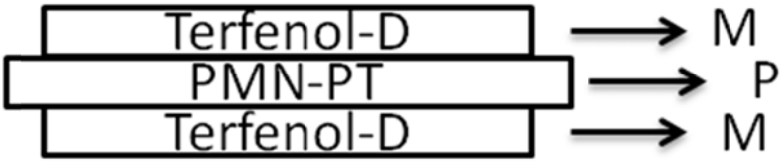

Figure 1.2. Schematic of Terfenol-D/PMN-PT laminate

1.2. **Magnetoelectric Laminate Composites**

Although, many different laminate composites have been studied over the past 10 years, they can be broadly classified into four basic categories by identifying the direction of their magnetization and polarization. These four types are (1) the longitudinally magnetized and longitudinally poled or (L-L) mode composites, (2) the longitudinally magnetized and transversely poled or (L-T) mode composites, (3) the transversely magnetized and longitudinally poled or (T-L) mode composites, and (4) the transversely magnetized and transversely poled or (T-T) mode composites.[23] The fundamental structures of these four modes are shown in Figure 1.3. The dependence of the ME voltage coefficient on the DC bias field for these modes is depicted in Figure 1.4, which confirms that the optimized DC bias field for the L-modes (L-L, L-T) are lower in comparison to that of the T-modes (T-L, T-T). This difference is due to the fact that the demagnetization field in T-modes laminates is much higher. Also, the peak value of the ME voltage coefficient for ME laminates in the L-mode is larger than in the T-mode.

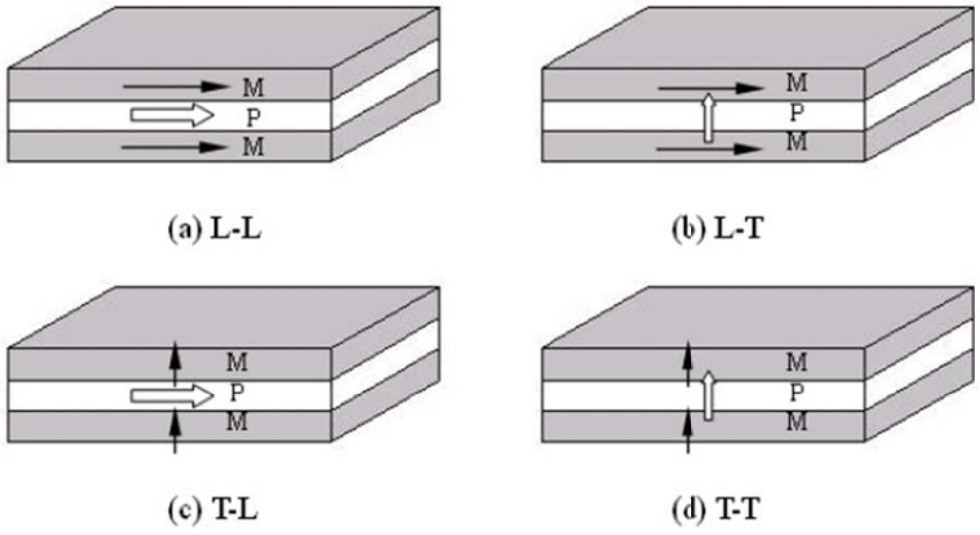

Figure 1.3. The four fundamental ME composite structures.

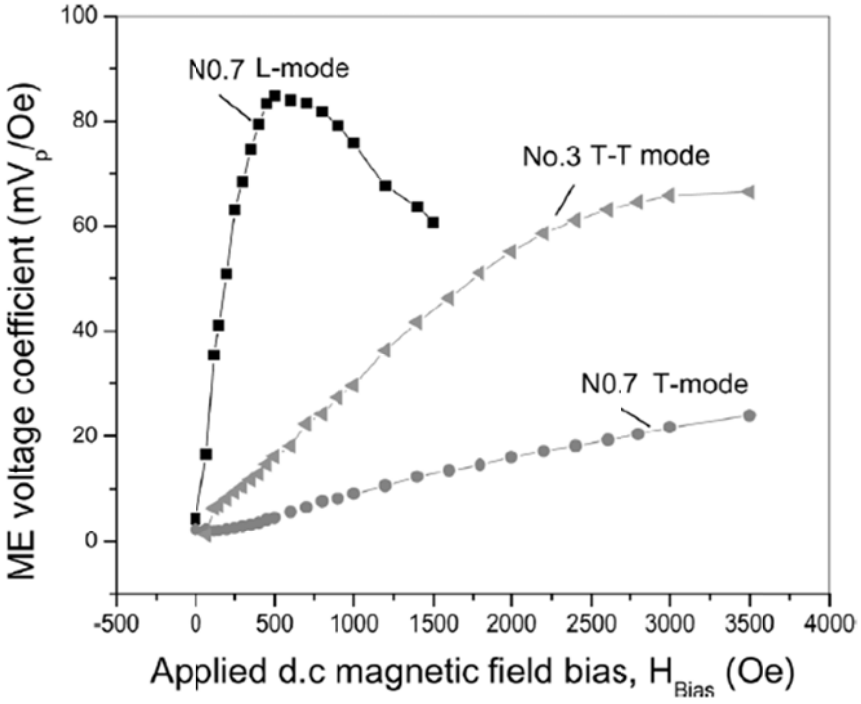

Figure 1.4. ME voltage coefficient as a function of DC bias field for L-mode and T-mode.[24] (Copyright © 2004, IEEE)

Theoretically, the (L-L) mode should have the largest ME voltage coefficient of all the four basic modes. The reason is that the (L-L) mode fully uses the piezoelectric coefficient d_{33}, while the three others prefer d_{31}; moreover, d_{33} is larger than d_{31} for the giant piezoelectric materials such as PZT, PMN-PT and PZN-PT. However, the small capacitance of the piezoelectric layer makes it hard to fabricate and limits the output voltage. When using Metglas with a thickness of < 30 μm as the magnetostrictive phase, the piezoelectric phase must be thin to achieve a high ME voltage coefficient. Unfortunately, this requirement further reduces capacitance. To solve this problem, ME laminates in L-L push-pull mode were developed, as illustrated in Figure 1.5.[25] This type

of laminate consists of a tri-layer structure with 2 layers of Terfenol-D sandwiched between an inner layer of PZT. The piezoelectric layer of the push-pull configuration is symmetrically poled around its center node in reverse directions along the longitudinal axis. The capacitance of an ME laminate in (L-L) push-pull mode is 4× larger than that of an ME laminate in (L-L) mode. In general, the magnetic field sensitivity of a magnetic sensor based on such an ME laminate is on the order of 10^{-10} T/Hz$^{0.5}$ at a frequency of f = 1 Hz.

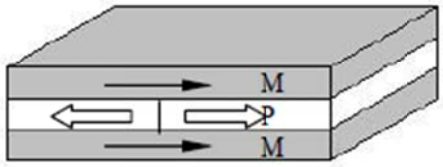

Figure 1.5. Structure of an (L-L) push-pull mode Tefenol-D/PZT laminate.

The highest ME voltage coefficient for an ME laminate was reported for one in (L-L) multi-push-pull mode, which is shown in Figure 1.6.[21,23] The Metglas foil has a relative permeability of μ_r >40000 due to a low magnetocystalline anisotropy, and has a low saturation magnetostriction of $\lambda_s \approx 40$ ppm at $H_{dc} < 10$ Oe. The piezofibers are composed of PZT-5A ceramic, and are 100 μm in thickness, 350 μm in width, and 30 mm in length. Thin Kapton insulting films with interdigititated (ID) electrodes have been bonded on PZT fibers using an epoxy resin. This (1-3) piezoelectric active fiber/epoxy composite (AFC) thin layer has the same structure of an actuator. Each piezofiber

features numerous alternating symmetric longitudinally poled push-pull units with a length of $2l_p$ = 1 mm. This multi-push-pull (L-L) configuration optimizes stress transfer, and also enhances the dielectric capacitance of the laminate. Very high ME voltage coefficients of up to 22 V/cm·Oe at 1 Hz for Metglas/PZT laminates can be achieved, which is an order of magnitude higher than other ME laminates reported previously.

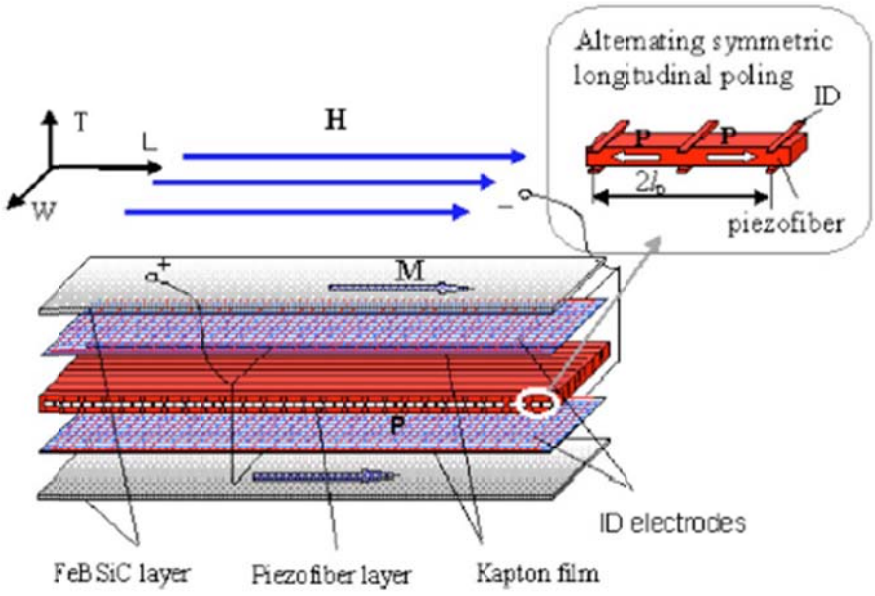

Figure 1.6. Structure of an (L-L) multi-push-pull mode Metglas/piezofiber laminate.[21] (Reprinted with permission from Ref. 21, Copyright © 2006, AIP Publishing LLC.)

A theoretical model of the ME effect in ME laminates has been proposed.[26,27] Specifically, researchers assumed the existence of an ideal coupling between the interfaces of each layer, and that an ME laminate operates at quasi-static frequencies. Additionally, this model assumes that the thickness, the polarization directions, and the

magnetic field are all along the 3 axis. The piezoelectric constitutive equations can be written as:

$$\begin{aligned} {}^{p}S_3 &= {}^{p}s_{33}\,{}^{p}T_3 + {}^{p}d_{33}E_3 \\ D_3 &= {}^{p}d_{33}\,{}^{p}T_3 + {}^{p}\varepsilon_{33}E_3; \end{aligned} \tag{1.1}$$

where ${}^{p}S_3$ and ${}^{p}T_3$ are the strain and stress tensor components of the piezoelectric phase along the length direction, E_3 and D_3 are the vector components of the electric field and electric displacement, ${}^{p}s_{33}$ and ${}^{p}d_{33}$ are the compliance and piezoelectric coefficients, and ${}^{p}\varepsilon_{33}$ is the dielectric permittivity. The magnetostrictive phase can be described by the following equations:

$$\begin{aligned} {}^{m}S_3 &= {}^{m}s_{33}\,{}^{m}T_3 + {}^{m}q_{33}H_3 \\ B_3 &= {}^{m}q_{33}\,{}^{m}T_3 + {}^{m}\mu_{33}H_3; \end{aligned} \tag{1.2}$$

where ${}^{m}S_3$ and ${}^{m}T_3$ are the strain and stress tensor components of the piezomagnetic phase along the length direction, H_3 and B_3 are the vector components of the magnetic field and magnetic flux induction, ${}^{m}s_{33}$ and ${}^{m}q_{33}$ are the compliance and piezomagnetic coefficients, and ${}^{m}\mu_{33}$ is the magnetic permittivity.

The ME voltage coefficient can be calculated from Equations (1.1) and (1.2) by assuming a perfect boundary conditions. In other words, the ME voltage coefficient of the (L-L) can be given as:

$$\alpha_{E,33} = \frac{|dE_3|}{|dH_3|} = \frac{2v(1-v)d_{33}^{p}q_{33}^{m}}{2(d_{33}^{p})^2(1-v) + \varepsilon_{33}^{s}[(v-1)(s_{11}^{p}+s_{12}^{p}) - kv(s_{11}^{m}+s_{12}^{m})]}; \tag{1.3}$$

where v is the thickness ratio of the piezoelectric layer.

Furthermore, an interfacial coupling parameter (k) was introduced by Bichurin,[8,28] where the ideal value is $k = 1$, and real interfaces have values of $k < 1$. Figure 1.7 shows the values of α_{ME} as a function of v for various k. The higher the coupling parameter, the higher the ME effect. However, the value of k cannot be determined or measured.

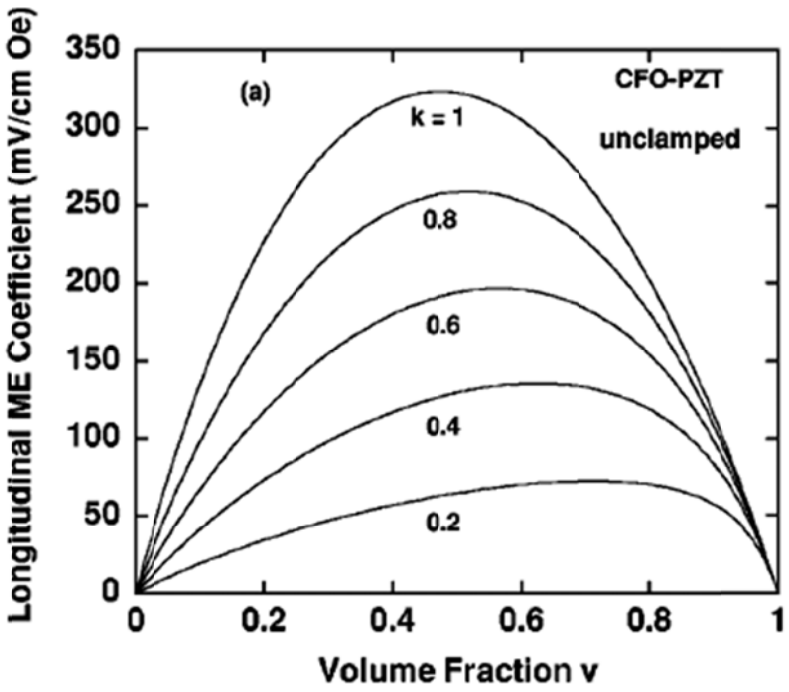

Figure 1.7. Dependence of the ME voltage coefficient on the interface coupling factor k and the volume fraction v for a CFO/PZT laminate.[28] (Reprinted with permission from Ref. 28, Copyright © 2003, APS)

Metglas is an amorphous metal alloy ribbon produced via a rapid solidification process. Metglas has magnetomechanical properties superior to those of any known magnetic material. The crystallization behavior for Metglas of differing concentrations

typically begins at temperatures ranging between 350-400°C.[29] For example, in Metglas 2605 SC, crystallization of α-Fe phase can be observed above 370°C. Once it undergoes crystallization, Metglas loses most of its magnetostrictive properties.

The major sources of magnetic anisotropy in Metglas are structural anisotropies induced by annealing under a magnetic field (and/or applied stress), as well as magnetostrictive anisotropies produced by the interaction between magnetostrictive strain and applied or residual stresses.[30] When the stress along the longitudinal direction is σ, the anisotropy field can be expressed as:

$$H_{A\sigma} = \frac{2K_u - 3\lambda_s\sigma}{M_s}; \tag{1.4}$$

where K_u is the energy per unit volume, λ_s is the substantial magnetostriction constant, and M_s is saturation magnetization. Under an applied field H, The strain ε can be determined as:

$$\varepsilon = \frac{\sigma}{E_M} + \frac{3\lambda_s}{2}\left(\frac{H^2}{H_{A\sigma}^2} - \frac{1}{3}\right); \tag{1.5}$$

where E_M is the young's modulus. The piezomagnetic coefficient d is:

$$d = \left(\frac{\partial\varepsilon}{\partial H}\right)_\sigma = \frac{3\lambda_s H}{H_{A\sigma}^2}. \tag{1.6}$$

When $H=H_{A\sigma}$, d reaches a maximum value of

$$d_{\max} = \frac{3\lambda_s}{H_{A\sigma}} = \frac{3\lambda_s M_s}{2K_u - 3\lambda_s\sigma}. \tag{1.7}$$

Experimental results agree well with this mathematic model. To obtain optimum engineering magnetostriction, it is necessary to induce a transverse domain structure, which is best achieved by first subjecting the material to complete stress relief, followed

by a transverse field anneal. An optimal combination of annealing time and temperature is able to minimize the K_u in the material, thereby suppressing the effects of moment spread and maximizing the magnetostrictive response.[31]

1.3. ME Magnetic Sensors

New sensors are needed to detect low-frequency minute magnetic field (H) variations. The sensors should be sensitive to minute (10^{-12} Tesla) at low frequency range (10^{-2}–10^{3} Hz) magnetic field variations. Also, any new magnetic field sensors should be able to function at room temperature, should be passive, and ideally should be small in size. A superconducting quantum interference device (SQUID) typically has a sensitivity of 10^{-15} Tesla/Hz$^{0.5}$ at low temperature of $T < 4$K.[32] The highest sensitivity results for one of the giant magnetoresistance (GMR) sensors is $\sim 4\times10^{-10}$ Tesla/Hz$^{0.5}$ at 1 Hz.[33] For these sensors, thermal or shot-noise tends to limit their functionality. Thus, older magnetic sensors cannot match the enhanced functionality of newer sensors.

ME laminate sensors are small and work well at room temperature. Recent investigations of these sensors have shown their potential to detect changes of pico-Tesla magnetic field variations.[34-37] An (L-L) push-pull mode Terfenol-D/PZT ME sensor delivered magnetic field sensitivities of 2×10^{-11} Tesla/Hz$^{0.5}$ at 1 Hz when operated at room temperature.[35] Additionally, DC magnetic field changes of 4 nT could be detected by a Metglas/PMN-PT ME sensor under a constant drive of H_{AC} = 0.1 Oe at f = 10 kHz.[38,39]

Usually, the magnetic field sensitivities of sensors are limited by noise. Thus, the ability to reduce the noise effect on the detection unit is quite important for enhancing

magnetic field sensitivity. Noise can be classified as either external and internal. External noise, also known as interference or environmental noise, is mainly induced by the environment. Such interference can be electrical, magnetic, vibrational, thermal, humidity-related, chemical, etc.[40-42] Most of the external noise can be eliminated by shielding, grounding, filtering, and isolation.[36] When measuring the magnetic field sensitivity of an ME laminate sensor, it is best conducted in a shielding chamber. Such an experimental setup can eliminate most of the external noise at low frequency range ($0.1 < f < 30$ Hz)—except in the extremely low frequency range ($f < 0.1$ Hz) and the power line frequency around 60 Hz.[43]

In contrast, internal noise cannot be removed. In an ME laminate sensor, there are two main noise sources: dielectric loss noise (N_{DE}) and DC leakage resistance noise (N_R).[43] They can be estimated as:

$$N_{DE} = \sqrt{\frac{4kTC\tan\delta}{2\pi f}}, \tag{1.8}$$

$$N_R = \frac{1}{2\pi f}\sqrt{\frac{4kT}{R}}. \tag{1.9}$$

The total charge noise density can then be given as:

$$N_t = \sqrt{N_{DE}^2 + N_R^2} = \sqrt{\frac{4kTC\tan\delta}{2\pi f} + \frac{1}{(2\pi f)^2}\frac{4kT}{R}}; \tag{1.10}$$

where k is Boltzmann's constant (1.38×10^{-23} J K^{-1}), T is the temperature in Kelvin, C is the capacitance, $\tan\delta$ is the dielectric loss, R is the DC resistance of the ME sensor, and f is the frequency in Hertz.

Equations (1.8–1.10) can predict the main internal charge noise density of an ME sensor as long as the following are known: the capacitance (C), the dielectric loss ($\tan\delta$),

and the DC resistance (R) of the ME sensor. Significant reduction in internal noise is possible through careful balancing of the individual noise components. Figure. 1.8 shows the measured and modeled charge noise density, as well as the equivalent magnetic noise, of an ME sensor unit in the frequency range of $0.125 < f < 100$ Hz. Except at frequencies where external vibrational sources are present, both the modeled and measured charge density noises show good agreement.

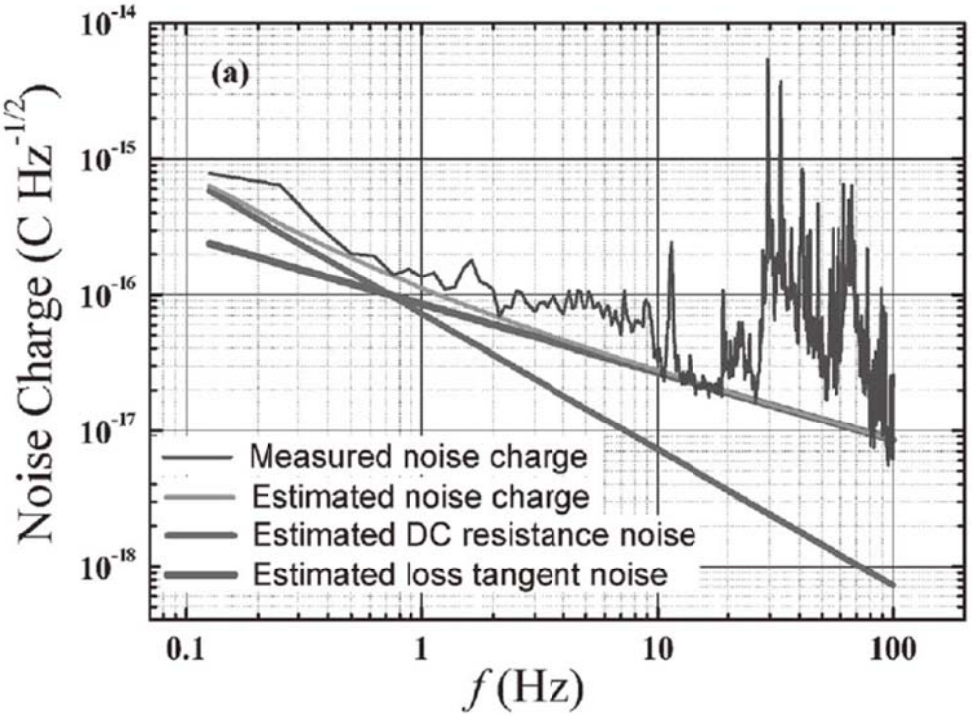

Figure 1.8. Measured and estimated charge noise density of the proposed sensor unit, including constituent dielectric loss and DC resistance loss, over the frequency range of $0.125 \text{ Hz} < f < 100$ Hz.[43] (Reprinted with permission from Ref. 43, Copyright © 2011 WILEY-VCH Verlag GmbH & Co. KGaA, Weinheim)

An enormous value of ME voltage coefficient of 52 V/cm·Oe has been reported in a Metglas/PMN-PT laminate in (L-L) multi-push-pull configuration.[43] Subsequently, it was packaged in a shielding box, and connected with a low-noise charge amplifier. An extremely low equivalent magnetic noise of 5.1 $pT/Hz^{0.5}$ was found at 1 Hz, which makes this ME sensor particularly promising for use in ultralow magnetic field detection applications.

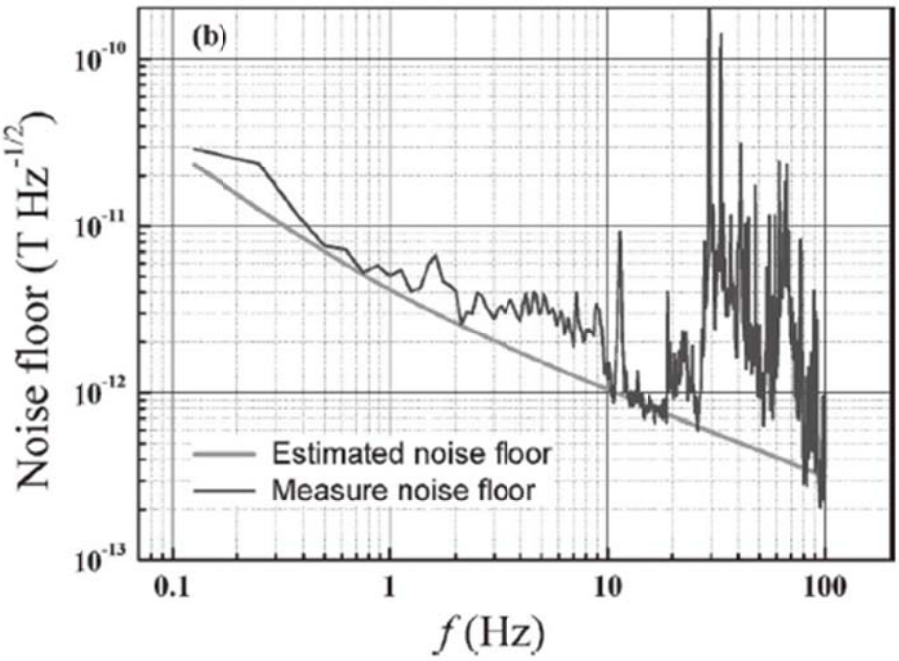

Figure 1.9. Measured and estimated equivalent magnetic noise of the proposed sensor unit. (Reprinted with permission from Ref. 43, Copyright © 2011 WILEY-VCH Verlag GmbH & Co. KGaA, Weinheim)

When an ME laminate is used as a magnetic field sensor, it need an applied external magnetic bias field to achieve the maximum ME response. This requirement

represents a significant disadvantage since it increases the required space, thus decreasing the possible spatial resolution. It also adds a potentially supplemental noise source, thereby lowering the signal-to-noise ratio. Additionally, it may interfere with neighboring sensors, which again limits the spatial resolution or any vector-field approaches based on the combination of individual sensors.[44] To overcome the limitations the arise from an external magnetic bias field, an ME voltage coefficient of 1.6 V/cm·Oe at zero bias field has been reported, which is shown is Figure 1.10.[45] This result is associated with the remnant magnetization effect in these graded magnetostriction materials. A giant ME effect has also been reported in exchange biased AlN and multilayers of Ta/Cu/$Mn_{70}Ir_{30}$/$Fe_{70.2}Co_{7.8}Si_{12}B_{10}$. However, the magnetic field sensitivities of these ME laminates in the absence of a DC bias field were not sufficiently high in the low frequency range.[44]

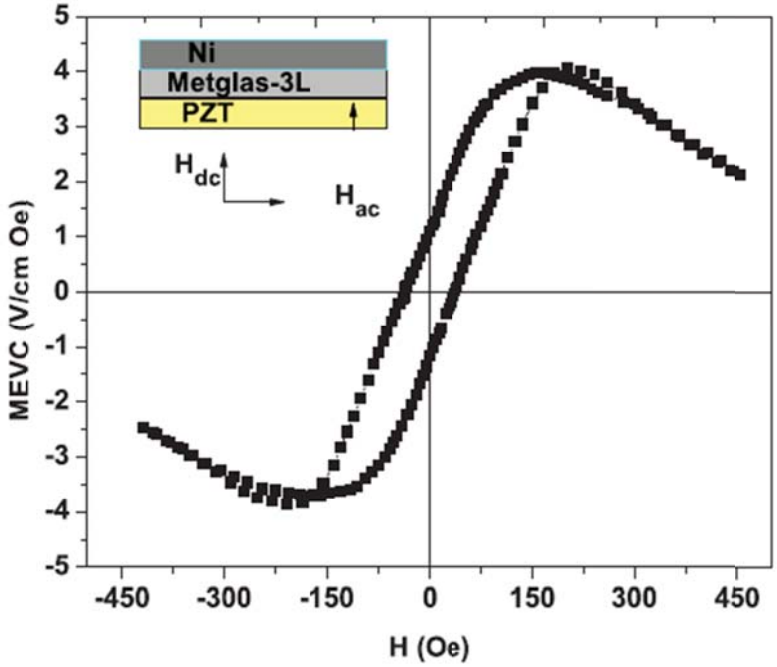

Figure 1.10. ME voltage coefficient as a function of bias field for a sample of PZT-3L Metglas/Ni. (Reprinted with permission from Ref. 44, Copyright © 2012, APS)

CHAPTER 2.

PURPOSE OF THIS THESIS

This study was designed to investigate and subsequently enhance the magnetoelectric (ME) effect in Metglas/piezo-fiber laminate composites, with the goal of developing their applications in magnetic sensors. This research targeted three specific areas of investigation, as follows.

(1) Metglas/piezo-fiber laminate composites

Previous investigations have confirmed that large ME coefficients could be achieved in ME laminate composites consisting of amorphous Metglas foils with high magnetic permeability and piezo-fibers with high piezoelectric properties. However, due to the fact that these ME laminates were fabricated manually via the lay-up process, the thickness of the epoxy layers was quite variable. This variation resulted in uneven stress transfer between the layers, and thus decreased the ME effect.

For this study I derived a theoretical model for ME effects in multi-push-pull mode Metglas/piezo-fiber laminate composites. The effects of the thickness ratio of the magnetostrictive phase (Kapton) and multiple layers of epoxy on the value of α_{ME} were investigated. I then used spin-coating, vacuum bagging, hot pressing, and screen printing techniques to decrease the thickness of the epoxy layer, to maintain its homogeneity, and the obtain excellent repeatability of the 16 ME laminates fabricated at the same time. Additionally, since it is known that suitable stress can increase the effective piezomagnetic coefficient of Metglas layers, I used a more convenient way to induce self-stress to the Metglas/PZT laminates. No extra device or volume was needed. I would like

to increase the ME coefficient by this experimental protocol, as well as increase the magnetic field sensitivity in self-stressed ME sensors.

In addition to magnetic field sensitivity, other parameters are also important for evaluating a magnetic field sensor. Specifically, a sensor's reliability must also be tested by measuring its linearity to an AC magnetic field, by assessing its durability over a lengthy duration (in this case, over a three-year period), and by determining its fatigue level when exposed to a strong AC magnetic field.

(2) ME magnetic sensor and arrays

In applications involving magnetic anomaly detection[46] and space exploration[47], new sensors are needed for detecting low frequency minute magnetic field variations. For a sensor to be effective, it should feature four essential parameters: (i) extreme sensitivity (< pT/√Hz) at low frequencies (10^{-2}–10^{3} Hz); (ii) low power consumption (passive mode); (iii) ability to operate at room temperature; and (iv) small size. Currently, there is no existing magnetic sensor that can meet all of these requirements. Because the magnetoelectric effect offers an alternative method for measuring variations in magnetic fields, an ME magnetic sensor has the potential to meet all four requirements.

The magnetic field sensitivity of an ME sensor unit could be increased by enhancing the ME effect in Metglas/piezo-fiber laminates. The ME sensor unit, consisting of a Metglas/PMN-PT laminate and a low noise charge amplifier, displayed a magnetic field sensitivity of 10 pT/$Hz^{0.5}$ in a well shielded environment. However, it remains very difficult to further decrease the equivalent magnetic noise based on current materials and structures. Stacking and arraying ME laminates have been theoretically predicted to increase the signal-to-noise (SNR) ratio of ME magnetic sensors. However,

there is no experimental result reported so far that confirms this theory. To address this knowledge deficit, I tried to find out the optimized distance between a pair of Metglas/PZT ME laminates. Second, I investigated the charge and equivalent magnetic noise of up to four stacked ME sensors, to confirm that magnetic field sensitivity could be effectively enhanced by stacking compared to results obtained with a single laminate. Finally, various arrays of four Metglas/PZT sensor units were constructed to further increase sensitivity.

It must be noted that the need for an external magnetic bias for an ME sensor brings many drawbacks. By using the remnant magnetization of a hard-soft ferromagnetic bilayer, a significant ME effect could be generated without any DC bias field. I studied the ME effect in Ni/Metglas/PZT laminates at zero bias field. To further enhance this effect, annealed Metglas was bonded on the Metglas/PZT laminate. Enormous values of α_{ME} could be achieved at a zero bias field using this type of self-biased ME laminate. Moreover, the sensor unit consisting of self-biased ME laminate arrays saves large volume.

(3) Converse ME effect and nonlinear ME effect

In addition to the direct ME effect, Metglas/piezo-fiber laminates are associated with other effects, such as the converse ME effect and the nonlinear ME effect. Based on these effects, Metglas/piezo-fiber laminates could be used for a variety of applications. Previously reported studies of converse ME effects have principally focused on laminates that were longitudinally magnetized and transversely poled ((L-T) mode).[48-50] The effect of the thickness of the magnetostrictive phase was not considered, which is known to notably affect ME properties.[51,52] Here, I would like to theoretically and experimentally

study the converse ME effects in laminates with longitudinally magnetized and longitudinally poled, or (L-L) mode, to reveal the optimum structure for producing the maximum effect in Metglas/PZT laminates.

Due to the nonlinearity of magnetostriction in Metglas layers, ME laminate composites can be used in an active mode to sense small DC magnetic fields or weak AC magnetic fields via a frequency modulation technique.[53,54] Therefore, I would like to study how to enhance the nonlinear ME effect by optimizing the structure of the Metglas layers, by inducing stress to increase the magnetic susceptibility χ_0, by selecting different piezo-fibers, and by modulating at different frequencies. As a result, magnetic field sensitivities were enhanced by this modulation-demodulation technique.

CHAPTER 3.

ENHANCED ME EFFECTS IN ME LAMINATE COMPOSITES

3.1 Introduction

In recent years researchers have investigated various combinations of the relative directions of the magnetization and polarization of the different magnetostrictive and piezoelectric phases.[23] The highest value reported for an ME voltage coefficient was that of the tri-layer Metglas/piezo-fiber/Metglas structure with a multi-push-pull mode.[55] Since a theoretical model for the multi-push-pull mode has yet to be reported, I derived a theoretical model for the ME coefficient for a Metglas/piezo-fiber multi-push-pull configuration. The importance of the thickness effect of Metglas, Kapton and multiple epoxy layers on the ME voltage coefficient were considered for this model in order to obtain more accurate results.

Previous work on $Pb(Zr,Ti)O_3$ (PZT) macro-fiber composite (MFC) actuators have detailed methods for laminating interdigitated Kapton electrodes onto PZT fibers using manually applied epoxy cures in a hot-press.[56-58] However, the majority of studies examining the coupling factor of laminates has been in developing theoretical treatments; in contrast, relatively little is known about techniques to improve coupling factors through epoxy selection and processing. To obtain a high ME coefficient in ME laminates with good repeatability, specific techniques must be utilized to deposit thin, uniform epoxy layers, which cannot be achieved manually.

In this chapter, I introduce several lamination techniques for obtaining thin layers of epoxy between the piezo-fibers, Kapton and Metglas layers. As a result of the addition

of the layers, the ME coefficient of Metglas/PZT laminate can be increased, while at the same time decreasing the noise floor. In fact, more than 16 laminates can be manufactured at one time via a screen printing method in the lab. Moreover, stress can be induced to the Metglas/PZT laminates by applying a DC bias field to the Metglas layers, or by applying an electrical field to the PZT layers during the cure of the adhesive epoxy layers. In self-stressed ME laminates, the ME coefficient can be enhanced by 24% via this technique, which represents a more convenient way to induce stress into ME laminates compared to previous methods. Lastly, I studied the reliability of the ME magnetic sensor using both durability and fatigue testing. Ensuing results—coupled with linearity measurement—confirmed that the ME sensors possessed stable and reliable sensing properties.

3.2 Theoretical Modeling of ME Laminate Composites

In Metglas/piezo-fiber/Metglas laminates with a multi-push-pull configuration, one layer of Kapton is bonded on both the top and bottom sides of the piezoelectric layer to insulate it from conductive Metglas ones. Multiple layers of epoxy, which bond the piezo-fiber, Kapton and Metglas layers transfer the strain between layers. Kapton and multiple layers of epoxy are known to significantly affect the ME coefficient in these laminates.[8,28,52,59]

We considered a multi-push-pull mode Metglas/Pb(Zr,Ti)O_3 (PZT)/Metglas sandwich structure in the (2,3) plane, as shown in Figure 3.1 (a). The core composite, consisting of a pair of insulating Kapton/interdigitated electrodes with a bundle of piezo-fibers, was sandwiched by *N*-layers of Metglas on both sides. The polarization direction of the piezo-fibers between the adjacent ID-electrodes is also illustrated in Figure 3.1 (a). We assumed that the polarization of the piezo-fibers was uniformly arranged along the longitudinal direction (3-axis). Thus, the multi-push-pull configuration can be considered as a multi-L-L mode, as illustrated in Figure 3.1 (b).

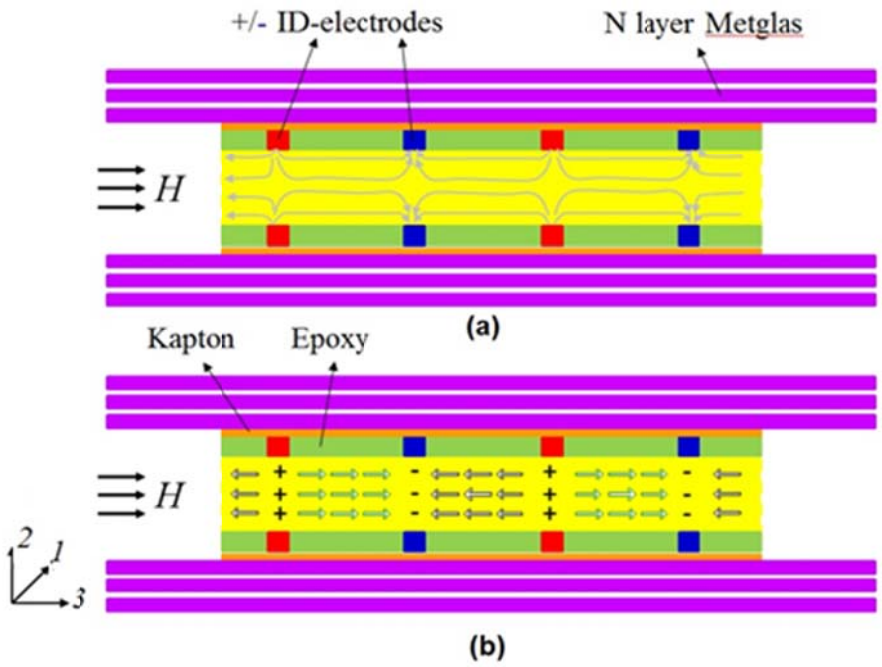

Figure 3.1. (a) Schematic diagram of Metglas/PZT/Metglas multi-push-pull mode laminate consisting of a Kapton/piezofiber core composite and *N* layer Metglas on the bottom and top of the core composite, where the polarization of the piezofibers and the "dead zone" are illustrated. (b) Schematic diagram of the simplified multi-L-L mode structure, where the polarization of the piezofibers was idealized to be arranged in the longitudinal direction.

Based on Dr. Hasanyan's modeling of ME effect in magnetostrictive-piezoelectric layered composited on resonance frequency, similar averaging method was used for deriving the effective material parameters of the composites under off-resonant frequencies.[28,60,61] For the poled piezoelectric phase with symmetry of ∞m[28], the following equations can be written for the strain and electric displacement:

$$
\begin{aligned}
{}^{p}S_i &= {}^{p}s_{ij}\,{}^{p}T_j + {}^{p}d_{ki}E_k \\
D_k &= {}^{p}d_{ki}\,{}^{p}T_i + {}^{p}\varepsilon_{kn}E_n;
\end{aligned}
\tag{3.1}
$$

where ${}^{P}S_i$ and ${}^{p}T_j$ are the strain and stress tensor components of the piezoelectric phase; E_k, E_n and D_k are the vector components of the electric field and electric displacement; ${}^{p}s_{ij}$ and ${}^{p}d_{ki}$ are the compliance and piezoelectric coefficient; and ${}^{p}\varepsilon_{kn}$ is the permittivity matrix of the piezoelectric phase. The magnetostrictive phase is assumed to have a cubic symmetry and is described by the equations:

$$
\begin{aligned}
{}^{m}S_{ik} &= {}^{m}s_{ij}\,{}^{m}T_{jk} + {}^{m}q_{pi}H_p \\
B_{pk} &= {}^{m}q_{pi}\,{}^{m}T_{ik} + {}^{m}\mu_{pn}H_n;
\end{aligned}
\tag{3.2}
$$

where ${}^{m}S_{ik}$ and ${}^{m}T_{jk}$ are the strain and stress tensor components of the magnetostrictive phase in the k^{th} layer of Metglas; H_p, H_n and B_{pk} are the vector components of the magnetic field and magnetic flux induction; ${}^{m}s_{ij}$ and ${}^{m}q_{pi}$ are the compliance and piezomagnetic coefficients; and ${}^{m}\mu_{pn}$ is the permittivity matrix of the magnetostrictive phase. The strain in the Kapton layer and in k^{th} epoxy layer can be described as:

$$
{}^{c}S_i = {}^{c}s_{ij}\,{}^{c}T_j \tag{3.3}
$$

$$
{}^{g}S_{ik} = {}^{g}s_{ij}\,{}^{g}T_{jk}; \tag{3.4}
$$

where ${}^{c}S_i$ and ${}^{c}T_j$, ${}^{g}S_{ik}$ and ${}^{g}T_{jk}$ are strain and stress tensor components of Kapton and epoxy in k^{th} layer, respectively; and ${}^{c}s_{ij}$ and ${}^{g}s_{ij}$ are compliance coefficients.

We assume the coupling between each layers is ideal, so the strain is transferred ideally. Also, we consider the total net force in the laminate is zero. Equations (3.1)-(3.4) were then solved for the following boundary conditions:

$$ {}^{m}S_{ik} = {}^{p}S_{i} = {}^{c}S_{i} = {}^{g}S_{ik} \ (i = 2, 3), \tag{3.5} $$

$$ 2\sum_{k=1}^{N} {}^{m}T_{ik}\,{}^{m}A_{ik} + 2\sum_{k=1}^{N+1} {}^{g}T_{ik}\,{}^{g}A_{ik} + 2\,{}^{c}T_{i}\,{}^{c}A_{i} + {}^{p}T_{i}\,{}^{p}A_{i} = 0 \ (i = 2, 3); \tag{3.6} $$

where ${}^{m}A_{ik}$, ${}^{g}A_{ik}$, ${}^{c}A_{i}$ and ${}^{p}A_{i}$ are the cross sectional areas of the Metglas and k^{th} epoxy, Kapton, and PZT layers along the 2 and 3 directions, respectively. We only considered the stresses along the 3 directions, and assumed that the stress in 2 direction is zero: ${}^{i}T_{2} = 0$. Further, based on the assumption that each epoxy layer is of the same thickness, the equations were solved using open circuit conditions: $D_3 = 0$. The ME coefficient of the Metglas/PZT/Metglas multi-push-pull mode laminates can then be obtained as:

$$ \alpha_{E,33} = \frac{E_3}{H_3} = -\frac{d_{31}(B_2A_4 - B_4A_2) + d_{33}(B_4A_1 - B_2A_3)}{\varepsilon_{33}(A_1A_4 - A_2A_3) + d_{31}(B_3A_2 - B_1A_4) + d_{33}(B_1A_3 - B_3A_1)}; \tag{3.7} $$

where A_i and B_i (i=1,2,3,4) are the coefficients shown in appendix A.

Figure 3.2 shows the theoretical values of α_{ME} for the Metglas/PZT/Metglas laminates as a function of v (line 1), where $v = 2Nt_m/(2Nt_m + t_p)$ is the thickness ratio of the magnetostrictive phase, in which t_m and t_p are the thickness of Metglas and PZT, respectively. The values of α_{ME} were obtained using the material parameters given in table 3.1. As v increased, the value of α_{ME} increased to a maximum of 28.6 V/cm·Oe for v = 0.63. The value of α_{ME} then decreased with further increase in v. Line 2 is the predicted results based on the equations in Reference [28]. In this modeling, the effects of Kapton and epoxy layers were ignored. Our modeling shows that the predicted values of α_{ME} are lower than these prior predicted ones.

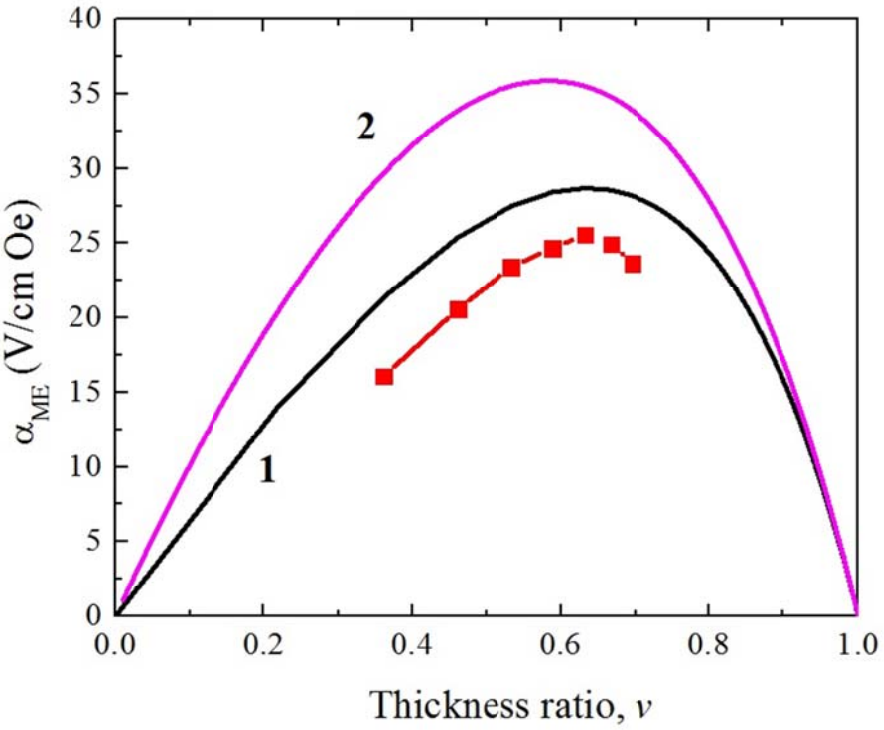

Figure 3.2. Theoretical and experimental values of α_{ME} for multi-push-pull mode Metglas/PZT/Metglas laminates as a function of v.

Table 3.1. Material parameters for calculating the ME coefficient

	PZT[28]	**Metglas[51]**	**Kapton[20]**	**Epoxy[21]**
Elastic constants (10^{-12} m^2/N)	15.3 (${}^{p}s_{11}$)	10 (${}^{m}s_{11}$, ${}^{m}s_{33}$)	440 (${}^{c}s_{11}$, ${}^{c}s_{33}$)	315 (${}^{g}s_{11}$, ${}^{g}s_{33}$)
	-5 (${}^{p}s_{13}$)	-5.2 (${}^{m}s_{12}$)	-110 (${}^{c}s_{12}$)	-78 (${}^{g}s_{12}$)
	17.3 (${}^{p}s_{33}$)			
Piezoelectric constant (10^{-12} C/N)	440 (${}^{p}d_{33}$)			
	-185 (${}^{p}d_{31}$)			
Dielectric constant	1850 (${}^{p}\varepsilon_{33}/\ \varepsilon_0$)			
Piezomagnetic constant[a] (10^{-9} m/A)		50.3 (${}^{m}d_{33}$)		
		-21.3 (${}^{m}d_{31}$)		
Thickness (10^{-6} m)	180 (t_p)	21(t_m)	20 (t_c)	5 (t_e)

[a] Measured values

Next, several Metglas/PZT/Metglas multi-push-pull L-L mode laminates were made. A 40 mm × 10 mm PZT bundle served as the core of the laminates, which consisted of five 40 mm × 2 mm PZT-5A fibers (Smart Materials, Sarasota, FL) oriented along the length direction of the laminates. Two interdigitated Kapton electrodes were bonded to the top and bottom surfaces of the piezoelectric bundle with epoxy resin (Stycast 1264, USA). The width and the separation of the electrodes were chosen to be 0.15mm and 1 mm, respectively, so that the piezoelectric response of the PZT fibers was close to the ideal ones in which there are no "dead zone".[62] Metglas foils (Vitrovac 7600F, Hanau, German) of dimensions 80 mm× 10 mm were then laminated to both the top and bottom surfaces of the interdigitated electrode/PZT core composites. The

laminates were placed into a vacuum bag and subsequently evacuated during the cure of the epoxy. Different pressures were applied to control the thickness of the epoxy. Laminates with different numbers N of Metglas layers bonded to both sides of the PZT core composite were fabricated for $N = 1$ to 7.

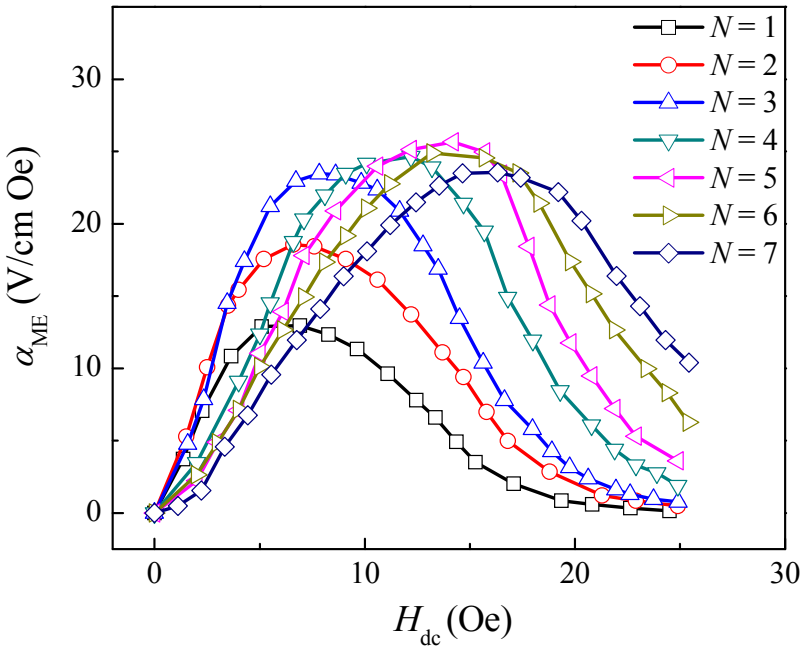

Figure 3.3. The value of α_{ME} as a function of H_{dc} for a Meglas/PZT/Metglas laminate with different numbers of layers of Metglas, N.

The value of α_{ME} was measured using a lock-in amplifier (SR-850) in response to a pair of Helmholtz coils driven at an AC magnetic field of $H_{ac} = 0.1$ Oe at a frequency of $f = 1$ kHz. The dc magnetic field was applied by a large electromagnet. Figure 3.3 shows the values of ME voltage coefficient α_{ME} as a function of H_{dc} for Metglas/PZT/Metglas laminates with different N. It can be seen that α_{ME} increased as H_{dc} is increased; and

subsequently decreased as H_{dc} was further increased. The maximum value of α_{ME} increased with increasing number of Metglas layers until $N = 5$, and then decreased with further increase in N. As shown in figure 3.2, the experimental maximum values of α_{ME} for the Metglas/PZT/Metglas laminates agreed well with the theoretical ones. When $v = 0.63$ ($N = 5$), the value of α_{ME} of 25.6 V/cm·Oe is maximum, which is 83% of the predicted one. It can be seen that the theoretical results in our model are more accurate than those reported previously.

Furthermore, the effects of epoxy and Kapton layers on the value of α_{ME} were investigated. The thicknesses of the epoxy between each of the layers can be controlled by spin coating and vacuum bagging techniques. After curing, the thicknesses were measured by an optical microscope. Kapton layers with different thicknesses were used in the laminates. The numbers of layers of Metglas bonded on both sides were kept at $N = 5$, yielding an optimal value for v. Figure 3.4 shows the theoretical and experimental values of α_{ME} as a function of (a) the thickness of the epoxy layer t_e, when the thickness of the Kapton layer was $t_c = 12$ μm; and (b) t_c, when $t_e = 5$ μm. Both theoretical lines reached maximum values when the thicknesses were less than 1 μm, and decreased as both thicknesses were increased. Experimental values showed similar trends as the predicted ones. The thinnest epoxy layer that we could obtain was 5 μm for each layer, which led to the highest value of $\alpha_{ME} = 25.6$ V/cm·Oe. The laminate with a Kapton of 12 μm exhibited the highest value of α_{ME}. Thus, to get high values of α_{ME}, the thicknesses of the Kapton and epoxy layers should be as thin as possible.

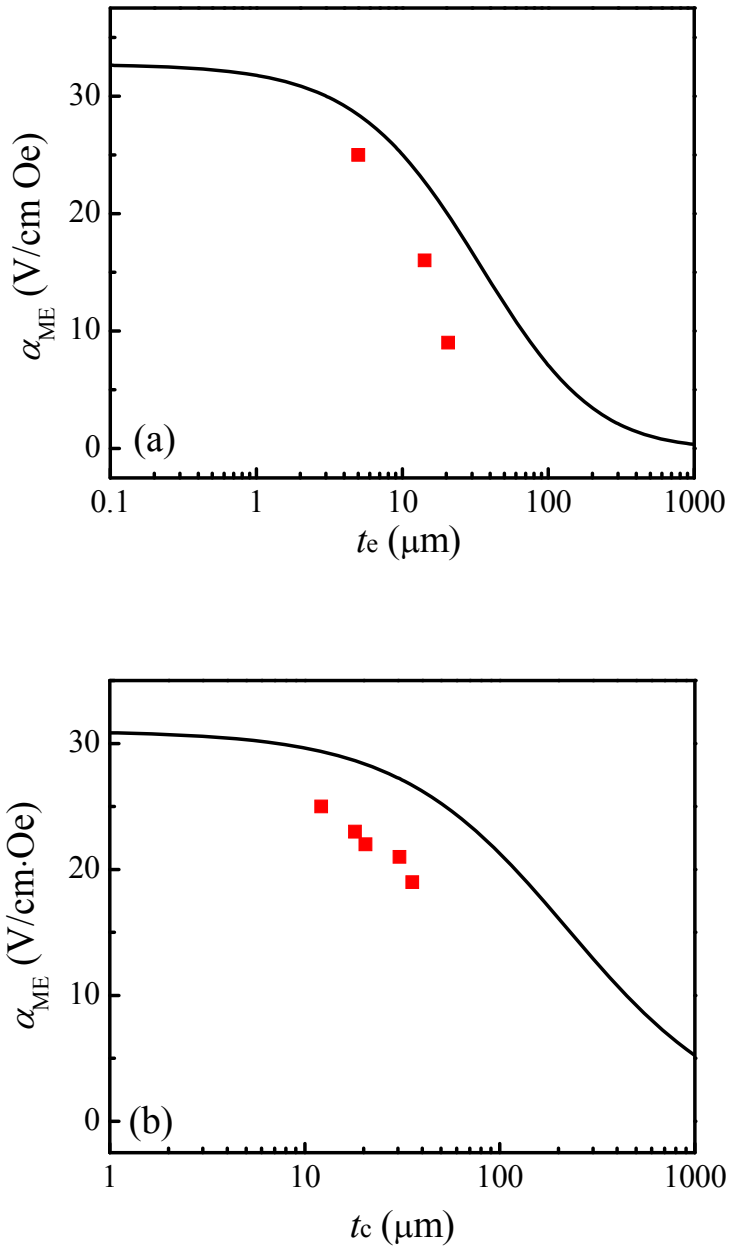

Figure 3.4. The value of α_{ME} as a function of thickness of (a) epoxy layer t_e, and (b) Kapton layer t_c. Solid lines are predicted values, where dots are measured ones.

3.3 Improved lamination process

3.3.1 Spin coating, vacuum bagging techniques

The ME coefficient of composite laminate structures is not an intrinsic quantity, but is rather a product tensor property that depends on the individual properties of each of the constituent materials, as well as the degree of strain coupling between the layers. A general expression for the magnetoelectric coefficient is

$$\frac{\partial P}{\partial H} = \alpha_{ME} = k_c e^m e; \tag{3.8}$$

where

$$e^m = \frac{\partial S}{\partial H} \text{ and } e = \frac{\partial P}{\partial S}, \tag{3.9}$$

and k_c is a interfacial coupling factor ($0 \leq k_c \leq 1$).[63] Accordingly, a high magnetostriction coefficient, a high piezoelectric coefficient, and good coupling between the layers will result in a high ME coefficient. Moreover, optimization of the thickness and interfacial bonding qualities of the magnetostrictive and piezoelectric layers are needed in order to achieve the maximum ME coupling in laminates.[11,64,65]

Longitudinal-longitudinal (L-L) mode ME laminates were fabricated by attaching interdigitated electrodes to both the top and bottom surfaces of a planar piezoelectric fiber bundle. The piezoelectric core was poled in the plane of the assembly to capitalize on increased performance of the magnetostrictive component. Finally, magnetostrictive layers were then attached to the top and bottom surfaces of the poled piezoelectric assembly. A schematic of the ME laminate is shown in Figure 3.5(a). The details of the processing steps are given below.

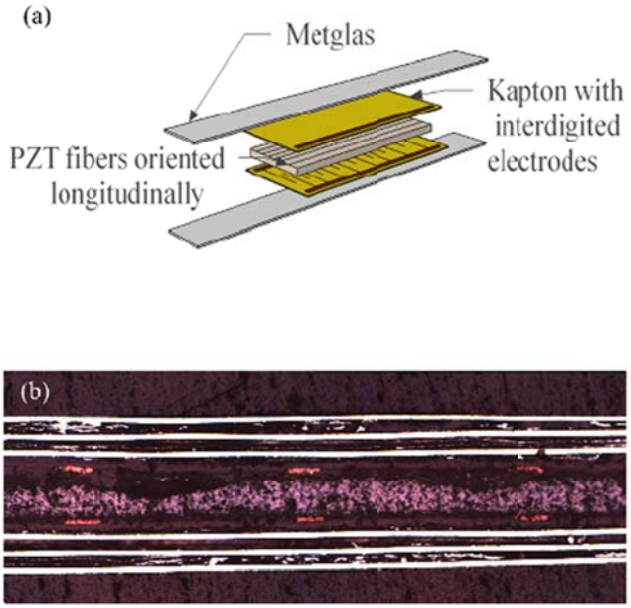

Figure 3.5. (a) Schematic representation and (b) optical micrograph of Metglas/PZT L-L mode composite ME laminate.

We used West System 105/206 resin/hardener as the epoxy in the laminates. Resin/hardener were mixed at a 5:1 mass ratio, per the manufacturer's recommendation. Resin was applied manually to one interdigited Kapton electrode. The electrode was mounted onto a Laurell WS-400BZ spinner and processed at 3000 rpm for 2 minutes to distribute the epoxy. A 4 cm × 1 cm PZT fiber bundle consisting of five 4 cm × 0.2 cm fibers mounted on a low-tack tape was attached to the coated electrode. The assembly was then placed into a modified commercially available vacuum bag and subsequently evacuated by the vacuum bagging system set up by Dr. David Berry. The epoxy was allowed to cure at room temperature for 24 hours. Once the bottom electrode epoxy had cured, an identical Kapton electrode was coated using the spin-coater. The low-tack tape

was removed from the PZT fibers and the second electrode was attached. The assembly was once again placed into a vacuum bag, evacuated, and cured at room temperature for 24 hours. After curing, the top and bottom electrodes were soldered together at solder pads. The PZT fibers were poled in a room-temperature oil bath for 15 minutes under a field of 19 kV/cm.

Six pieces of Vitrovac 7600F Metglas (Vitrovac 7600F, Vitrovac Inc. Hanau, German) were trimmed to 8 cm × 1 cm pieces. The Metglas pieces were then assembled into two stacks of three layers using the same West System 105/206 epoxy system. The stacks were pressed in a hydraulic press to evenly distribute the wet epoxy. One Metglas stack was bonded to both the top and the bottom of the PZT core using the previously described vacuum-bag technique. The epoxy was then vacuum-bag cured at room temperature for 24 hours.

The ME laminates were studied by optical microscopy, in order to determine epoxy thickness. Laminates were mounted in West System 105/206 epoxy and longitudinal cross sections made using a low-speed cut-off saw. The cross-sections were then manually ground and polished to 1200 μm alumina grit. Micrographs were taken using a Zeiss inverted-stage metallographic optical microscope with calibrated measurement optics. Figure 3.5(b) shows an optical micrograph of the structure of our ME laminate. In this figure, one can see the PZT-fiber layer in the center, the electrodes, the Kapton® layer, and the three layers of Metglas on each side of the PZT; in addition to the epoxy layers.

The ME properties were measured as a function of DC magnetic bias field (H_{DC}). The laminates were placed inside a Helmholtz coil between two poles of a Varian

Associates water-cooled electromagnet. A Kepco BOP 100-4M DC power supply was used to generate a DC bias field that was calibrated with a Walker Scientific MG-10D Gauss meter. The Helmholtz coil was driven by the sine output of a Stanford Research SR850 lock-in amplifier to produce a 0.1 Oe field at 1 kHz. The output voltage of the ME laminate was then measured by the lock-in amplifier and recorded as a function of DC bias for $-20 \leq H_{DC} \leq 20$ Oe.

Noise floor measurements were obtained by placing the sensor inside a custom-built Amuneal zero-Gauss chamber mounted on a pneumatic vibration isolation stage. The sensor was packaged in a plastic enclosure, and wrapped with metal foil to provide EMI shielding. Permanent magnets were used inside the packaging to bias the sensor to its maximum output charge. The output charge of the sensor was collected via a low-noise BNC cable and converted to a voltage signal using a wide-band charge amplifier designed and fabricated following a prior report. The charge amplifier output voltage was fed into a Stanford Research SR785 dynamic signal analyzer for noise floor measurements between $1 < f < 1600$ Hz, and the equivalent magnetic noise floor calculated using a transfer function.

Figure 3.6 shows a comparison of the ME voltage coefficient α_{ME} of a ME laminate made using the spin-coat/vacuum-bag technique (see blue curve), compared to that made by a manual epoxy application and ambient cure (see red curve). These data were taken using ME laminate containing the Metglas foils with $\lambda = 42$ ppm (Vitrovac 7600F). Due to the symmetric response of the ME laminate output voltage with respect to the sign of H_{dc}, only the positive half of the α_{ME} - H_{dc} curve is shown. The laminate fabricated by the spin-coat/vacuum bag technique had a maximum ME coefficient of α_{ME}

= 21.6 V/Oe·cm at 1kHz under a DC bias of 10.8 Oe, whereas that made by a manual lay-up had a value of 14.8 V/Oe·cm at 1kHz under H_{dc} = 7.2 Oe. In this figure, we also show results for a laminate made by manual lay-up using the source of Metglas foils with λ = 27 ppm (Magnetic Alloy 2605SA1, Metglas Inc., Conway, SC) that we had used in prior studies[15]. One can see that α_{ME} was increased from 6 V/Oe·cm to 14.8 V/Oe·cm using the same manual lay-up process. The increase in α_{ME} is a direct consequence of an increased interphase interfacial coupling factor between the magnetostrictive and piezoelectric layers. Spin-coat/vacuum-bag processing leads to a decrease in thickness, and a decrease in variance of the interfacial epoxy layers, within the laminate.

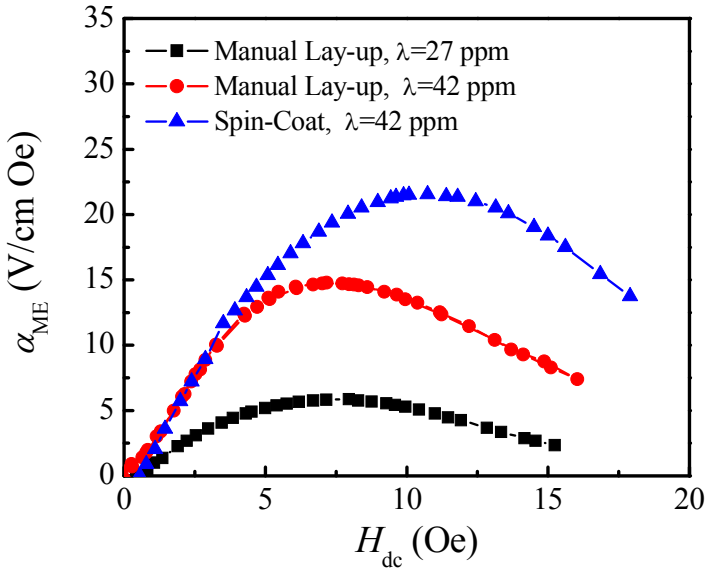

Figure 3.6 α_{ME} (V/cm·Oe) as a function of DC bias for a manual lay-up process using Metglas with λ=27 ppm (black curve) and λ=42 ppm (red curve), and a spin-coat/vacuum bag process using Metglas with λ=42 ppm (blue curve).

Figure 3.7(a) shows an optical micrograph of a cross-section of a ME laminate fabricated by manual epoxy application. The thickness of the epoxy between the PZT

fiber and the Kapton tape in this figure is ~17 μm. Additional microscopy (images not shown) demonstrated that the epoxy thickness at the Kapton®/PZT interface varied between about 5 μm to over 30 μm, using the manual layup process. This is a large variation, which was difficult to control. Such variability of the interphase interfaces will result in variability in stress transfer between layers, and thus in the value of α_{ME}.

For laminates fabricated using the spin-coat/vacuum bag techniques, both the thickness of the epoxy and the variation in thickness along the length of the laminate were reduced. Figure 3.7(b) shows a micrograph for such a laminate method. The resulting even deposition of the epoxy by the spin-coating process, coupled with a uniform applied pressure by the vacuum bag method, yields laminates with intimate contact between copper electrodes and the PZT fibers. The epoxy at the interface can be seen to decrease from a thickness of ~17-20 μm (which is the thickness of the copper traces) to about 4-6 μm at distances of more than ~20 μm from the edge of the copper trace (Figure 3.7(c)). Thus, the non-planarity of the Kapton® layer is not reflected in the topology of the Metglas, to which the Metglas is subsequently bonded. This ensures that the strain due to an external magnetic field will be coplanar with the poling direction of the PZT fibers. These images clearly demonstrate improved uniformity and reduced thicknesses of the interphase interfacial resins results in a larger α_{ME}.

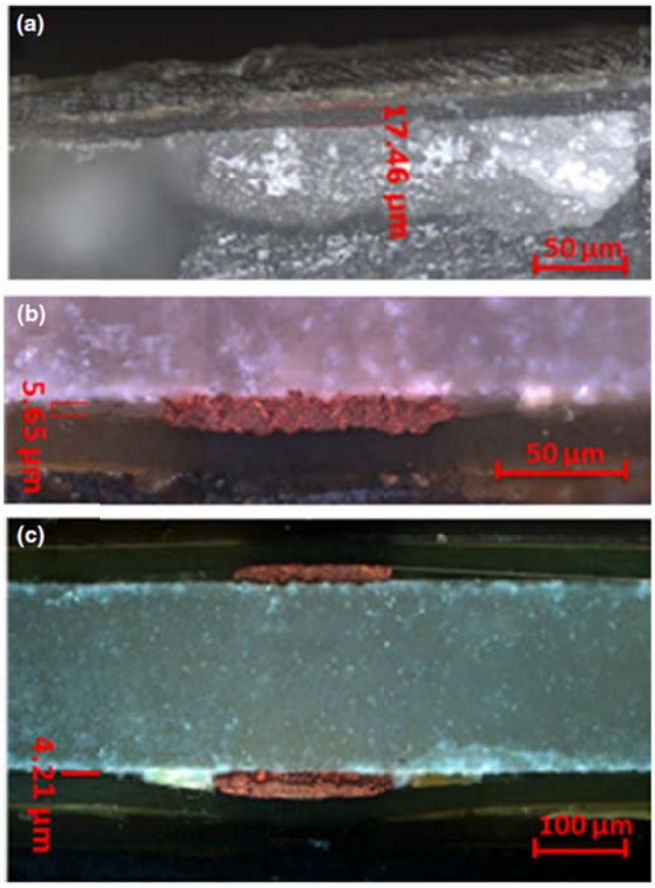

Figure 3.7. Optical micrographs showing (a) thick (~18 µm) epoxy layer when epoxy is applied manually, (b) electrode-to-PZT interface with no epoxy visible at the interface for spin-coat/vacuum bag technique, (c) for spin-coat/vacuum bag technique, epoxy at the Kapton/PZT interface tapers from a maximum of 20 µm near the electrode to 4 µm within 20µm of the electrode edge.

Figure 3.7(c) shows a cross-sectional view of an optical microscopy image of a completely fabricated laminate by the spin-coat/vacuum bags method. In this image, one can see the three layers of Metglas on each side of the PZT-fiber layer, the Kapton layers,

and the electrodes. The laminate can be seen to be void free and uniform. The electrodes can be seen to be quite parallel and uniformly spaced.

The increase in α_{ME} for laminates fabricated by the spin-coat/vacuum-bag technique resulted in a lower equivalent magnetic noise floor, compared to those made by the manual lay-up process. Figure 3.8(a) shows the equivalent magnetic noise for a ME sensor unit with a detection circuit containing a laminate made by the spin-coat/vacuum-bag. The noise floor at f = 1Hz was ~4×10^{-11} T/√Hz, which was almost a factor of 2× lower than the ~7×10^{-11} T/√Hz for a ME unit containing a laminate made by the manual lay-up process.

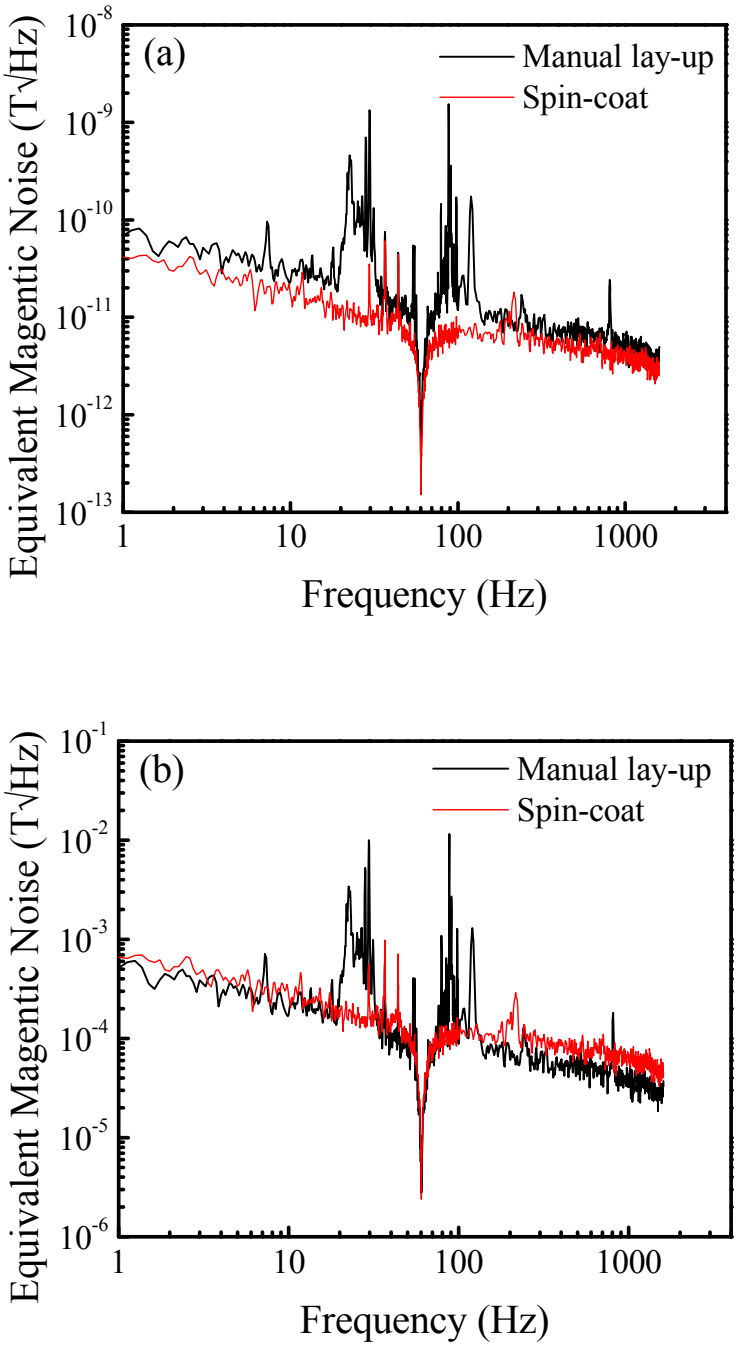

Figure 3.8. (a) Equivalent magnetic noise spectrum and (b) real voltage noise of manual lay-up (black curve) and spin-coat/vacuum bag technique (red curve).

The spin-coat technique increased α_{ME} of the laminate and decreased the equivalent magnetic noise floor of the ME sensor. However, the ~2× increase in α_{ME} did not result a direct 2× reduction in measured voltage noise. Rather, as can be seen in Figure 3.8 (b), the voltage noise of the sensor containing the laminate fabricated by the spin coat method was actually slightly higher than that of the sensor with laminate made by the manual lay-up process: 0.642 mV/√Hz versus 0.516 mV/√Hz, respectively. This discrepancy in the voltage noise relative to the equivalent magnetic noise can be explained by an increase in the sensor capacitance, due to the spin-coat/vacuum-bag technique. Typical values of capacitance for the spin-coat sensors were on the order of 1 nF at 1 kHz, whereas the manual lay-up sensors had values on the order of 600 pF. Due to impedance matching conditions for our charge amplifier, an increase in the sensor capacitance leads to an increase in the detected voltage noise. The equivalent magnetic noise floor for the spin-coat laminate sensor was then lower due to the larger value of the transfer function.

In addition to improvements in sensor performance by the spin-coat/vacuum-bag epoxy processing, the incorporation of improved Metglas alloys was also very important to reducing the equivalent magnetic noise floor of the ME laminate sensors. Prior ME laminate sensors employed a Metglas alloy with a magnetostriction of λ = 27 ppm (Magnetic Alloy 2605SA1), but here we used a Metglas alloy with a higher magnetostriction of λ = 42 ppm (Vitrovac 7600F). This, along with the improved epoxy processing techniques, allowed for an increase in α_{ME} of the sensor, from the value of 6 V/Oe·cm to 21.6 V/Oe·cm, as can be seen in Figure 3.6.

In Figure 3.9, we show the equivalent magnetic noise floor for ME sensors containing laminates with Metglas having enhanced magnetostriction (λ = 42 ppm) that were fabricated by our spin-coat/vacuum-bag epoxy processing. In this figure, the results are compared to those ME laminates containing Metglas with lower magnetostriction (λ = 27 ppm) that were fabricated by the manual lay-up process. The results in this figure show a decrease in the equivalent magnetic noise floor for laminates with Metglas layers having enhanced magnetostriction made by spin-coat/vacuum-bags epoxy process, from 2×10^{-10} T/√Hz, for laminates made by manual lay-up process with λ = 27 ppm, to 4×10^{-11} T/√Hz, for laminates made by spin-coat/vacuum bag epoxy process with λ = 42 ppm.

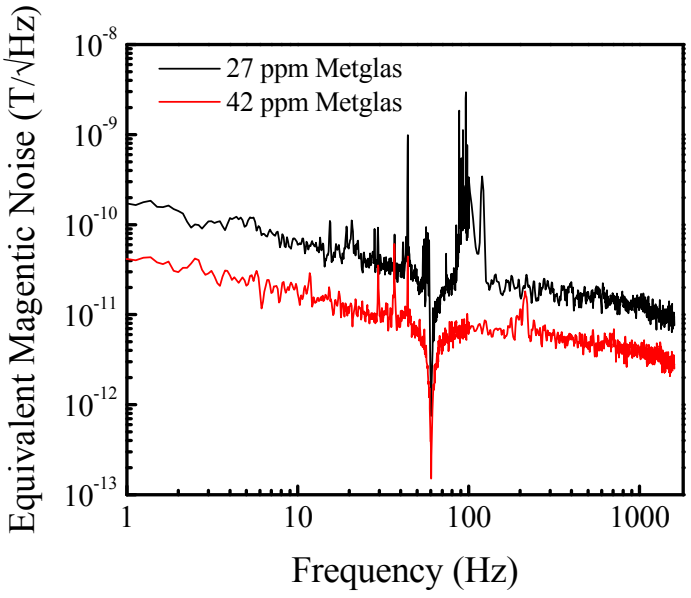

Figure 3.9. Noise floor of sensor made with manual layup process (black curve) and sensor fabricated using a Metglas alloy with higher saturation magnetostriction (42 ppm vs. 27 ppm) and improved processing techniques.

(Reprinted with permission from Ref. 66, Copyright © 2011 The American Ceramic Society)

3.3.2 Screen printing and manufacturability of ME laminates

Figure 3.10 illustrates the equivalent magnetic noise floor for three Metglas/PZT fiber laminate sensors, whose laminates were fabricated by the spin-coat/vacuum-bag epoxy method, using the Metglas with λ = 42 ppm. This figure confirms that the noise floors are nearly equivalent for the various sensors. These results clearly demonstrate the ability to fabricate laminates with easily repeatable properties for highly sensitive low frequency magnetic sensors.

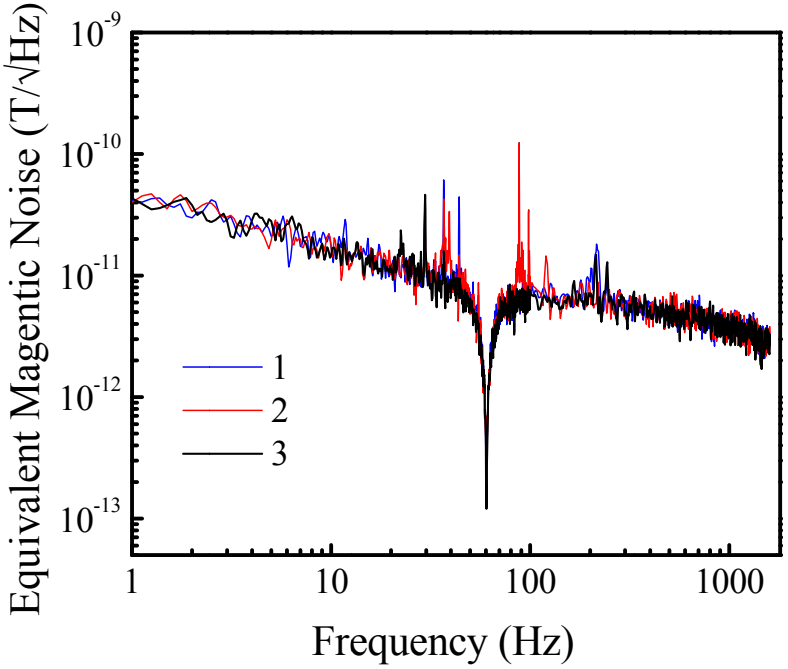

Figure 3.10. Noise floor of three sensors made by the spin-coat/vacuum-bag epoxy method, using the Metglas with higher saturation magnetostriction (λ=42 ppm).

A Metglas/PZT laminate is typically fabricated individually via the spin-coating method. Thus, when more than 10 laminates are required, it is not convenient to do this in the laboratory due to the time and effort needed to fabricate so many one by one. Moreover, the epoxy resin used to bond the Metglas and PZT layers has a usability window of only 15 minutes—any longer than that and the epoxy could cure during the spin-coating process. To overcome this problem, a screen printing method can be used to deposit a uniform layer of epoxy on the Kapton ID electrodes, as illustrated in Figure 3.11. A squeegee was used to spread the epoxy onto the Kapton, as well as remove any residue.

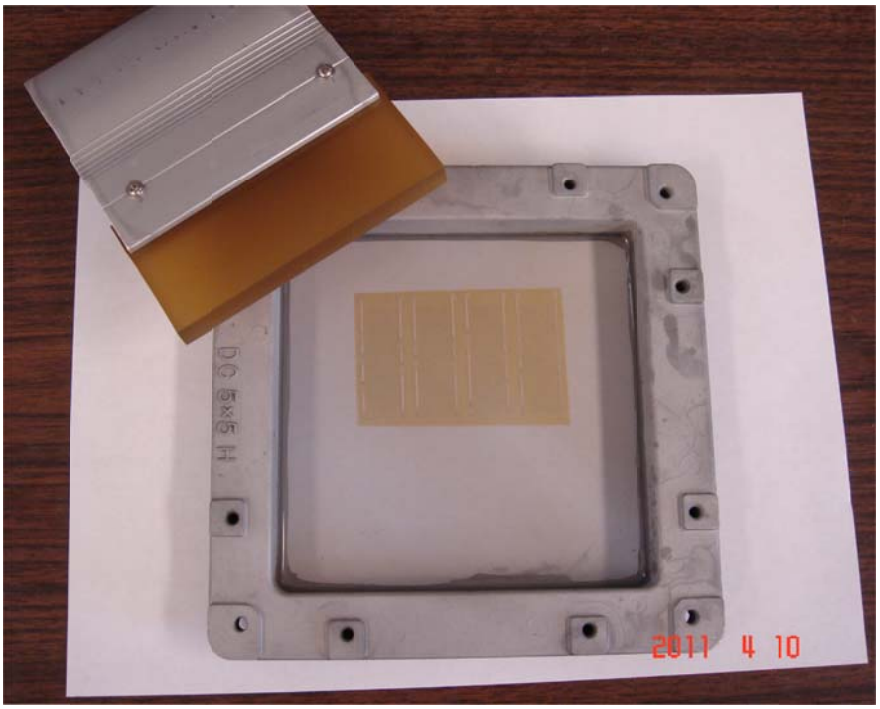

Figure 3.11. Photo of depositing epoxy on Kapton ID electrodes by screen printing method.

Figure 3.12 illustrates the capacitance results for four Metglas/PZT laminates made simultaneously by the screen printing/vacuum bagging method at a frequency range of f < 10 kHz. Specifically, the capacitance levels for these four laminates were quite similar: 441.2 pF, 431.9 pF, 426.0 pF and 430.9 pF at 1 kHz. In fact, between the four the capacitance difference was smaller than 3.5%. The α_{ME} values for these four laminates were also assessed, as follows: 25 V/cm·Oe, 24.2 V/cm·Oe, 24.6 V/cm·Oe and 24.3 V/cm·Oe, respectively. This experiment was repeated for four times. Figure 3.13 shows the α_{ME} values for all the laminates. Both the capacitance results at 1 kHz and the α_{ME} values for these 16 laminates showed variations smaller than 5%.

These results confirm the feasibility of producing at least 16 ME laminates with similar capacitance variations and ME properties (i.e., differences smaller than 5%) at one time in a laboratory setting. Indeed, the efficiency of fabricating ME laminates is highly enhanced in the laboratory environment. This finding means that ME sensor arrays can be built consisting of multiple ME laminates with similar ME properties.

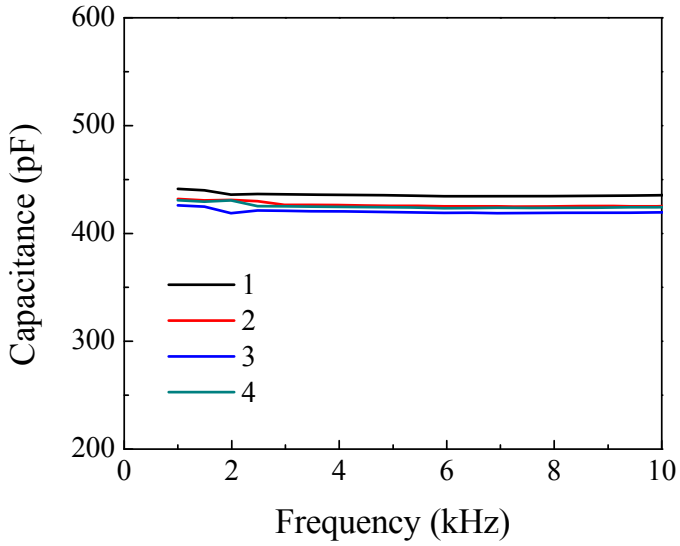

Figure 3.12. Capacitance results for four Metglas/PZT laminates made by the screen-printing/vacuum-bag method.

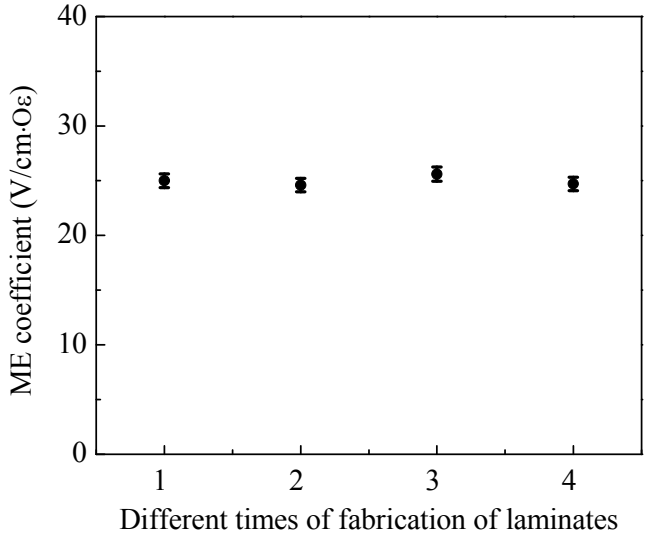

Figure 3.13. Values of α_{ME} for the 16 Metglas/PZT laminates (four assays).

3.4 Self-stressed Metglas/PZT Laminates

It is know that application of suitable stress to magnetostrictive materials results in a maximum value of the effective linear piezomagnetic coefficient.[67] Under moderate stress, the piezoelectric coefficient of piezoelectric materials can also be increased.[68] Thus, when suitably stress biased, the ME effect of magnetostrictive/piezoelectric laminate composites should also be enhanced. To apply a static stress to ME composites, a stiff frame and pre-stress screws can be used, which makes the unit size large and inconvenient to assemble.[69,70] Alternatively, the application of an optimum dc electric voltage bias to the piezoelectric layer is similar in context to applying a static stress to the composites.[71,72] Since the layers of ME laminates are epoxied together, inducing self-stress could be a good way by which to apply static stress to both phases. However, to data, there have been no reports of enhanced ME effects in self-stressed ME laminates.

Metglas/PZT/Metglas multi-push-pull L-L mode laminates were fabricated. A 40 mm × 10 mm PZT bundle served as the piezoelectric core of the laminates, which consisted of five 40 mm × 2 mm PZT-5A fibers (Smart Materials, Sarasota, FL) oriented along the length direction of the laminates. Two interdigitated Kapton electrodes were bonded to the top and bottom surfaces of the piezoelectric bundle with epoxy resin (Stycast 1264, USA). Spin-coat and vacuum-bag techniques were used to keep good repeatability of the capacitances of the interdigitated electrode/PZT core composites. The core composites were poled under 20 kV/cm electric field. Three Metglas foils (Vitrovac 7600F, Hanau, German) of dimensions 80 mm× 10 mm were then laminated to both the top and bottom surfaces of the core piezoelectric composites.

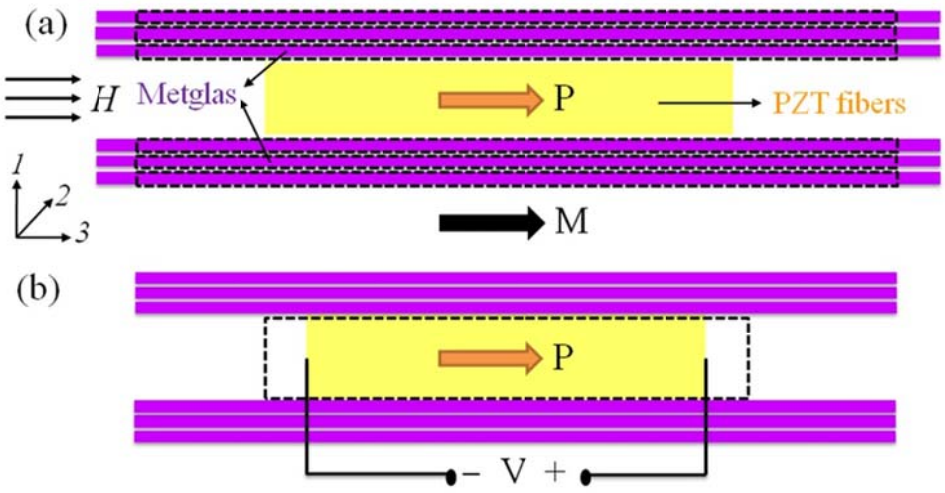

Figure 3.14. Schematic of the induced self-stress in the longitudinal section of a ME laminate configured in multi-push-pull mode. (a) H_{bias} applied to the Metglas layers and (b) E_{bias} applied to the interdigitated electrode/PZT core composite. The dashed lines illustrate the original shape without H_{bias} or E_{bias}.

When bonding Metglas layers to the core piezoelectric composites, there are two methods by which to induce self-stress: (i) application of a dc magnetic field (H_{bias}) to the Metglas layers, or (ii) application a DC electric field (E_{bias}) to the piezoelectric ones. After the cure of the epoxy and the removal of H_{bias} or E_{bias}, a self-stress will remain between the different layers of the laminates. Figure 3.14 shows the schematic of the induced self-stress in the longitudinal section of a ME laminate in the multi-push-pull configuration. As illustrated in Figure 3.14 (a), H_{bias} induces magnetostriction in each Metglas layer. After the cure of the epoxy, removal of H_{bias} will result in Metglas transferring stress to the PZT fibers. Values of H_{bias} from 0 to 60 Oe were applied to the Metglas layers during the process of bonding the core piezoelectric composites.

Alternatively, a compressive piezoelectric strain induced by E_{bias} applied opposite to the polarization direction will result in a tensile stress applied to the Metglas layers, as shown in Figure 3.14 (b). Values of E_{bias} from 0 to 4.7 kV/mm were applied to the core PZT composite layer during bonding to the Metglas layers.

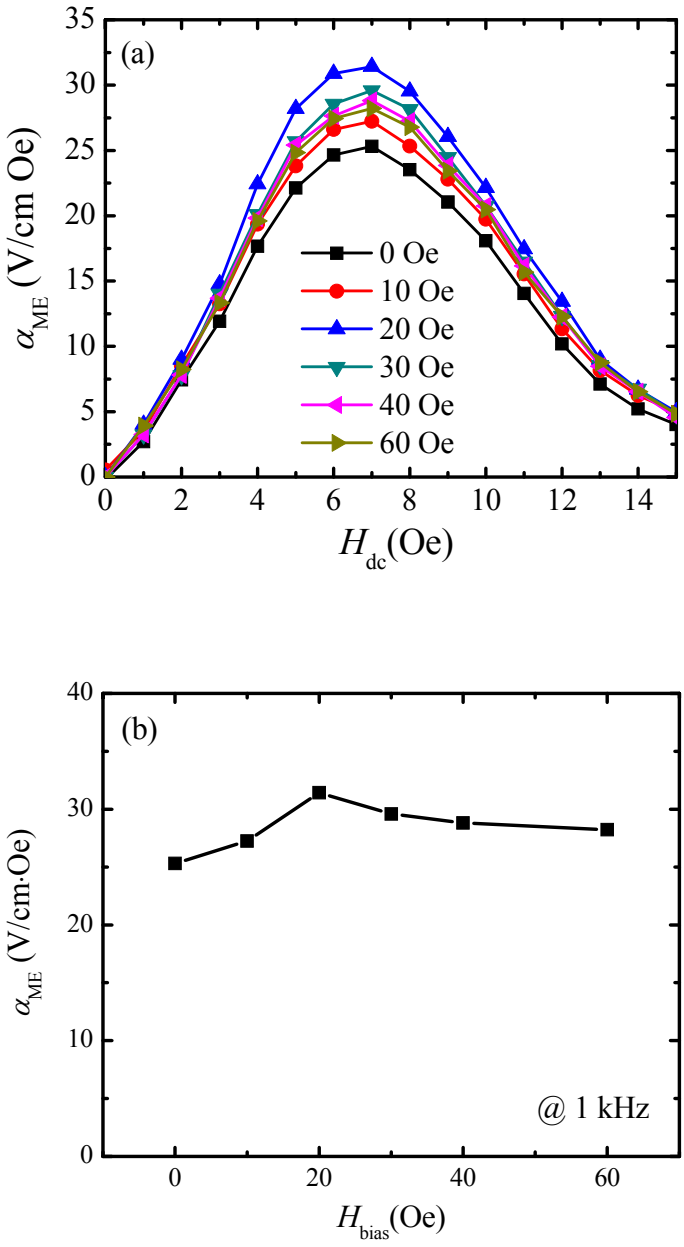

Figure 3.15. (a) The values of the ME voltage coefficient α_{ME} as a function of H_{dc} for Metglas/PZT/Metglas laminates epoxied together under various H_{bias}. (b) Maximum value of α_{ME} as a function of H_{bias}. The data were measured at an AC magnetic field of H_{ac} = 0.1 Oe and at a frequency of f = 1 kHz.

The value of α_{ME} was measured using a lock-in amplifier (SR-850) in response to a pair of Helmholtz coils driven at an AC magnetic field of H_{ac} = 0.1 Oe at a frequency of f = 1 kHz. The dc magnetic field was applied by a large electromagnet. Figure 3.15 (a) shows the value of α_{ME} as a function of H_{dc} for the Metglas/PZT/Metglas laminates with different H_{bias} applied during the cure of the epoxy. It can be seen that α_{ME} increased as H_{dc} was increased; and subsequently decreased as H_{dc} was further increased. The maximum value of α_{ME} increased with increasing magnetic fields until H_{bias} = 20 Oe, and then decreased with further increase in H_{bias}. As shown in Figure 3.15 (b), without self-stress in the laminate, the maximum value of α_{ME} was 25.3 V/cm·Oe, which agrees well with data previously reported. However, for H_{bias} = 20 Oe, the maximum value of α_{ME} was 31.4 V/cm·Oe, which was a factor of 1.24× higher than that for H_{bias} = 0. This value of α_{ME} in the self-stressed state is higher than any data ever reported for ME laminates having a core PZT layer.

The enhanced value of α_{ME} was mainly due to the increases in the magnetostrictive properties induced by the self-stress in Metglas layers of the laminates. In pure Metglas materials, the stress ${}^{m}T_{r}$ in Metglas layers after the remove of the bias field is:

$$ {}^{m}T_{r} = -\frac{\lambda}{{}^{m}S_{33}}, \tag{3.10} $$

where λ is the magnetostriction under the DC bias field H_{bias}. To simplify the calculation, I just consider the stresses in the longitudinal direction (3 direction). If such Metglas layers are bonded with PZT layers, considering the following boundary conditions of ideal strain transfer between each layers:

$$ {}^{m}S_{3} = {}^{p}S_{3} = {}^{e}S_{3}, \tag{3.11} $$

and Newton's third law of motion:

$$({}^{m}T_r + {}^{m}T_3)A_m + {}^{p}T_3 A_p + {}^{e}T_3 A_e = 0, \tag{3.12}$$

the residual stress ${}^{m}T_3$ in Metglas layers could be determined as:

$${}^{m}T_3 = \frac{\lambda t_m {}^{p}s_{33} {}^{e}s_{33}}{{}^{m}s_{33}({}^{p}s_{33} {}^{e}s_{33} t_m + {}^{m}s_{33} {}^{e}s_{33} t_p + {}^{m}s_{33} {}^{p}s_{33} t_e)}, \tag{3.13}$$

where t_m, t_p and t_e are the thickness of Metglas, piezoelectric and epoxy layers. Therefore, under various DC bias field H_{bias} during the cure of the epoxy layers, the residual stress could be calculated. Using the same elastic coefficients and thickness parameters in Table 3.1, the residual stress ${}^{m}T_3$ as a function of DC bias field H_{bias} is shown in Figure 3.16. The sign of ${}^{m}T_3$ is positive, meaning that it is tensile stress. As tensile stress is applied to Metglas layers, the anisotropy field is reduced. Thus, the effective piezomagnetic coefficient $d_{33,m}$ of Metglas layers is enhanced, leading to enhanced value of ME coefficient α_{ME}. When H_{bias} = 20 Oe, the value of ${}^{m}T_3$ is 0.40 MPa, which is very close to the critical stress $\sigma_c = 2K_u/3\lambda_s$ in Metglas layer. The value of $d_{33,m}$ of Metglas layers is maximum. From equation (1.3) it could be seen that the value of α_{ME} is proportional to the value of $d_{33,m}$. Thus, when $d_{33,m}$ reaches the maximum value, the value of α_{ME} is maximum. When H_{bias} > 20 Oe, the value of ${}^{m}T_3$ is larger than σ_c, which makes the magnetic easy axis switched towards the longitudinal direction from transverse direction. The effective magnetostriction is lower, so the value of α_{ME} decreases as increasing H_{bias} to higher values.

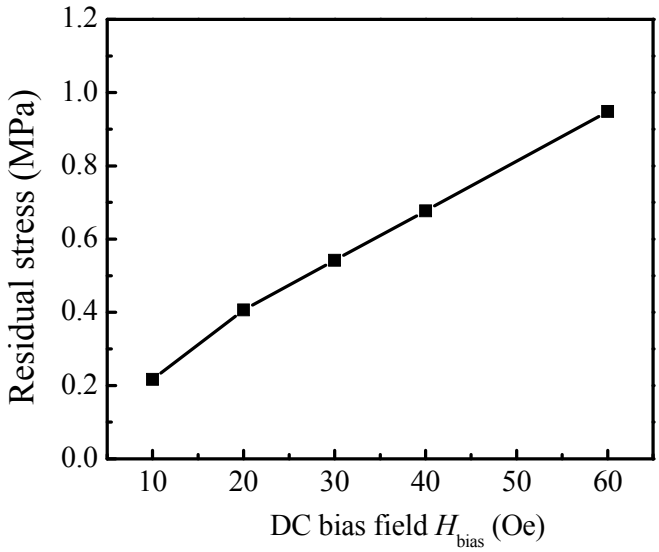

Figure 3.16. Residual stress in Metglas layers after cure of epoxy and the removal of different DC bias field H_{bias}.

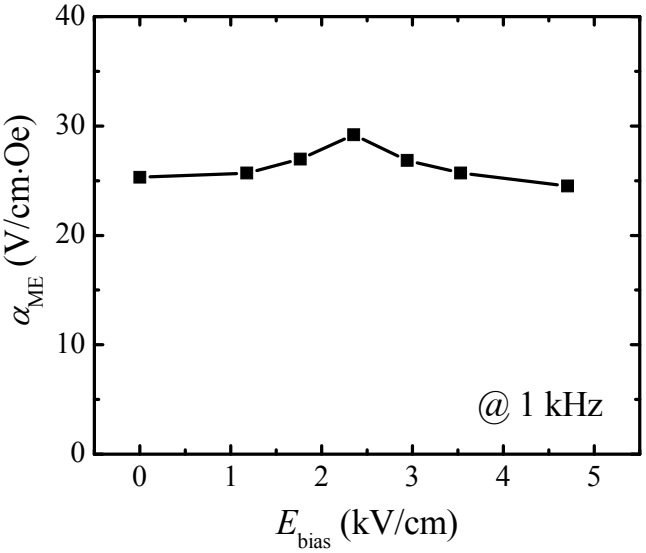

Figure 3.17. Maximum value of α_{ME} as a function of E_{bias}. The data were measured at an AC magnetic field of H_{ac} = 0.1 Oe and at a frequency of f = 1 kHz.

Figure 3.17 shows the maximum value of α_{ME} of the laminates as a function of E_{bias}. The highest value was 29.2 V/cm·Oe for E_{bias} = 2.4 kV/cm, which was 1.15× higher than the laminate without self-stress. This highest value under E_{bias} is a little lower than that of laminates epoxied together under H_{bias}. This may be due to the stress transferred to Metglas not being uniform in each layer. There are three Metglas layers bonded on both sides of the core piezoelectric composite. The stress from the PZT is transferred to each Metglas layer by the adhesive epoxy. The stress in the outmost two Metglas layers is smaller than that in the innermost two layers. Under such nonuniform stress, it is difficult to maximize the effective linear piezomagnetic coefficient in each Metglas layer. Thus, the highest value of α_{ME} of laminates epoxied under E_{bias} may be lower than that under H_{bias}.

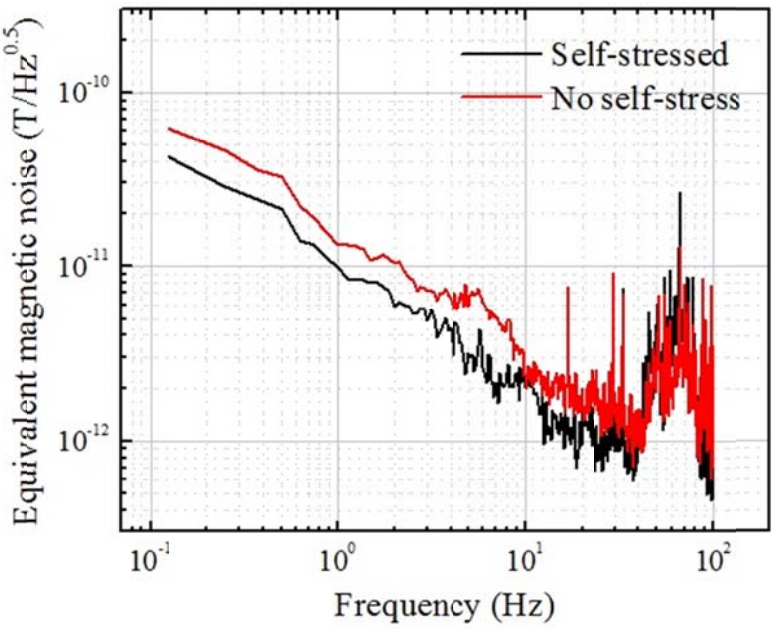

Figure 3.18. Equivalent magnetic noise floor of self-stress Metglas/PZT/Metglas laminates epoxied together under H_{bias} = 20 Oe, and laminate without self-stress.

The noise charge density of a ME laminate is mainly determined by the dielectric properties: the capacitance (C) and the dielectric loss (tan δ). The values of C and tan δ were measured using an impedance analyzer (Agilent 4292A). No obvious changes were found between laminates with or without self-stress at low frequencies. If having similar dielectric properties, ME laminates with higher values of α_{ME} should exhibit lower equivalent magnetic noise floors. Self-stressed Metglas/PZT/Metglas laminates epoxied under H_{bias} = 20 Oe and H_{bias} = 0 (i.e., without self-stress) were then packaged with a simple low-noise charge amplifier having a gain of 5.1 V/pC over the frequency range of $0.1 < f < 100$ Hz (designed by SAIC). The unit was placed inside a high-mu-metal magnetic shielded chamber, and connected to a dynamic signal analyzer (SR-785) to measure the voltage noise. The voltage noise was then converted to the equivalent magnetic noise floor using α_{ME} and C of the laminate. Figure 3.18 shows the equivalent magnetic noise floor of the self-stressed Metglas/PZT/Metglas laminate epoxied together under H_{bias} = 20 Oe, which is compared to the laminate prepared without self-stress. The results show a decrease in the equivalent magnetic noise floor for the self-stressed laminate over the frequency range of $0.1 < f < 30$ Hz. At f = 1 Hz, the noise floor was reduced from 13.3 pT/Hz$^{0.5}$ to 9.8 pT/Hz$^{0.5}$, which was by a factor of about 1.35×.

3.5 ME Sensor Reliability Testing

In addition to magnetic field sensitivity, other parameters associated with magnetic sensor are also important. This section details the process by which I tested the following essential properties of Metglas/piezo-fiber laminates: (1) the linearity of ME output voltage to AC magnetic field; (2) the durability of ME coefficients over three years; and (3) the fatigue of ME coefficient to strong AC magnetic field at different frequencies.

3.5.1 The linearity of ME laminates

The linearity of Metglas/PZT laminates was measured by applying various AC magnetic field H_{ac} at f = 1 kHz. Figure 3.19 shows the ME output voltage of a Metglas/PZT laminate at the range of $0 < H_{ac} < 6$ Oe under an optimum DC bias field of 8 Oe. The ME laminate showed good linear response at the range of $H_{ac} < 3$ Oe. When $H_{ac} > 3$ Oe, the value of V_{out} was smaller than the linear fitted results (red line in Figure 3.19). This outcome can be linked to the magnetostrictive properties of Metglas materials. The magnetostriction λ of Metglas layers with a dimension of 8 cm × 1 cm was almost linear in the range of 5 Oe < H_{dc} < 11 Oe. The value of V_{out} was directly proportional to λ. When biased at 8 Oe, the linear range of V_{out} was the same as the linear range of λ. When biased at 0 Oe,t value of V_{out} was much smaller. The linear range of V_{out} corresponds to when $H_{ac} < 2$ Oe, which is associated with the same causation factors whereby λ was approximately linear in this range.

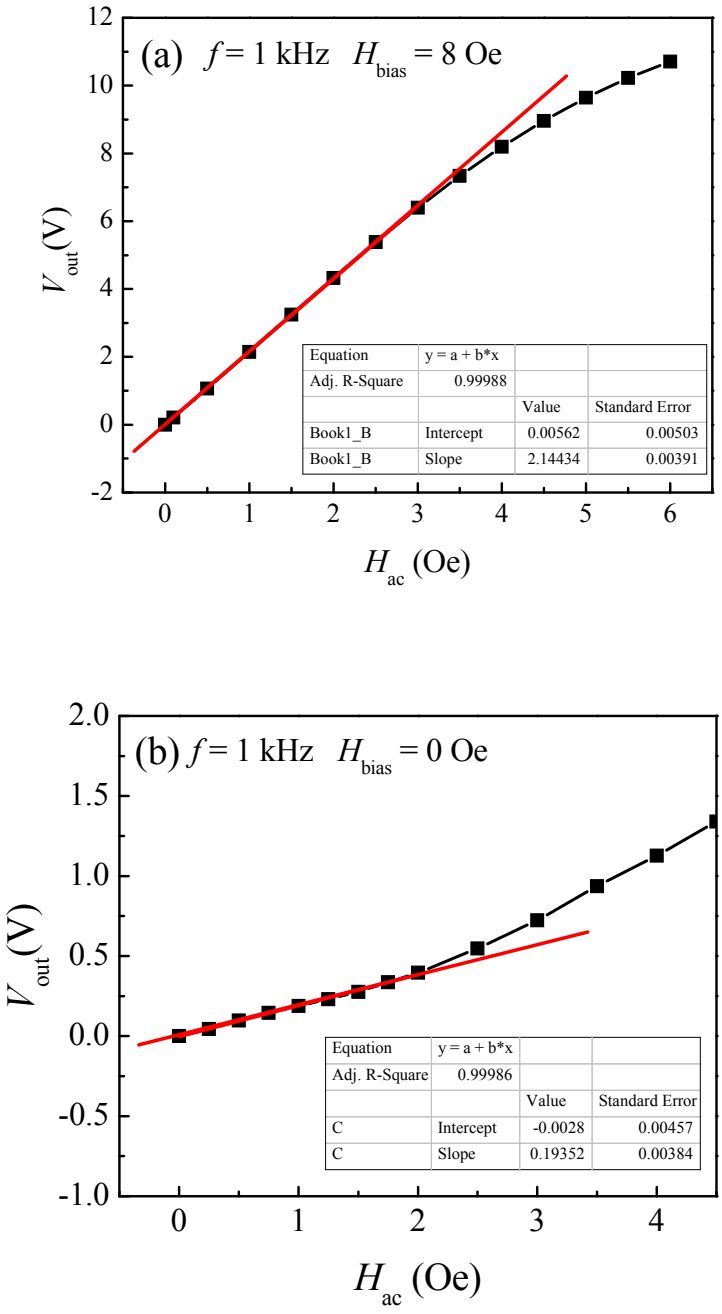

Figure 3.19. ME output voltage V_{out} of Metglas/PZT laminate as a function of AC magnetic field H_{ac} under (a) H_{bias} = 8 Oe and (b) H_{bias} = 0 Oe. The red lines are extended from the linear fitted equations.

3.5.2 Durability testing of ME laminates

To characterize the durability of an ME magnetic sensor, I measured the ME voltage coefficient of Metglas/PZT laminates over a three-year period. Although every measurement was obtained under the same experimental conditions, the laminates were stored in different environments. One laminate was kept in a desiccator at room temperature; another laminate was maintained in the natural environment at room environment. It should be noted that in the summer, humidity levels in Blacksburg, VA (the location of Virginia Tech), could be as high as 90% (or even higher). The laminate maintained outside the desiccator was used to characterize the effect of moisture on ME coefficients.

The ME coefficient was measured at 1 kHz. The laminates were exposed to an optimum DC bias field applied by small magnets. Figure 3.20 shows the change of ME voltage coefficient verses time. It can be seen that there is no obvious change in ME voltage coefficient for either laminate (the one in the desiccator versus the one in the room environment). This finding confirms that our ME laminates possess stable ME properties at room temperature, regardless of humidity levels.

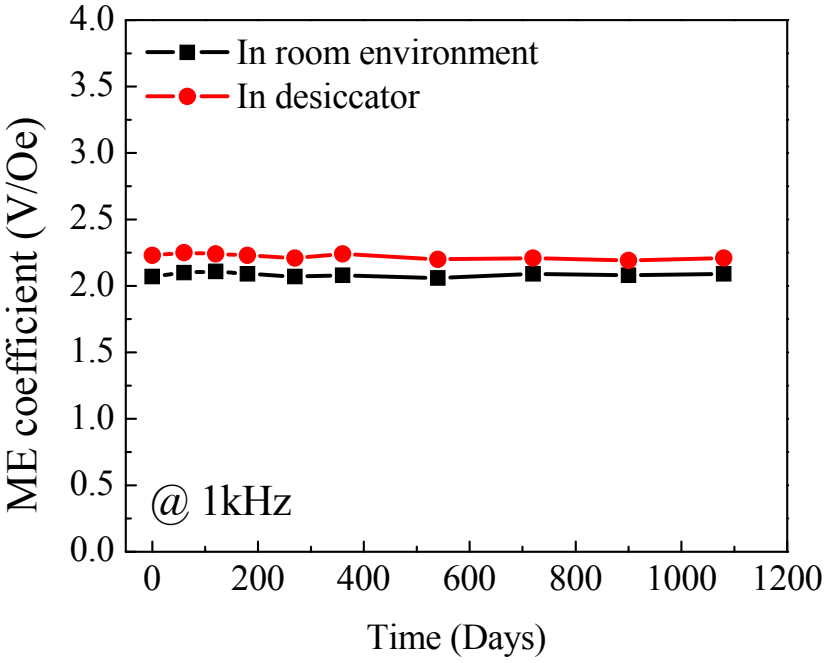

Figure 3.20. Change of ME voltage coefficient for Metglas/PZT laminate verses time. The laminates were stored at room environment or in a desiccator.

3.5.3 Fatigue testing of ME laminates

Fatigue testing of the Metglas/PZT laminates was done by applying a continuous AC magnetic field. As shown in Figure 3.21, the ME voltage coefficient did not change even after applying 1×10^9 cycle change of 4 Oe AC magnetic field at 1 kHz. However, when increasing the frequency of the field to EMR (f = 30.1 kHz), the ME voltage coefficient slightly decreased after 5×10^8 cycles. After 1×10^9 cycles, the ME voltage coefficient decreased by 10%.

In the low frequency range, each layer of the ME laminate maintained stable properties throughout the test. The ME voltage coefficient remained stable after applying more than 1×10^9 cycles. In contrast, at EMR and driven by a strong AC magnetic field, much larger strain was transferred from the Metglas layers to the PZT materials. This large strain resulted in fatigue of the adhesive epoxy layers, yielding a decrease in the coupling factor between the Metglas and PZT layers. In summary, the ME voltage coefficient decreased after a 1×10^9 cycle change in the magnetic field. The dielectric properties of PZT fibers, however, did not display any obvious change after 1×10^9 cycles, but the piezoelectric properties might have decreased due to domain switches induced by strong strains at EMR. Thus, future investigations should target all additional effects of fatigue testing on ME laminates.

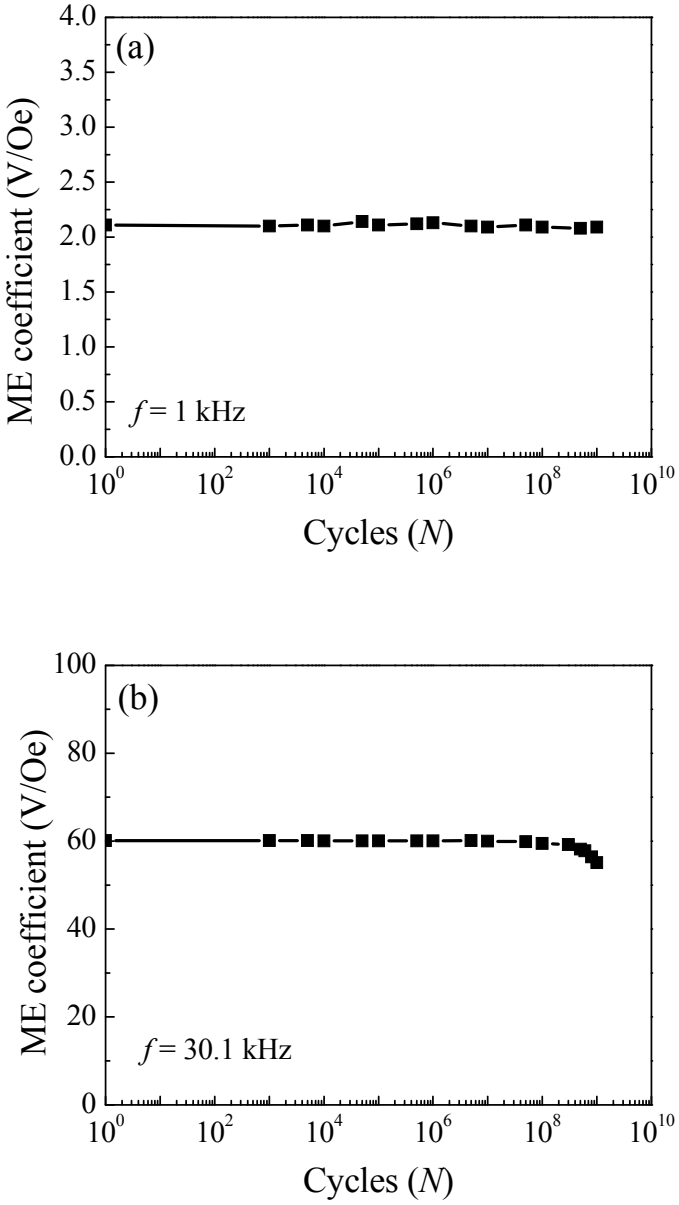

Figure 3.21. Change of ME voltage coefficient for Metglas/PZT laminate verses cycles of change of magnetic field (a) at 1 kHz and (b) at 30.1 kHz. The ME laminate was under optimum bias field of 8 Oe.

3.6 Section Summary

Firstly, a theoretical model was presented for magnetoelectric (ME) effects in multi-push-pull mode magnetostrictive/piezo-fiber laminate composites. Analytical solutions for the ME coefficient were derived. The effects of thickness ratio of the magnetostrictive phase, Kapton and multiple layers of epoxy on the value of α_{ME} were discussed. This model presents theoretical guidelines by which to achieve higher values of α_{ME}.

Secondly, a novel method of epoxy application and epoxy cure was described, which significantly improves the ME voltage coefficient (α_{ME}) of laminate composites. Also, spin-coating, vacuum bagging, hot pressing and screen printing techniques were used to reduce variations of α_{ME} values—i.e., smaller than 5%. These results confirm the efficacy of this method for fabricating Metglas/PZT laminates with repeatable ME properties in the laboratory. Indeed, up to 16 laminates can be manufactured in this way at one time.

Furthermore, application of a DC magnetic field to the Metglas layers, or a DC electric field to the core piezoelectric composites, can effectively induce self-stress to the laminate when bonding Metglas and PZT layers. The value of α_{ME} for the laminate epoxied under H_{bias} = 20 Oe was enhanced by a factor of 1.24×, compared to the laminate prepared without self-stress. Subsequently, the equivalent magnetic noise floor was reduced over the frequency range of $0.1 < f < 30$ Hz.

Finally, the linearity, durability and fatigue of the Metglas/piezo-fiber laminates were tested. Resulting parameters confirmed that the Metglas/piezo-fiber laminates are good candidate for magnetic sensors.

CHAPTER 4.

ME LAMINATE STACKS AND ARRAYS

4.1 Introduction

Sensor arrays have been used in many practical applications where improvements in the signal-to-noise ratio (SNR) are important. Some common applications include radar[74], odor recognition[75] and sonar[76]. For magnetic sensors, array configurations have been used in cases where significant enhancements in sensitivity are essential—e.g., for SQUIDs (superconducting quantum interference devices)[77], Hall sensors[78] and others. Xing *et al*. predicted that an array of N number of ME laminate sensors will increase the SNR by a factor of $\sqrt{N}$, [79] however, similar experimental studies for ME Metglas/piezo-fibers laminate sensors have not been reported.

For this study phase, I investigated strategies for optimizing the distance between a pair of Metglas-PZT-Metglas ME laminates to achieve enhanced α_{ME} values. I then investigated the charge and equivalent magnetic noise levels of stacked ME laminate sensors. Predicted and experimental data confirmed that the equivalent magnetic noise decreased and the magnetic field sensitivity increased, both by factors of $\sqrt{N}$. Finally, I construct an array of four Metglas/PZT sensor units. The magnetic field sensitivity of the array increased by a factor of two relative to the individual unit. These experimental results confirmed predicted findings—namely, that array configurations of ME sensors are capable of increased sensitivity.

4.2 Separation Distance Effect on Magnetic Field Sensitivity

In the application of magnetic materials with very high permeabilities, magnetic flux concentration effects can be quite significant.[51,80] The permeability of Metglas is μ_r > 40000. Clearly, the magnetic flux density can vary for each Metglas foil, due to the effect of mutual inductance, when two foils are placed at different distances with respect to each other, as shown in Figure 4.1(a). Finite element simulation using *MAXWELL 13.0* was performed for Metglas foils of the same dimensions as our laminates. We show simulation results in Figure 4.1(b) of the flux density for one Metglas foil when another identical foil was placed nearby it at various distances (i.e. center of one Metglas foil to another). The exteral magnetic field was 0.1 Oe. As can be seen, when the distance between the two Metglas foils was 20 mm, the magnetic flux density at the center region (-20 mm to 20 mm), where the Kapton/PZT core composite was bonded, was low. The flux density became higher in this region as the spacing between the two foils was increased. When the distance was 40 mm and 50 mm, the flux density was nearly equal: which means that mutual inductance between foils is small. Such effect was depended on the size of the sensors. For sensors with various dimensions, the distance at which the effect of mutual inductance can be neglected should be different.

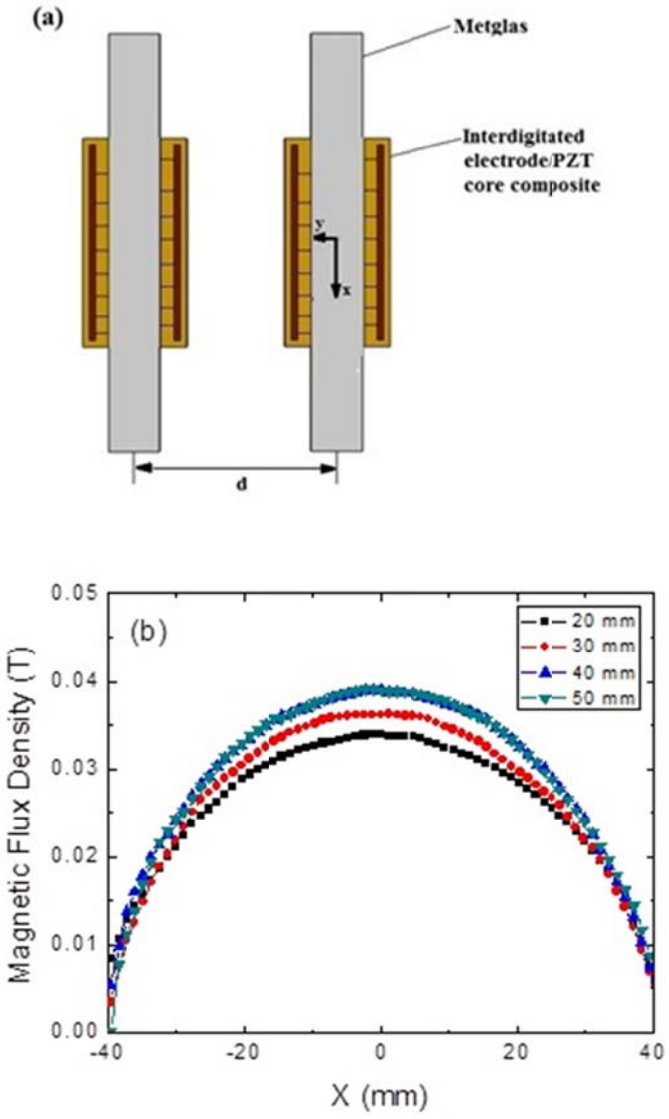

Figure 4.1. Schematic representation of a pair of Metglas/PZT L-L mode ME laminates separated by a distance d. (b)Magnetic flux density of the Metglas foil along the x-axis (length direction) at y=0, z=0 (the origin was at the center of the Metglas foil), when another identical foil was placed at various distances from it. The external magnetic field was 0.1 Oe.

When the distance separating the two ME laminates was changed, the value of α_{ME} also varied: this is due to changes in the magnetic flux density in the Metglas foil. The value of α_{ME} was measured using a lock-in amplifier (SR-850) in response to a pair of Helmholtz coils driven at an AC magnetic field of H_{ac} = 0.1 Oe at a frequency of f = 1 kHz. The two laminates were placed on a horizontal plane, separated by different distances within the Helmholtz coil. As shown in Figure 4.2(a), the value of α_{ME} was largest when the laminates were separated from each other by at least 40 mm. The maximum value of α_{ME} was then 28.5 V/cm·Oe under a DC bias of 8.86 G. When the distance between these two laminates was < 40 mm, the value of α_{ME} was reduced: for example at 20 mm, the maximum value of α_{ME} was 23.6 V/cm·Oe under a DC bias of 8.90G: a 17% reduction with respect to that at 40 mm. Figure 4.2(b) shows the maximum value of α_{ME} as a function of distance between two Metglas/PZT laminates. In this figure, one can see that the maximum value of α_{ME} increased as the distances between the two laminates was increased. When the distance was > 40 mm, the maximum value of α_{ME} was the same as for each sensor with an infinite separation.

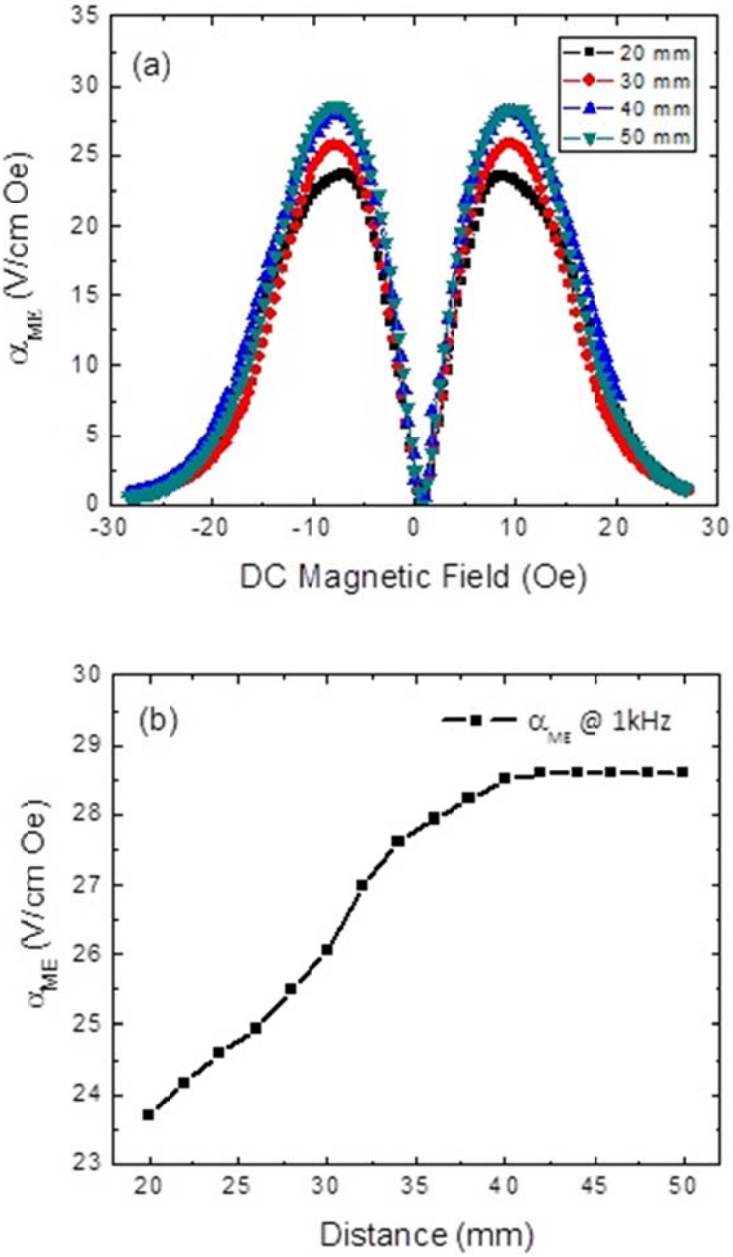

Figure 4.2. The value of α_{ME} as a function of DC bias field for one Metglas/PZT laminate when another one was placed at different distances from it. (b) The maximum value of α_{ME} as a function of distance between two Metglas/PZT laminates. The data were measured at 1 kHz and H_{ac}=0.1 Oe.

A pair of Metglas/PZT laminates connected in parallel was then packaged with a simple low-noise charge amplifier having a gain of 5.18 V pC^{-1} over the frequency range of $0.1 < f < 100$Hz (designed by SAIC); which we designated as a ME sensor unit. The unit was placed inside a high-mu-metal magnetic shielding chamber, and connected to a dynamic signal analyzer to measure the noise voltage and output signal. The magnetic field sensitivity can be expressed as:

$$\text{Magnetic field sensitivity} = \frac{H_{ac-f}}{V_{ME-f}} \times SNR \times V_{noise}; \tag{4.1}$$

where $H_{ac\text{-}f}$ is the ac magnetic field generated by the Helmholtz coil, $V_{ME\text{-}f}$ is the ME output voltage of the ME sensor unit, SNR = 2, and V_{Noise} is the voltage noise at the frequency of interest.

Figure 4.3(a) shows the voltage noise spectrum over the frequency range of $0.125 < f < 100$ Hz, which also contained an output signal in response to a 10 nT incident AC magnetic field at 1Hz, when the two laminate were 40 mm from each other. The output of the sensors was 1.58 V, and the background voltage noise at the corresponding frequency was 1.13×10^{-3} $V/Hz^{1/2}$. From Equation (4.1), the magnetic field sensitivity of this pair of Metglas/PZT laminate sensors was 14.2 pT at 1 Hz. In Figure 4.3(b), the output voltage and magnetic field sensitivity of the sensor pair in response to H_{ac} = 10 nT is shown, when the laminates were placed at various distances. The output voltage increased with increasing distance between laminates; correspondingly, the sensitivity also improved. When the distance was > 40 mm, the sensors had a maximum output voltage and the highest magnetic field sensitivity (14.2 pT): a 27% increase, relative to a distance of 20 mm.

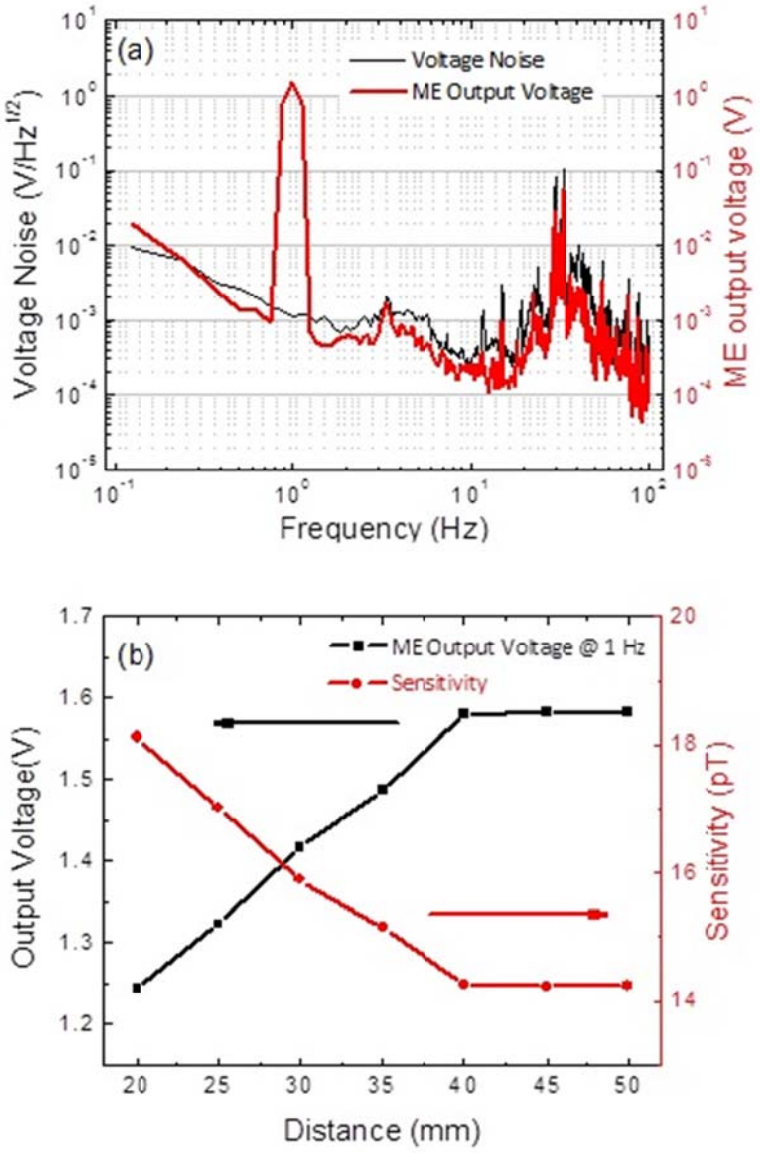

Figure 4.3. (a) ME output signal of the ME sensor unit and background voltage noise in the absence of intentional excitation. (b) The output signal and sensitivity of the sensor unit when the two laminates were placed at various distances. The incident AC magnetic field was 10 nT at 1 Hz.

4.3 ME Laminate Stacks

For ME sensors, the dominant internal noise sources have been identified to be the dielectric loss (N_{DE}) and the DC leakage resistance (N_R) contributions.[82] Secondary noise sources, such as thermal and electrical circuit noises, have been neglected due to a lower charge noise density relative to these internal sensor noise contributions.[82] The charge noise density of these two dominant noise sources can be estimated as:

$$N_{DE} = \sqrt{\frac{4kTC\tan\delta}{2\pi f}}, \tag{4.2}$$

$$N_R = \frac{1}{2\pi f}\sqrt{\frac{4kT}{R}}. \tag{4.3}$$

The total charge noise density can then be given as:

$$N_t = \sqrt{N_{DE}^2 + N_R^2} = \sqrt{\frac{4kTC\tan\delta}{2\pi f} + \frac{1}{(2\pi f)^2}\frac{4kT}{R}}; \tag{4.4}$$

where k is Boltzmann's constant (1.38×10^{-23} J K^{-1}), T is the temperature in Kelvin, C is the capacitance, $\tan\delta$ is the dielectric loss, R is the DC resistance of the ME sensor, and f is the frequency in Hertz.

The equivalent magnetic noise N_m can then be obtained from the α_Q of the sensor and the total noise charge density:

$$N_m\left(T/\sqrt{Hz}\right) = \frac{N_c\left(C/\sqrt{Hz}\right)}{\alpha_Q\ (C/T)} = \frac{\sqrt{\frac{4kTC\tan\delta}{2\pi f} + \frac{1}{(2\pi f)^2}\frac{4kT}{R}}}{\alpha_V C}. \tag{4.5}$$

If N ME laminates are stacked in parallel, the capacitance of the array is N times that of C, the DC resistance is $1/N$ and the dielectric loss is unchanged. Therefore, the equivalent magnetic noise of the ME array N_{mA} can be estimated as

$$N_{mA} = \frac{\sqrt{N\left(\frac{4kTC\tan\delta}{2\pi f} + \frac{1}{(2\pi f)^2}\frac{4kT}{R}\right)}}{N\alpha_V C} = \frac{1}{\sqrt{N}} N_m. \tag{4.6}$$

From Equation (4.6) and the predictions by Xing *et al*., one can see that the equivalent magnetic noise is decreased and the SNR is increased both by factors of $\sqrt{N}$.

The value of α_{ME} was measured using a lock-in amplifier (SR-850) in response to a pair of Helmholtz coils driven at an AC magnetic field of H_{ac} = 0.1 Oe at a frequency of ƒ = 1 kHz. Figure 4.4 (a) shows the ME voltage coefficient α_V and ME charge coefficient α_Q as a function of H_{dc} for a single Metglas/PMN-PT laminate. The maximum value of α_v was 52 V/cm·Oe under a DC bias of 8.6 G; correspondingly, the maximum value of α_Q was 2078 pC/Oe. The ME coefficient reported here is significantly higher than that previously reported for two phase ME composites, which is mainly due to the high piezoelectric constant ($d_{33,p}$) of the PMN-PT piezofibers. The maximum values of α_v and α_Q as a function of the number of laminates under the optimum H_{dc} are shown in Figure 4.4 (b). The value of α_v was unchanged and that of α_Q increased linearly with N , agreeing well with predictions. Figure 4.4(c) shows the capacitance and the dielectric loss factor of the laminate array as a function of N . The capacitance increased linearly with N , and the dielectric loss factor was relatively invariant to N .

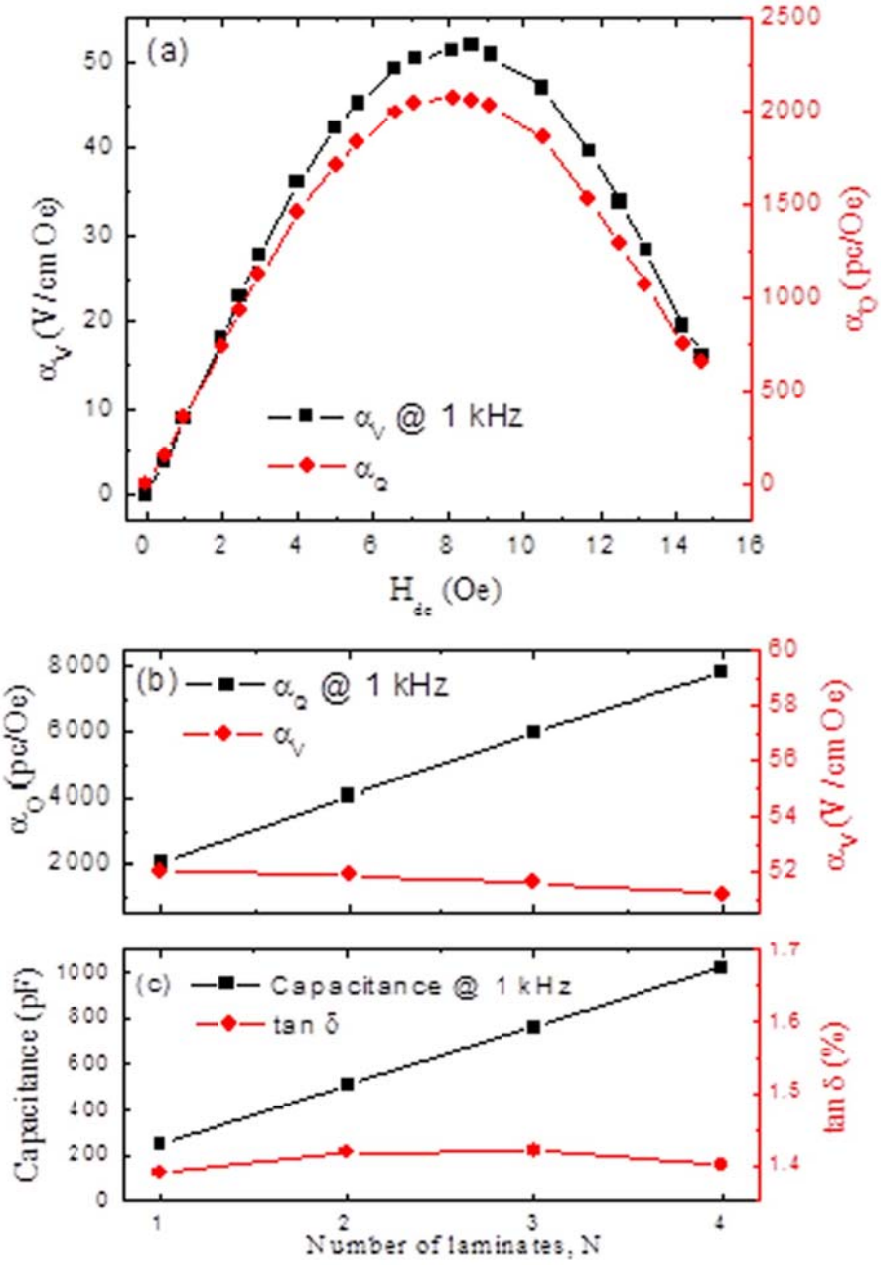

Figure 4.4. ME voltage coefficient (α_V) and ME charge coefficient (α_Q) of Metglas/PMN-PT laminates as a function of (a) DC bias H_{dc} at 1 kHz, and (b) the number of laminates stacked, *N*. (c) Capacitance and dielectric loss factor as a function of number laminates stacked, *N*.

The laminates were then packaged with a simple low-noise charge amplifier having a gain of 5.1 V pC^{-1} over the frequency range of $0.1 < f < 100$Hz (designed by SAIC): which we designate as a ME sensor unit. The unit was placed inside a high-mu-metal magnetic shielded chamber, and connected to a dynamic signal analyzer to measure the voltage noise and output signal. Due to the DC resistance saturating the amplifier (<30 GΩ), the largest number of laminates that we could connect in parallel and measure was $N = 4$.

Figure 4.5(a) shows the measured and estimated charge noise spectra for a ME sensor unit which contained a single laminate. The noise density was estimated based on Equations (1) to (4), using appropriate ME laminate parameters. The estimated and measured charge noises exhibited good agreement, except at frequencies near external vibrational sources. Figures 4.5 (b) and (c) show the estimated and measured charge noises for a ME sensor unit as a function of N at f =1 Hz. In these figures, one can see that the estimated and measured noises increased proportionally to $\sqrt{N}$. Figure 4.5 (d) shows the estimated and measured equivalent magnetic noises at 1 Hz. The measured noise decreased with increasing N, which agreed well with the predicted noise. In particular, the equivalent magnetic noise of the ME sensor unit for $N = 4$ was as low as 2.84 $pT/Hz^{0.5}$, which was a factor of 2.1× lower than that for $N = 1$. This low equivalent magnetic noise was also a factor of 1.8× lower than that previously reported for ME sensors.[43] Such a low equivalent magnetic noise holds promise for ultra-low magnetic field detection applications at room temperature.

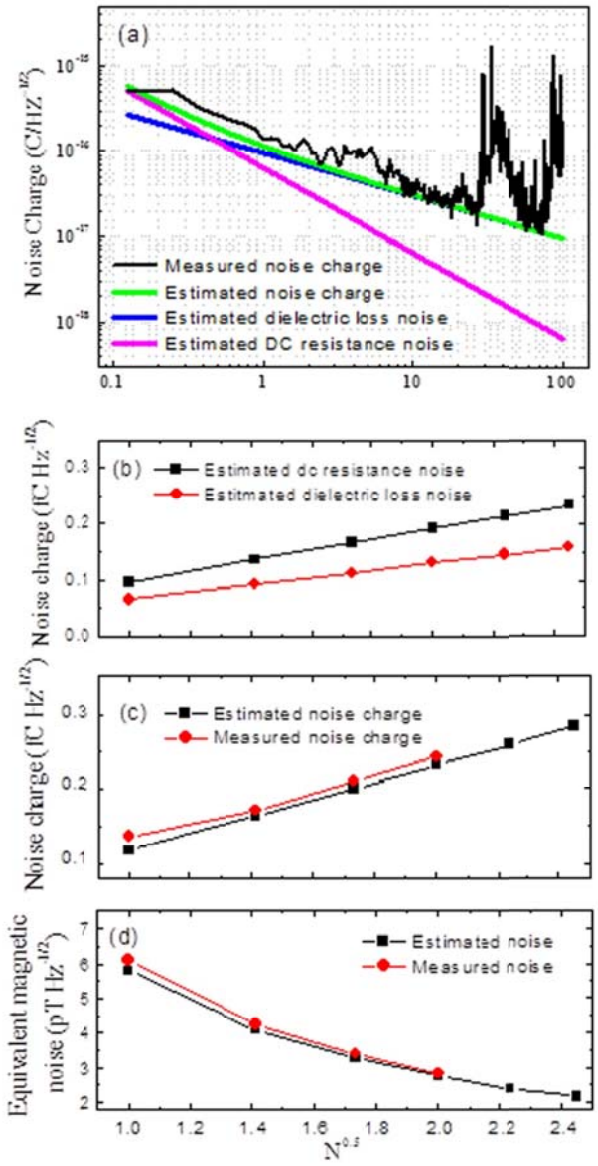

Figure 4.5. (a) Measured and estimated charge noise density of the ME sensor unit for N = 1, including constituent dielectric loss and dc resistance, over the frequency range of 0.125< f <100 Hz. (b) Estimated dc resistance and dielectric loss noise charge. Measured and estimated (c) noise charge and (d) equivalent magnetic noise at 1Hz, as a function of $\sqrt{N}$.

Figure 4.6 (a) shows a voltage noise spectra and the output voltage of a ME sensor unit for N =1 over the frequency range of 0.125 < f < 100 Hz, in response to a 1 nT incident ac magnetic field at 1Hz. The output of the sensors was 0.106 V, and the background voltage noise at 1 Hz was 6.77 $\times 10^{-4}$ V/Hz$^{1/2}$. From (4.6), the magnetic field sensitivity for N =1 was determined to be 12.8 pT. In Figure 4.6 (b), the voltage noise and output voltage of the ME sensor unit is shown as a function of N in response to H_{ac} = 1 nT. The voltage noise and the output voltage increased with increasing N. Substituting the data of the voltage noise and the output voltage into (4.1), the magnetic field sensitivity was calculated as a function of N as shown in Figure 4.6 (c). The magnetic field sensitivity for N =4 was 5.5 pT at 1 Hz, which is a 2.3× enhancement relative to N =1. This increased sensitivity is a direct consequence of the increase in the ME charge coefficient that results from the ME laminate stacking.

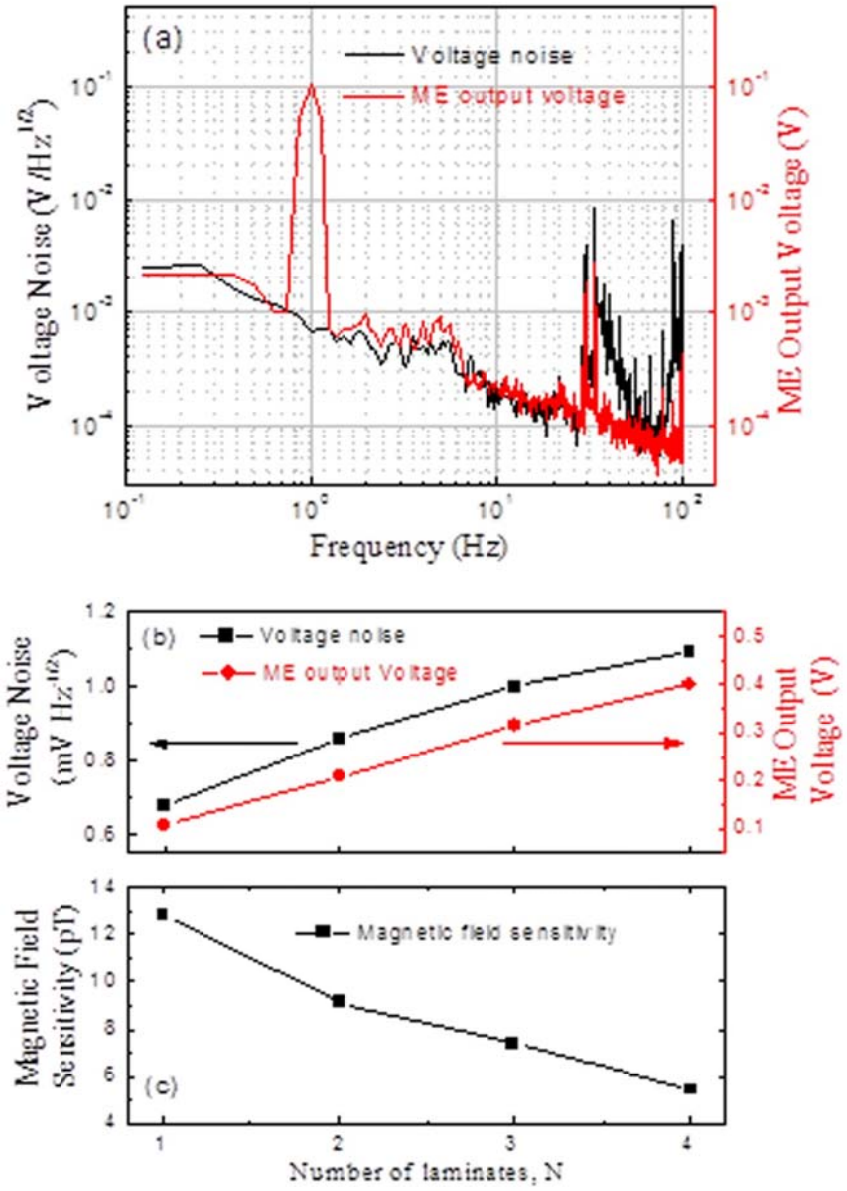

Figure 4.6. (a) ME output signal of the ME sensor unit and background voltage noise in the absence of intentional excitation. (b) Voltage noise and ME output signal, and (c) magnetic field sensitivity of the sensor unit as a function of $\sqrt{N}$. The incident AC magnetic field was 1 nT at 1 Hz.

(Reprinted with permission from Ref. 83, Copyright © 2012 AIP Publishing LLC)

4.4 ME Sensor Arrays

Based on an equivalent circuit model, the SNR of the ME sensor can be estimated as[84]

$$SNR = j\omega\alpha_0 e^{-j\phi} H / n_t; \tag{4.7}$$

where ω is the angular frequency, α_0 is the modulus of α^*_{ME}, ϕ is the phase delay of the signal to H, and H is the magnetic field.

For our ME sensor arrays, N ME sensors were connected in a parallel mode. The signal response of all the ME sensors were harmonic to the applied magnetic field H. Thus, the output signal of the array is

$$I_A = N \cdot j\omega\alpha_0 e^{-j\phi} H . \tag{3.8}$$

However, because the internal noise sources are uncorrelated, using a root-square sum method, the value of the total noise can be estimated as

$$n_{tA} = \sqrt{n_{t1}^2 + n_{t2}^2 \cdots + n_{tN}^2} = \sqrt{N} n_t . \tag{3.9}$$

The SNR of the ME sensor array can then be determined as

$$SNR_A = \sqrt{N} \cdot j\omega\alpha_0 e^{-j\phi} H / n_t . \tag{3.10}$$

By comparing (4.7) and (4.10), one can see that the SNR of the ME sensor array in parallel increases by a factor of $\sqrt{N}$.

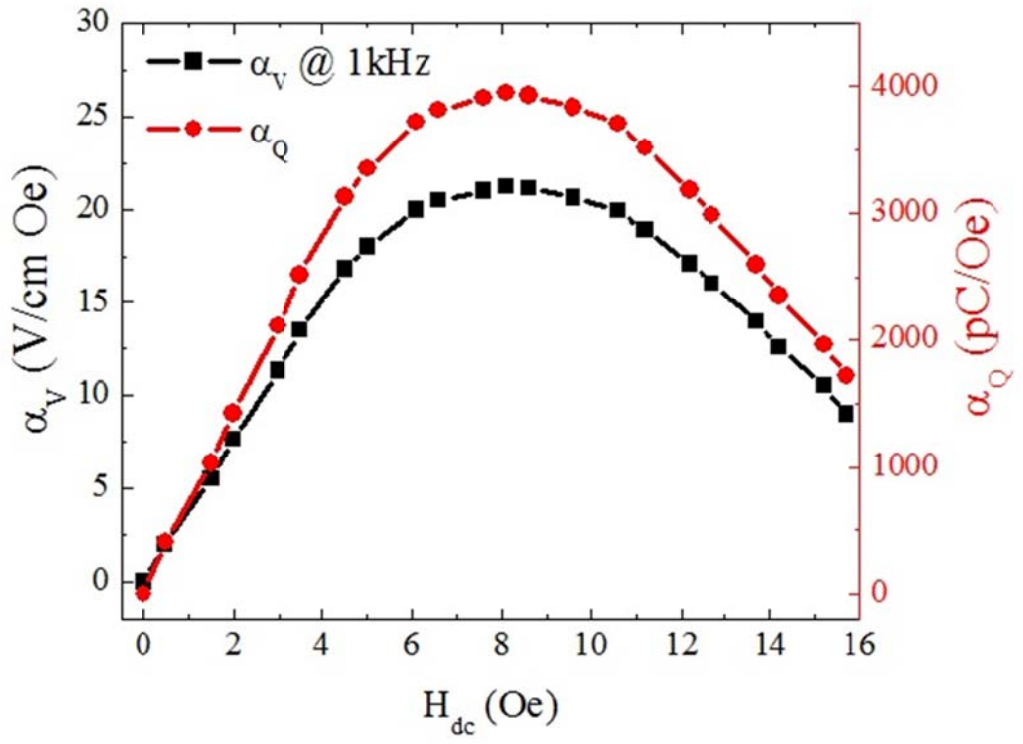

Figure 4.7. ME voltage coefficient (α_V) and ME charge coefficient (α_Q) of Metglas/PZT laminates as a function of DC bias H_{dc} at 1 kHz.

To achieve higher sensitivity, we stacked four laminates in parallel. The value of α_{ME} was measured using a lock-in amplifier (SR-850) in response to a pair of Helmholtz coils driven at an AC magnetic field of H_{ac} = 0.1 Oe and at a frequency of f = 1 kHz. Figure 4.7 shows the ME voltage coefficient α_V and ME charge coefficient α_Q as a function of H_{dc} for a configuration were the four Metglas/PZT laminates stacked in parallel mode. The maximum value of α_V was 22 V/cm·Oe under a DC bias of 8.6 G; correspondingly, the maximum value of α_Q was 3950 pC/Oe.

The laminates were then packaged with a simple low-noise charge amplifier having a gain of 5.1 V pC^{-1} over the frequency range of $0.1 < f < 100$Hz (designed by SAIC), which we designated as a ME sensor unit. The unit was placed inside a high-mu-metal magnetic shielding chamber, and connected to a dynamic signal analyzer to measure the noise voltage and output signal. Figure 4.8 shows the measured and estimated charge noise density spectra for one ME sensor unit. The noise densities were estimated based on Equation (4.4), using appropriate ME laminate parameters. The estimated and measured charge density noises exhibited good agreement, except at frequencies near external vibrational sources.

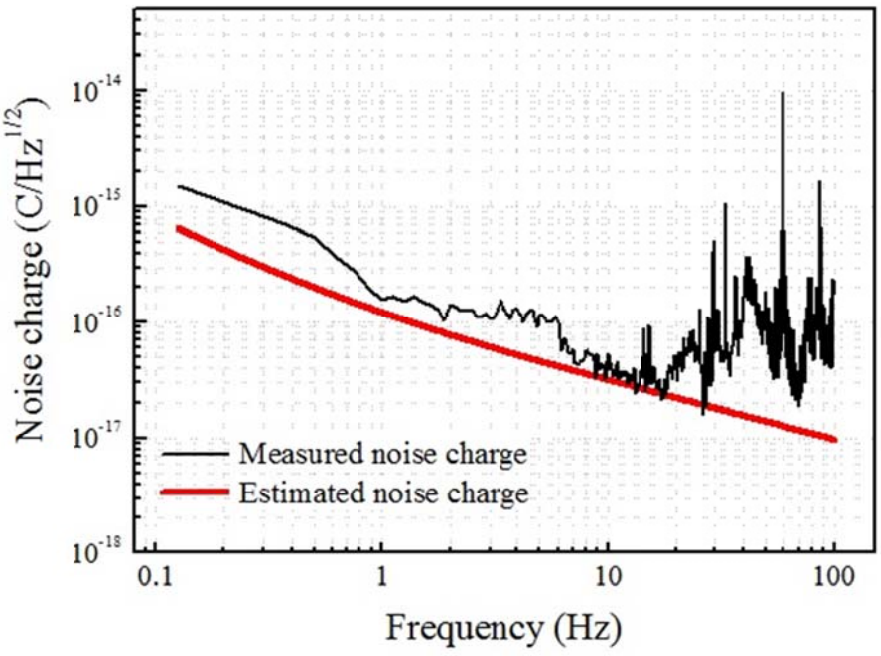

Figure 4.8. Measured and estimated charge noise densities of one ME sensor unit, over the frequency range of $0.125 < f < 100$ Hz.

In total, we fabricated four ME sensor units to construct the ME sensor array. The four units were placed in a square holder inside the shielding chamber. The distance between the centers of two units was 8 cm. A coil was placed in the center line 40 cm away from the center of the sensor unit arrays, so that the magnetic field applied was homogenous to each unit. Figure 4.9 shows the equivalent magnetic noise spectra for these four ME sensor units. Over the frequency range of $0.125 < f < 100$ Hz, the noise floors can be seen to be nearly equivalent for the various units. An extremely low noise floor of 7 pT/Hz$^{1/2}$ was identified at 1 Hz.

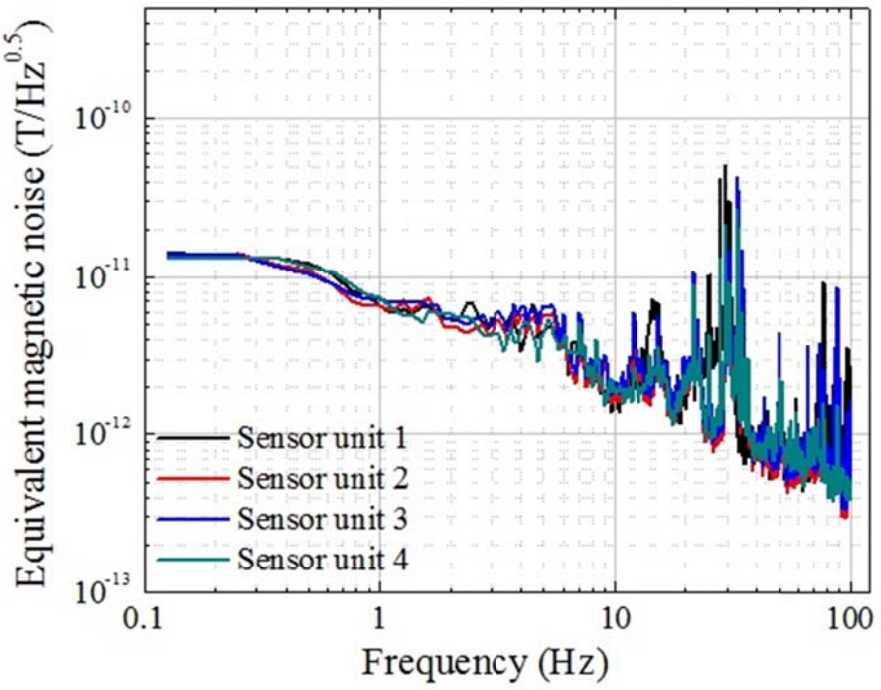

Figure 4.9. Equivalent magnetic noise spectra for four ME sensor units over the frequency range of $0.125 < f < 100$ Hz.

Figure 4.10 (a) shows the output signals of each ME sensor unit in response to a 1 nT incident AC magnetic field at 1Hz. Figure 4.10 (b) shows the voltage noise spectra of single ME sensor unit over the frequency range of $0.125 < f < 100$ Hz. The output voltages of one ME sensor unit were 0.24 V, and the background voltage noise at the corresponding frequency was 1.36×10^{-3} V/Hz$^{1/2}$. From Equation (4.1), the magnetic field sensitivity of each ME sensor unit was estimated as 11.3 pT. The voltage noise of the array was then calculated based on Equation (4.9), and is shown in Figure 4.10(b). From Equations (4.7) to (4.10), the magnetic field sensitivity of the four ME sensor unit array can be calculated to be 5.7 pT, which presents a 2× enhancement in the magnetic field sensitivity for the ME sensor unit arrays.

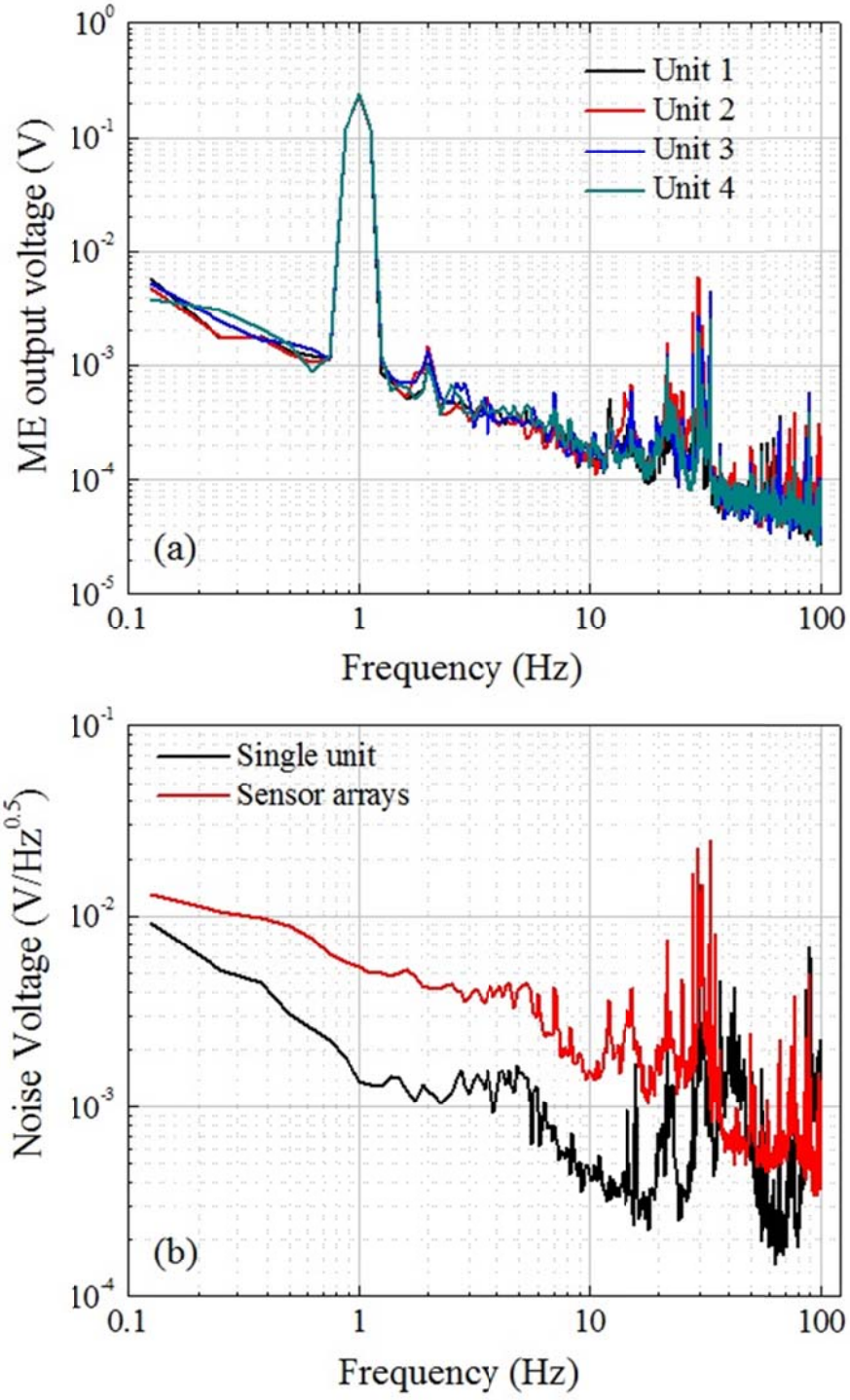

Figure 4.10. (a) ME output signal of four ME sensor units. The incident AC magnetic field was 1 nT at 1 Hz. (b) Background voltage noise of single unit and calculated noise of the sensor arrays.

4.5 Section Summary

An optimization of the distance between a pair of Metglas-PZT-Metglas ME laminates has been performed to achieve enhanced values of α_{ME}. Units of two laminates displayed relatively high magnetic field sensitivities of 14.2 pT when the distance between the laminates was > 40 mm. Our findings demonstrate the effect of geometrical arrangement of sensor pairs in arrays. Mutual inductions can have important effects. To achieve sensor units that feature the highest gain and sensitivity, these considerations should be taken into account.

The charge and equivalent magnetic noises of stacked ME laminate sensors have been investigated. Predicted and experimental data confirmed that the equivalent magnetic noise decreased and the magnetic field sensitivity both increased by a factor of $\sqrt{N}$. For $N = 4$, the ME sensor had a 2.1× lower equivalent magnetic noise and a 2.3× higher magnetic field sensitivity than for a single laminate.

The importance of ME sensor arrays has been confirmed with respect to an increase in SNR. Arrays of four Metglas/PZT sensor units were constructed. The magnetic field sensitivity of the arrays showed double the enhancement in comparison to an individual unit. This result confirmed predicted ones that array configurations of ME sensors are capable of increasing sensitivity. These findings reinforced the potential of ME laminate arrays as low-noise, extremely sensitive magnetic field sensors.

CHAPTER 5.

ME EFFECT AT ZERO BIAS FIELD

5.1 Introduction

A magnetoelectric composite is comprised of both magnetostrictive and piezoelectric materials. The magnetoelectric effect is produced by the combined effect of piezomagnetism and the piezoelectricity of the corresponding phases and their coupling. The strength of a magnetoelectric composite is determined by the piezoelectric (d_p) and piezomagnetic (d_m) coefficients. To achieve the highest value of α_{ME}, all previously reported ME laminated composites operated in a passive mode have required a magnetic bias field in order to maximize the value of d_m. In sensor applications, the need for an external magnetic bias presents some significant disadvantages, such as limiting the spatial resolution, increasing the required volume, and adding a potential noise source (among others).

To overcome the limitations associated with an external magnetic bias field, ME laminates with an internal magnetic bias are becoming increasingly important. For example, it has recently been reported that an epitaxial thin layer ME composite with an additional exchange bias layer is able to produce significant ME effects at zero magnetic bias.[44] However, such thin layer ME heterostructures are difficult to fabricate and are potentially costly compared to laminated ones. Magnetization-graded ME composites have also shown non-zero α_{ME} values under zero magnetic bias, but these values were small.[45,85]

First, this chapter describes my investigation of the ME effect in Metglas/Ni/PZT trilayer laminates in a working mode of (L-L) multi-push-pull. Second, annealed Metglas layers, which are harder magnetic layers compared to amorphous Metglas layers, were bonded to Metglas/PZT laminates. The internal bias between annealed Metglas and amorphous Metglas results in a large ME coefficient at a zero bias field. Third, I investigated the mutual effect between self-biased ME laminates via finite element simulations and experiments. Results showed that smaller stack size of four self-biased ME laminates can be achieved.

5.2 Metglas/Ni/PZT Laminates

Zero-bias ME coupling has been observed in PZT and Ni/Metglas magnetization-graded trilayer laminate.[45] Figure 5.1(a) shows the schematic of this ME laminate. The bias magnetic field H_{dc} and the AC magnetic field H_{ac} are parallel to the x axis. The piezoelectric layer is pole along z and the ac electric field E_3 is measured across PZT layer. The operation mode of this laminate is (L-T) mode. The largest value of α_{ME} was reported to be 1.6 V/cm·Oe at zero bias field. The reason is that a torque is induced by the interaction between the in-plane ac field H_{ac} and a transverse grading-induced magnetization. The torque produces a bending moment in the Metglas layers. Therefore, a value of α_{ME} could be observed at the zero bias field.

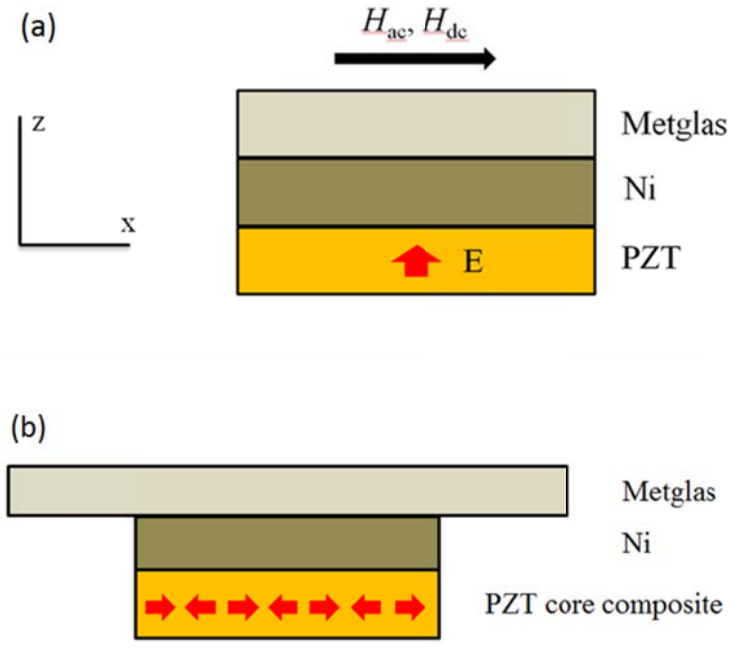

Figure 5.1. Schematic of Metglas/Ni/PZT laminate (a) L-T mode and (b) (L-L) multi-push-pull mode.

In Figure 5.1(a), the piezoelectric effect in PZT layer uses the piezoelectric coefficient d_{31}, which is about 40% of d_{33}. I fabricated a Metglas/Ni/PZT laminate in a (L-L) multi-push-pull configuration, which almost fully uses d_{33} in PZT layer, as shown in Figure 5.1(b). Ni layer was bonded between 3 layers of Metglas and PZT core composite. The value of α_{ME} was then measured using a lock-in amplifier (SR-850) in response to a pair of Helmholtz coils driven at an AC magnetic field of H_{ac} = 0.1 Oe at a frequency of f = 1 kHz. A DC magnetic field was applied by a large electromagnet. Figure 5.2 shows the value of α_{ME} as a function of H_{dc}. Due to a higher piezoelectric properties in this ME laminate, the value of α_{ME} was 6.3 V/cm·Oe at zero bias field, which is about 4 times larger than previously reported ones.

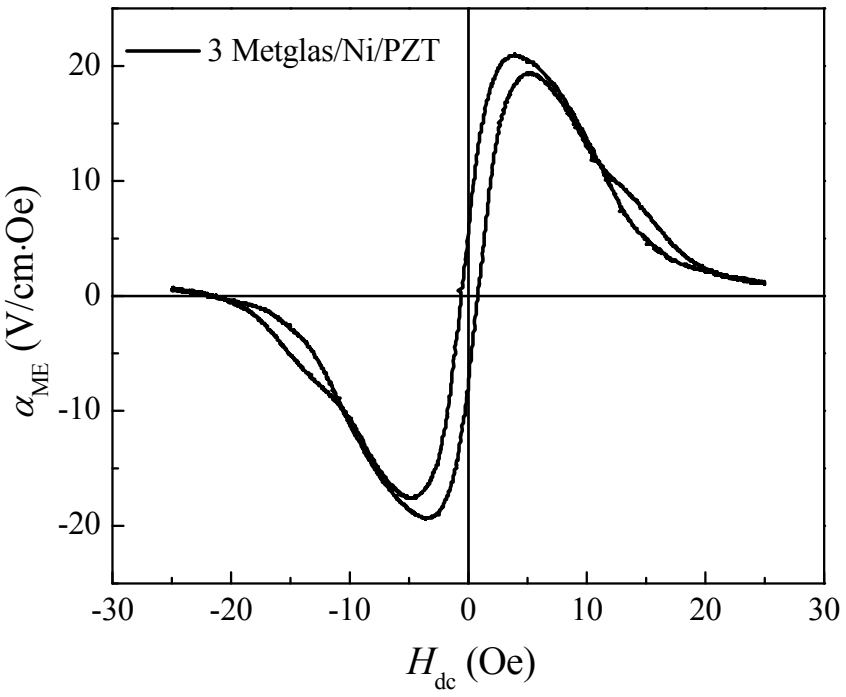

Figure 5.2. Value of α_{ME} as a function of H_{dc} at 1 kHz.

The laminates were then packaged with a low-noise charge amplifier having a gain of 5.1 V pC^{-1} over the frequency range of $0.1 < f < 100$Hz: which we designate as a ME sensor unit. The unit was placed inside a high-mu-metal magnetic shielded chamber, and connected to a dynamic signal analyzer to measure the voltage noise and output signal. Figure 5.3(a) shows a voltage noise spectrum over the frequency range of $0.3 < f < 100$ Hz. and the background voltage noise at the corresponding frequency was 1.0×10^{-3} $V/Hz^{1/2}$. Figure 5.3(b) shows the output signals in response to a 10 nT incident AC magnetic field at 1Hz for both Metglas/Ni/PZT laminate and Metglas/PZT/Metglas laminate. The output of the sensors with Metglas/Ni/PZT laminate was 0.057 V, which is much higher that of the sensors with Metglas/PZT/Metglas laminate. The magnetic field sensitivity of this self-biased sensor was 175 $pT/Hz^{1/2}$ at 1 Hz without external bias field.

Compared to ME sensor with bias magnets, the sensitivity of this self-biased sensor is not high, which is due to the ME effect at zero bias field is not strong enough. The value of α_{ME} at 0 Oe is only 30% of that at an optimum bias field. Moreover, the α_{ME}-H_{dc} curves show obvious hysteresis. This is not benefit for magnetic field measurement. Thus, to get a good ME magnetic sensor with high sensitivity, the ME coefficient at zero bias field needs to be further enhanced; and also a α_{ME}-H_{dc} with little hysteresis is needed.

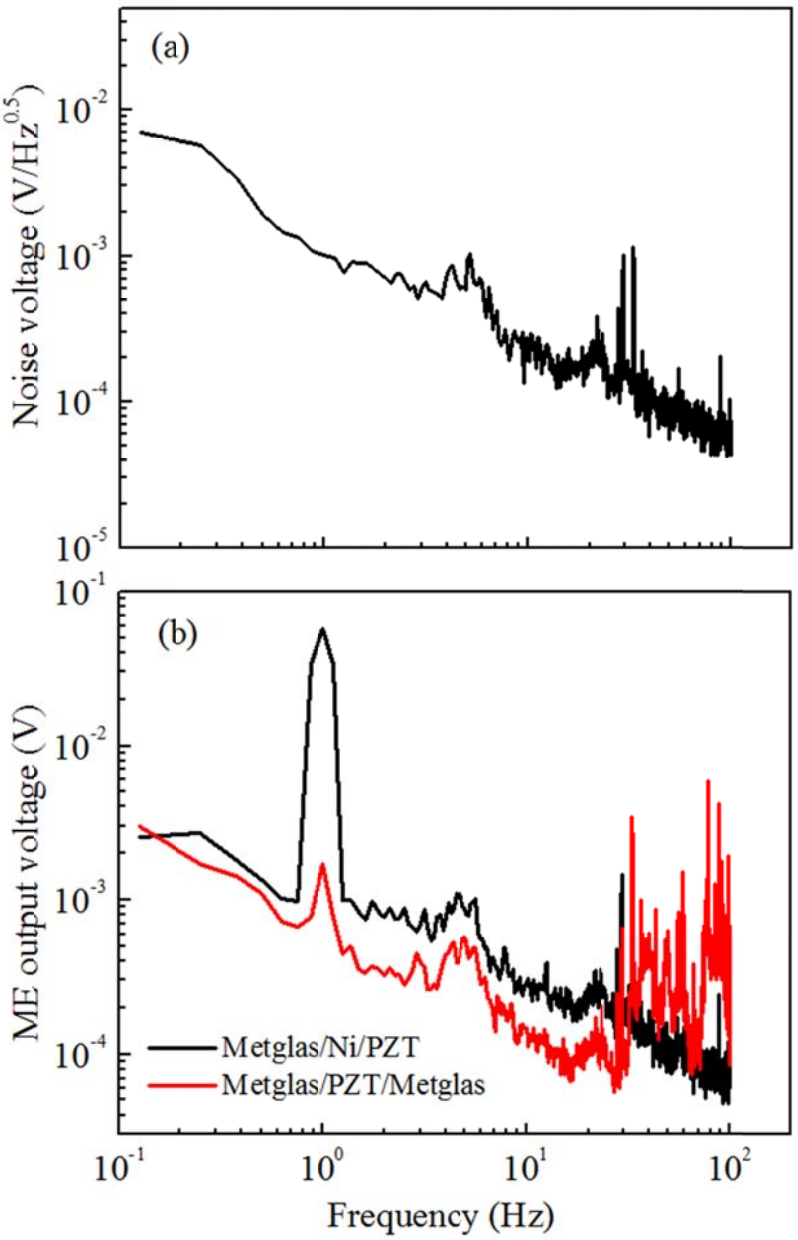

Figure 5.3. (a) The background voltage noise in the absence of intentional excitation for both Metglas/Ni/PZT laminate; and (b) the output signal for both Metglas/Ni/PZT laminate and Metglas/PZT/Metglas laminate over the frequency range of $0.3 < f < 100$ Hz.

5.3 Annealing Metglas Induced Internal Bias Field

Metglas foils (Vitrovac 7600F, Hanau, German) of dimensions 40 mm× 5 mm were annealed at 600 ℃ for 4 hours in air. Figure 5.4 shows X-ray diffraction (XRD) line scans for amorphous and annealed Metglas. No obvious peaks were observed for the amorphous Metglas. However, after annealing, there were intense peaks for α-Fe and hcp-Co near 2θ = 44°, indicating that the amorphous Metglas had partially crystallized. In addition, less intense peaks were apparent for the iron oxide phases (Fe_3O_4 and Fe_2O_3) at 2θ = 34° and 51°, indicating that the surface of the Metglas foil had oxidized. These crystalline and oxidized phases have "harder" magnetic properties than amorphous Metglas.[86,87] After being magnetized by a dc magnetic bias, these crystalline and oxidized phases can induce a unidirectional magnetic anisotropy in adjacent amorphous Metglas layers. [88,89]

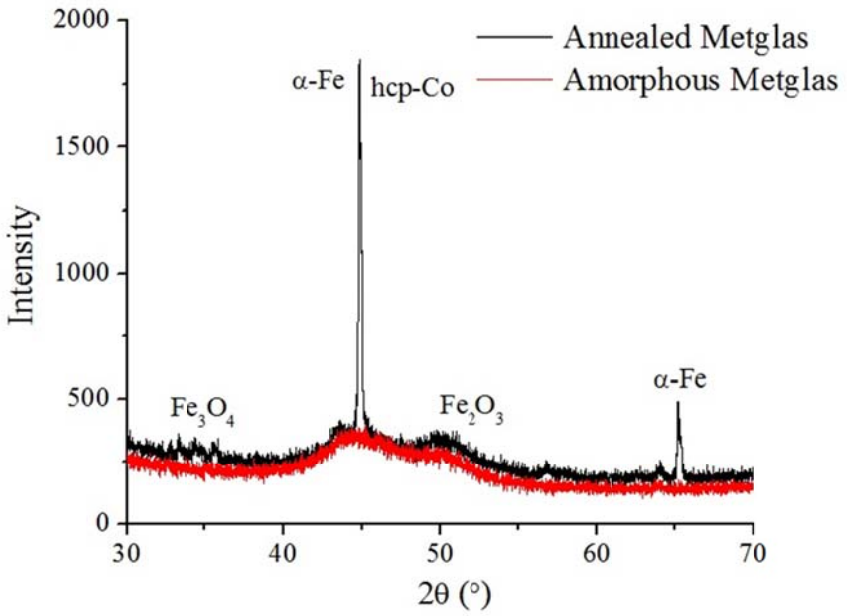

Figure 5.4. XRD line scan of amorphous and annealed Metglas foils.

Two layers of Metglas and two layers of annealed Metglas both of dimensions 40 mm× 5 mm were then epoxied together. After premagnetizing with a bias of H_{dc} = +2 kOe, the *M-H* hysteresis loops were measured by a vibrating sample magnetometer (VSM). A high-field *M-H* loop is given in Figure 5.5 (a). The data in this figure can be seen to consist of two sections: (i) a narrow low-field magnetization process for the "soft" magnetic phase of the amorphous Metglas, and (ii) a wider one for the "hard" annealed Metglas. The low-field *M-H* loop is given in Figure 5.5 (b), where "soft" magnetic characteristics with a low coercive field can be seen. There was an obvious shift of the *M-H* loop to positive fields, with a built-in bias of H_b = 2.7 Oe. Such a shift in the *M-H* curve has been shown to be mainly due to magnetic interactions between "soft" and "hard" phases.[90] Accordingly, premagnetizing the annealed Metglas layers creates an internal antiparallel magnetic field in the "soft" amorphous Metglas layers with respect to the "hard" ones, resulting in a 2.7 Oe shift of the *M-H* loops. These results indicate that an annealed and normal Metglas bilayer structure could be used in ME laminates, yielding a non-zero value of α_{ME} under H_{dc} = 0.

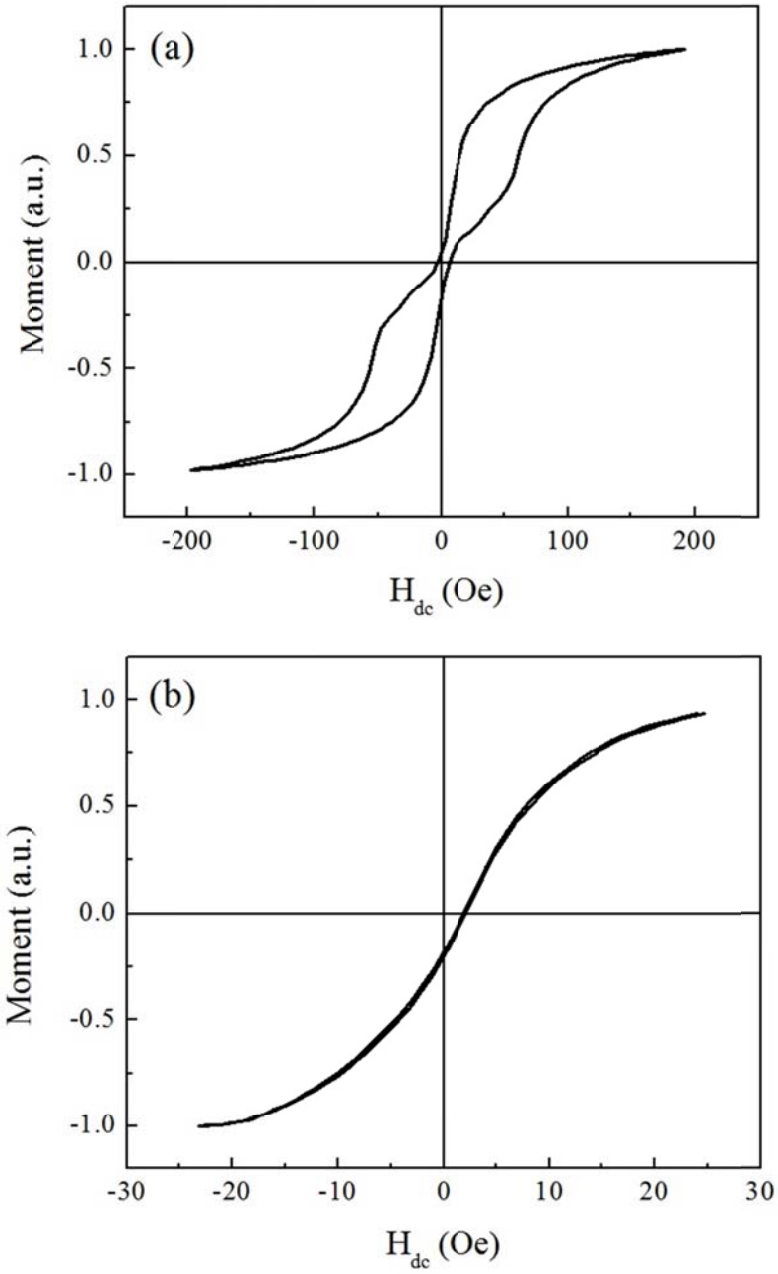

Figure 5.5. (a) High-field and (b) low-field *M-H* hysteresis loops by VSM for two layers of Metglas and two layers of annealed Metglas epoxied together.

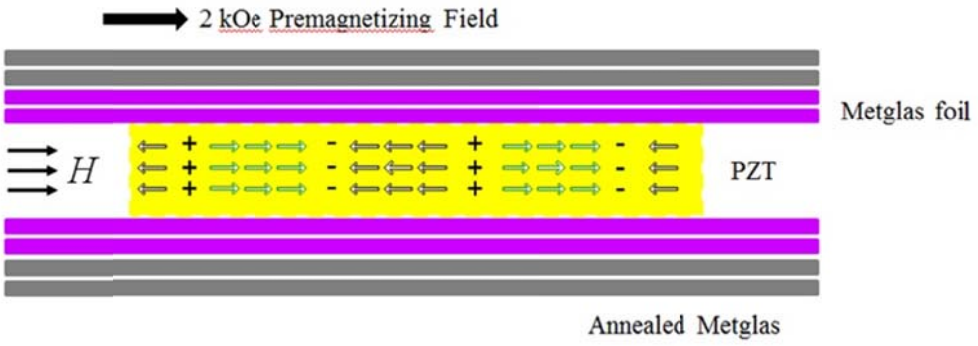

Figure 5.6. Schematic of Metglas/PZT/Metglas laminate consisting of annealed Metglas.

Next, several Metglas/PZT/Metglas multi-push-pull L-L mode laminates were made. A 40 mm × 10 mm PZT bundle served as the core, which consisted of five 40 mm × 2 mm PZT-5A fibers (Smart Materials, Sarasota, FL) oriented along the length direction of the laminates. Two interdigitated (ID) Kapton electrodes were bonded to the top and bottom surfaces of the piezoelectric bundle with epoxy resin (Stycast 1264, USA). The width and the separation of the electrodes were chosen to be 0.15mm and 1 mm, respectively. Two layers of Metglas of dimensions 80 mm× 10 mm were then laminated to both the top and bottom surfaces of the ID electrode/PZT core composites. Two layers of annealed Metglas also of dimensions 80 mm× 10 mm were then laminated to both surfaces. A schematic of this Metglas/PZT/Metglas laminate using annealed Metglas foils is shown in Figure 5.6.

The value of α_{ME} was then measured using a lock-in amplifier (SR-850) in response to a pair of Helmholtz coils driven at an AC magnetic field of H_{ac} = 0.1 Oe at a frequency of f = 1 kHz. A DC magnetic field was applied by a large electromagnet. Figure 5.7(a) shows the values of α_{ME} as a function of H_{dc} for Metglas/PZT/Metglas

laminates with and without annealed Metglas foils. For Metglas/PZT/Metglas laminates without annealed Metglas, the values of α_{ME} were 0 V/cm·Oe at zero magnetic bias and 20 V/cm·Oe under an optimum bias field of 7.5 Oe. For Metglas/PZT/Metglas laminates with annealed Metglas, the curve of α_{ME} - H_{dc} response was shifted, resulting in a value of α_{ME} = 12 V/cm·Oe at zero magnetic bias. Figure 5.7 (b) shows the values of α_{ME} as a function of frequency f under H_{dc} = 0. The maximum value of α_{ME} was 373 V/cm·Oe at an electromechanical resonance (EMR) frequency of 33.7 kHz. Such giant values of α_{ME} for H_{dc} = 0 are much higher than those previously reported for other composites under zero bias, both at low and EMR frequencies.

Please note that the peak value of α_{ME} was suppressed to 15 V/cm·Oe, which was a 25% reduction compared to Metglas/PZT/Metglas laminates without annealed Metglas. The reason for the reduction in the maximum value of α_{ME} was that the annealed Metglas layers had a lower magnetostriction. A further increase in the layers of annealed Metglas increased the built-in internal bias H_b, while reducing the values of α_{ME} both at peak position and under zero magnetic bias, as shown in Figure 5.8.

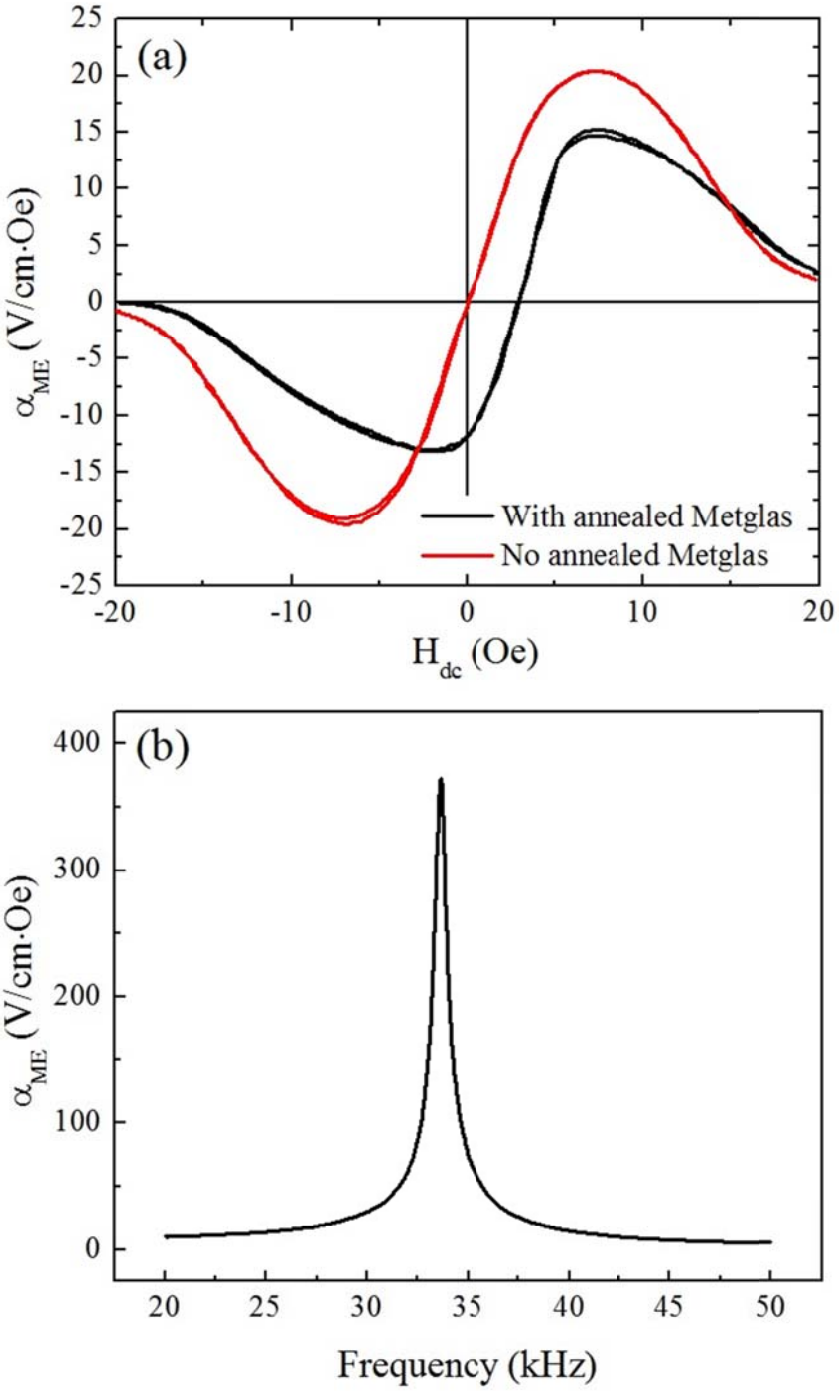

Figure 5.7. (a) Value of α_{ME} as a function of H_{dc} at 1 kHz. (b) Value of α_{ME} as a function of frequency with an AC magnetic field of 0.1 Oe.

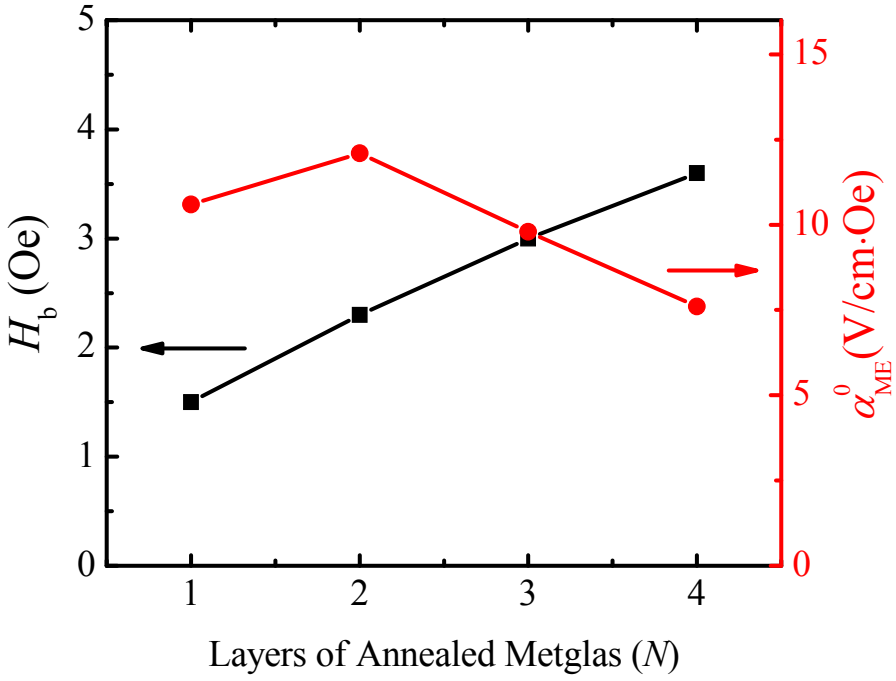

Figure 5.8. Value of internal bias field H_b and ME coefficient α^0_{ME} at zero bias field for various layers of annealed Metglas.

The laminates were then packaged with a low-noise charge amplifier having a gain of 5.1 V pC^{-1} over the frequency range of $0.1 < f < 100$Hz: which we designate as a ME sensor unit. The unit was placed inside a high-mu-metal magnetic shielded chamber, and connected to a dynamic signal analyzer to measure the voltage noise and output signal. Figure 5.9 shows a voltage noise spectrum over the frequency range of $0.3 < f <$ 100 Hz, which also contained an output signal in response to a 10 nT incident AC magnetic field at 1Hz. The output of the sensors was 0.27 V, and the background voltage noise at the corresponding frequency was 8.2×10^{-4} V/$Hz^{0.5}$. Thus, the magnetic field

sensitivity of this self-biased sensor was 30 pT/Hz$^{0.5}$ at 1 Hz without external bias field. This is in comparison to about 20 pT/Hz$^{0.5}$ at 1 Hz for ME sensors without annealed Metglas, as previously reported.

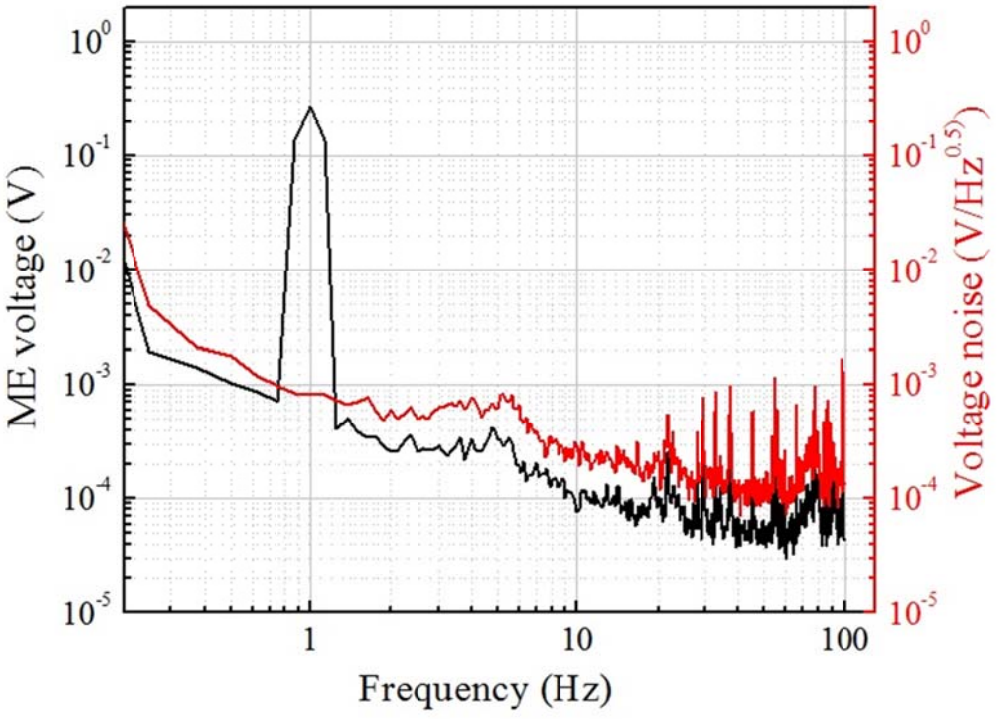

Figure 5.9. The output signal of a ME sensor unit containing annealed Metglas foils, and the background voltage noise in the absence of intentional excitation.

5.4 Self-biased ME Laminate Stacks and Arrays

In self-biased ME laminates, the magnets used to supply the DC bias field are not needed. This absence translates to an important advantage—namely, that in sensor stacks and arrays, the volume of the total sensor unit could be reduced. Additionally, the mutual effect from neighboring sensors could also be decreased. For this research phase I conducted a finite element simulation of the magnetic field strength of self-biased ME laminates, after which I compared those results to magnet-biased laminates. Subsequently, I measured the ME coefficient and noise floors of self-biased ME laminates arrays.

5.4.1 Finite element modeling

The finite element simulation was conducting using a Comsol 4.3. As shown in Figure 5.10, the magnetic field was calculated in a large air cylinder with a height of 150 mm and a radius of 60 mm. A background field of 0.1 Oe was applied along the *y*-axis in this cylinder. Metglas layers, each with a dimension of 80 mm × 10 mm × 0.12 mm (6 layers), were placed in the center of the cylinder. The relative permeability of the Metglas was 80,000, and the BH curve corresponds to the results of VSM measurements. For the magnet-biased ME laminate, the magnets were placed 10 mm away from the both ends of the Metglas layers, which is the same distance as when it is packaged as sensor unit. For the self-biased ME laminate, another two hard ferromagnetic layers were built on the top and bottom of the Metglas layers. The remnant magnetic flux density of these hard layers was set to 1 T, according to the VSM results in Section 5.3.

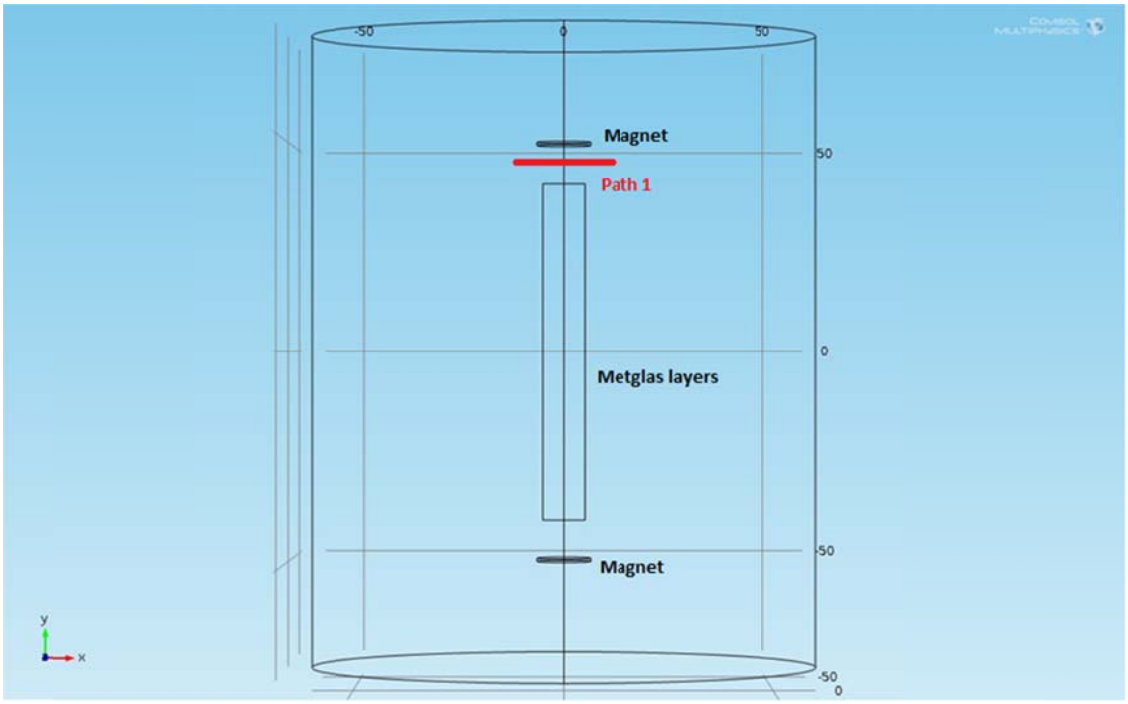

Figure 5.10. Finite element modeling of magnet-biased ME laminates by Comsol 4.3.

The distribution of the magnetic flux density is shown in Figure 5.11. With biased magnets, the maximum magnetic flux density averages about 780 mT in the center area of the Metglas foil. This result agrees well with previous studies.[39] Figure 5.11 (b) illustrates the simulated magnetic flux density of an ME laminate without magnets, while (c) indicates the self-biased result. As shown in this figure, in the absence of bias magnets, the magnetic flux density induced by the background field was smaller than 10 mT in the Metglas layers. In the presence of two hard ferromagnetic layers to apply the biased field, the magnetic flux density was about 700 mT. This value is quite close to that of magnet-biased ME laminates. Also important to note is that the flux density was homogenous along the cross section of Metglas layers. This is mainly due to long range ferromagnetic coupling at the hard/soft magnetic interface.[90]

This study also compared the flux density around the three different types of ME laminates. The B fields along path 1 in Figure 5.10 are compared, as shown in Figure 5.12. In the absence of biased magnets at both ends of the ME laminate, the B field increased slightly to 2×10^{-2} mT in the center range due to the presence of high-μ Metglas layers in the background field of 10^{-2} mT. For the self-biased ME laminate, the B field was about 3×10^{-2} mT in the center range, and 1.7×10^{-2} mT at the edge. The hard ferromagnetic layer on the surface of the Metglas changed the B field by a factor of ×1.5-1.7. However, the B field dramatically increased to 34.0 mT in the center range in the presence of biased magnets. An enhancement in the B field by a factor of >1000 can be expected for a magnet-biased ME laminate, compared to a self-biased one. In sensor arrays, a sensor based on a magnet-biased ME laminate will show significantly higher mutual effect to neighboring sensors than that based on a self-biased one.

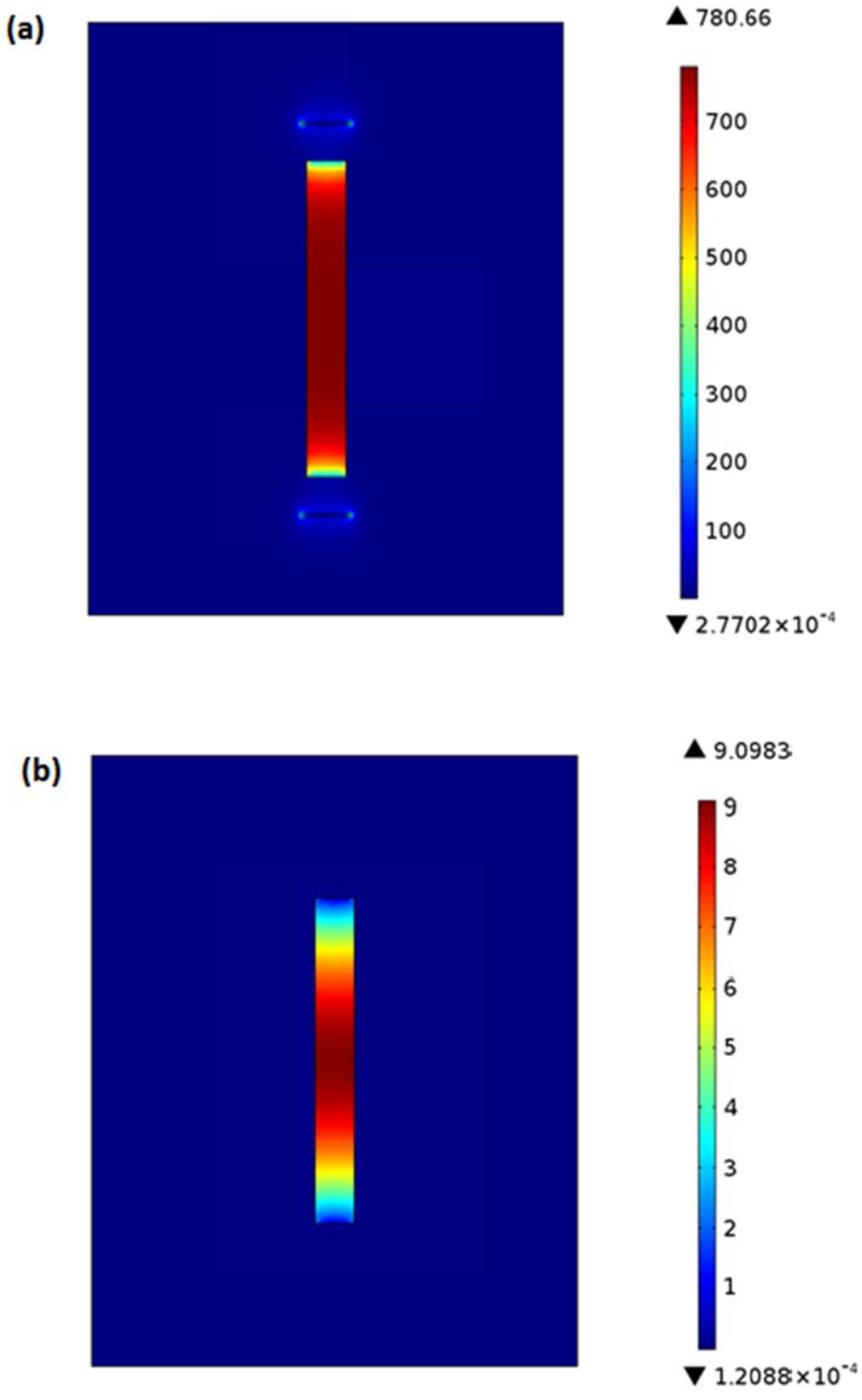
(a)
▲ 780.66
700
600
500
400
300
200
100
▼ 2.7702×10⁻⁴
(b)
▲ 9.0983
9
8
7
6
5
4
3
2
1
▼ 1.2088×10⁻⁴

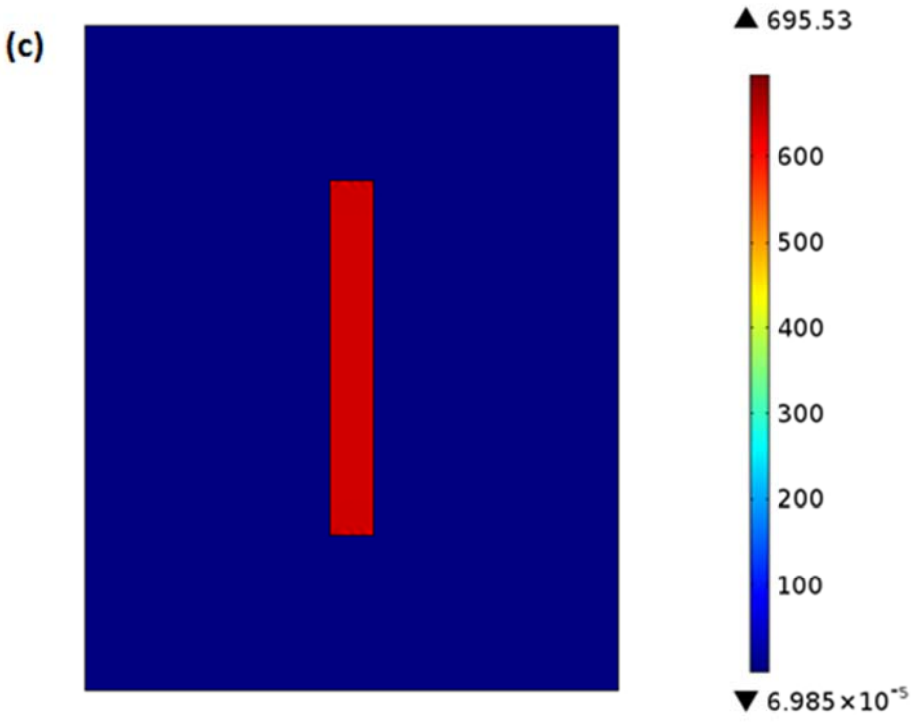

Figure 5.11. Simulated magnetic flux density of (a) ME laminate with biased magnets, (b) ME laminate without biased magnets, and (c) self-biased ME laminate. The unit of the scale bar is mT. The cross plane is the center of the plane of Metglas layers along *x*-*y* plane.

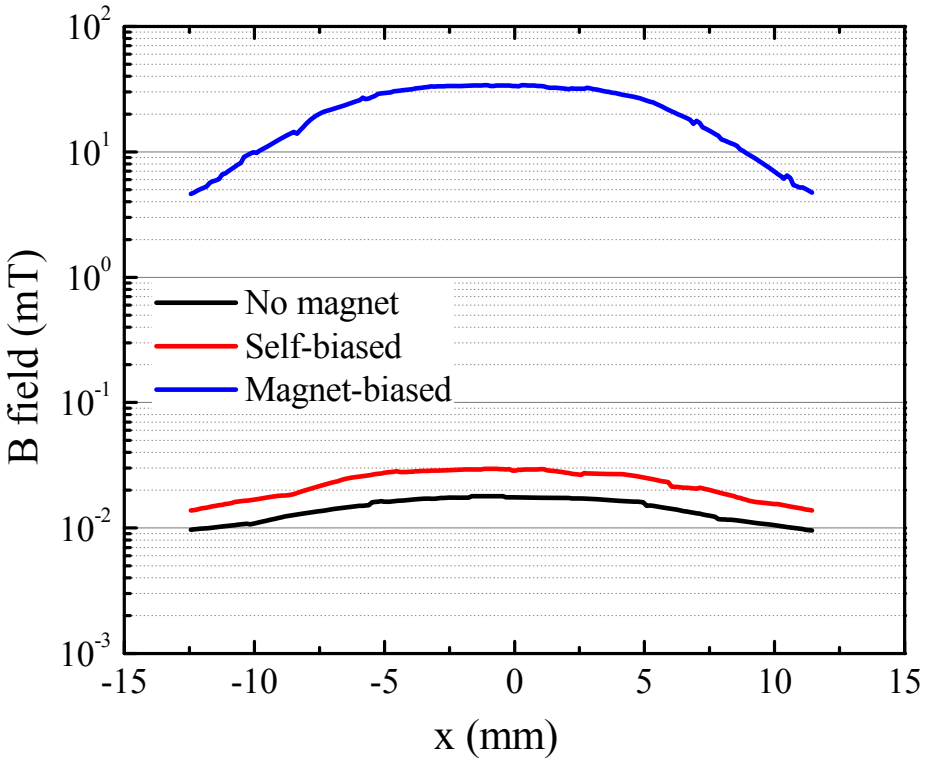

Figure 5.12. Magnetic flux density along Path 1 in Figure 5.10 for three types of ME laminates.

5.4.2 Experimental results

A pair of Metglas/PZT laminates were placed in a large Helmholtz coil (H-coil) at various distances d. One laminate was fixed in the center of the H-coil, and another was placed on top of it. I then measured the value of the ME voltage coefficient α_{ME} for the laminate fixed in the center in response to an AC magnetic field of H_{ac} = 0.1 Oe at a frequency of f = 1 kHz. Figure 5.13 shows the schematic of a pair of magnet-biased ME

laminates separated by a distance *d*. The DC bias field applied by the magnets was about 6 Oe, where the laminate had the maximum value of α_{ME}. For self-biased ME laminates, no magnets were used when obtaining measurements.

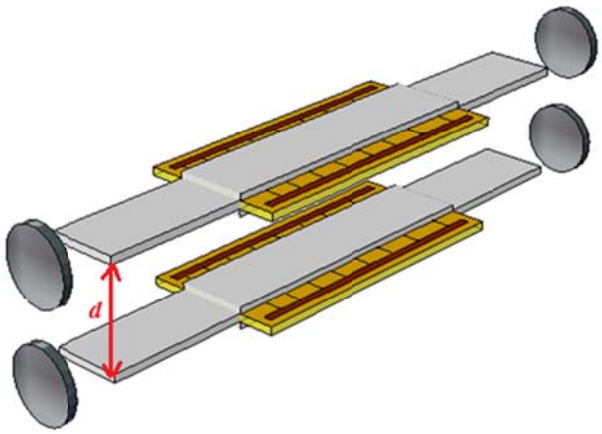

Figure 5.13. Schematic of a pair of magnet-biased ME laminates separated by a distance d. The value of αME for the bottom laminate is measured.

Figure 5.14 shows the ratio of $\alpha_{ME} / \alpha_{ME}^{\max}$ for self-biased and magnet-biased ME laminates, where *d* varied from 2.5 mm to 55 mm, and where $\alpha_{ME}^{\max}$ was the value of α_{ME} when there was no neighboring laminate (d→∞). When *d* was larger than 40 mm, the ratio of $\alpha_{ME} / \alpha_{ME}^{\max}$ was close to 100%, which means that the mutual effect between the two laminates was small. When *d* was smaller, meaning that the distance between the two laminates was smaller, the ratio of $\alpha_{ME} / \alpha_{ME}^{\max}$ decreased for both types of ME laminates. Moreover, it was clear that the ratio decreased more rapidly for the magnet-biased ME laminate in comparison to the self-biased one. When *d* = 2.5 mm, the ratio of $\alpha_{ME} / \alpha_{ME}^{\max}$

for magnet-biased ME laminate was 45.6%, which was much lower in comparison to results for the self-biased one (76.0%). This finding shows that biased magnets could affect the DC field of the neighboring laminate, leading to a reduction in the α_{ME} value by > 50%.

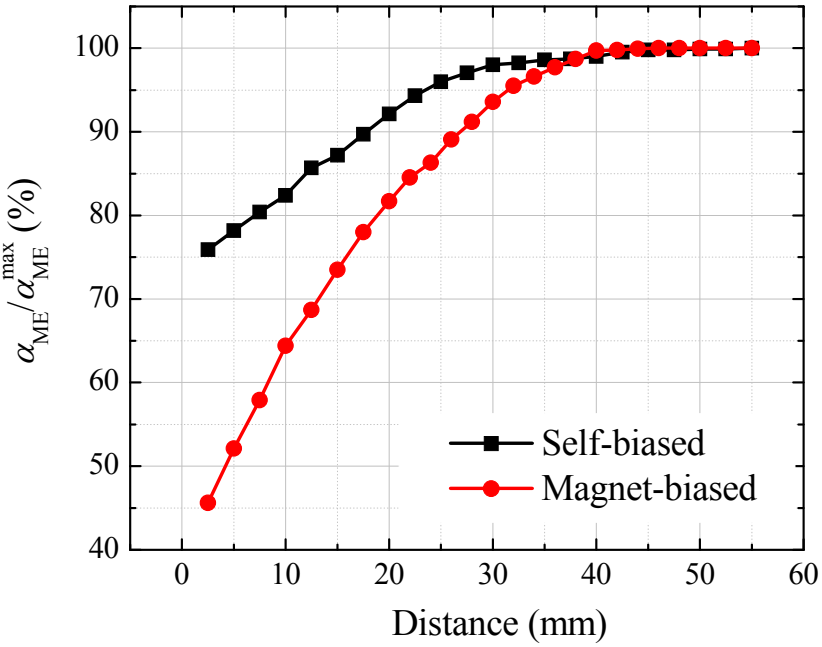

Figure 5.14. Ratio of $\alpha_{ME} / \alpha_{ME}^{max}$ for self-biased and magnet-biased Metglas/PZT laminates with various distance *d*.

I then measured the voltage noise floor of one ME laminate when another laminate with a different *d* was placed next to it. For both self-biased and magnet-biased laminates, the voltage noise was mainly determined by the dielectric loss noise and DC leakage resistant noise. The neighboring laminate did not introduce any additional noise.

Thus, the voltage noise level remained the same even when d was varied. Due to a change in the transfer function of the ME laminate, the equivalent magnetic noise will change. Figure 5.15 shows the equivalent magnetic noise at 1 Hz of self-biased and magnet-biased Metglas/PZT laminates with various d. When $d > 25$ mm, the equivalent magnetic noise of the magnet-biased ME laminate was lower in comparison to the self-biased one. This finding is associated with the higher value of $\alpha_{ME}^{\max}$, which leads to a higher transfer function. In contrast, when $d < 25$ mm, the self-biased ME laminate showed lower noise levels. For example, when $d = 2.5$mm, the noise level of the self-biased ME laminate was 32.5 pT/Hz$^{0.5}$, which was only 68.6% of the analogous magnet-biased result (47.4 pT/Hz$^{0.5}$). The self-biased ME laminate has an important advantage: when such laminates are placed very close (< 25 mm), the value of α_{ME} does not decrease much, and the noise level remains low. Therefore, when assembling an ME laminate array, there could be a significant volume savings in terms of the total size of the sensor unit.

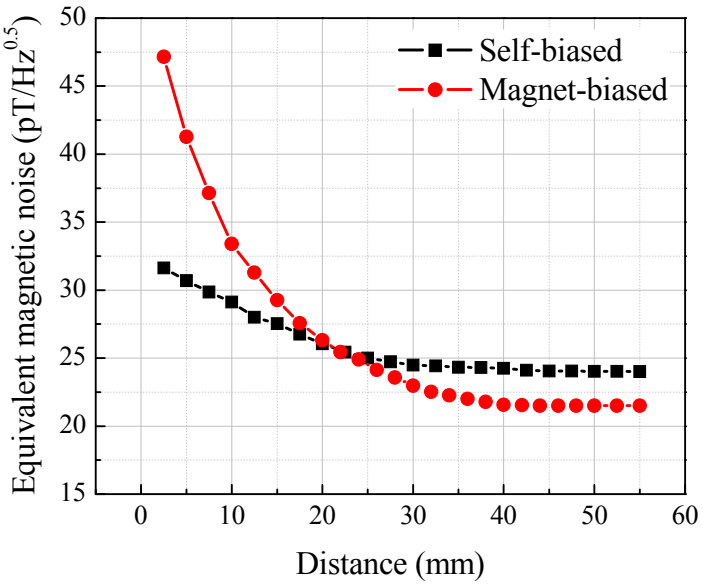

Figure 5.15. Equivalent magnetic noise at 1 Hz of self-biased and magnet-biased Metglas/PZT laminates with various distance *d*.

As reported in Chapter 4, I determined that stacking four ME laminates enhanced the ME charge coefficient α_Q by a factor of ×4, and correspondingly, decreased the equivalent magnetic noise by 50%. Due to the mutual effect from neighboring laminates, the four laminates were packaged into a square tube with a side-length of 4.5 cm, as shown in Figure 5.16 (a). Ideally, the value of ME charge coefficient for the stacking $\alpha_{Q,s}$ should be $\alpha_{Q,s}$ = 400%×α_Q. In this type of square structure, the actual value of $\alpha_{Q,s}$ was about 380%×α_Q. If the side-length of the square were smaller, the value of $\alpha_{Q,s}$ would decrease. By using self-biased ME laminates, the side-length of the square unit could be reduced to 2.5 cm, while the value of $\alpha_{Q,s}$ could remain at approximately 380%×α_Q. This reduces the area of the cross section of the sensor unit from 20.3 cm^2 to 6.25 cm^2, by

69.2%. In sensor arrays based on self-biased ME laminates, the space resolution could be enhanced when drawing the magnetic images.

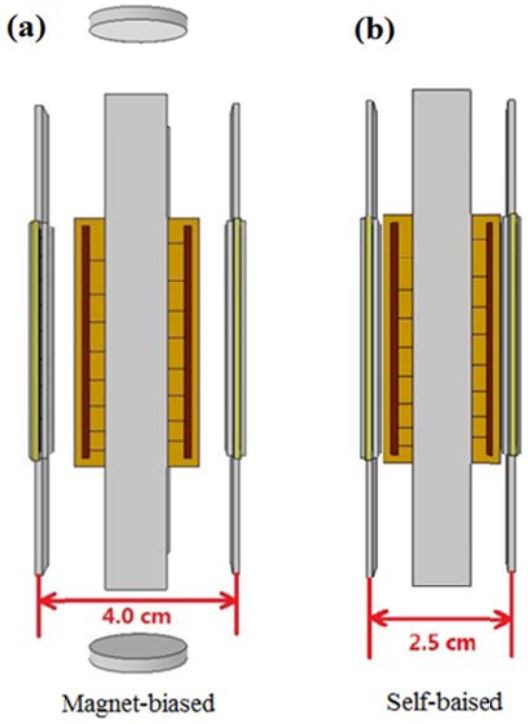

Figure 5.16. Schematic of stacking (a) four magnet-biased ME laminates and (b) self-biased ME laminates in a square tube. The tube is not shown.

5.5 Section Summary

In this chapter, the ME effect at zero bias field was studied in ME laminates. Different structures and materials were used to achieve high values of α_{ME} at 0 Oe. The noise and magnetic field sensitivities were measured in these self-biased ME laminates. The advantage of self-biased laminates in magnetic sensor application was also described in this section.

Firstly, the value of α_{ME} was increased to 6.3 V/cm·Oe in Metglas/Ni/ZPT laminate in a multi-push-pull configuration, which is about 4 times larger than that of (L-T) mode one. Giant values of α_{ME} have been found in self-biased annealed Metglas/ PZT/Metglas laminates under a zero magnetic field. A magnetic interaction can shift the *M-H* hysteresis loops in annealed Metglas/Metglas bilayers. In annealed Metglas/PZT/Metglas laminates, values of α_{ME} = 12 V/cm·Oe (1 kHz) and 380 V/cm·Oe (EMR) were found. This self-biased laminate shows a high sensitivity to small ac magnetic fields, which is quite close to the sensitivity of magnet-biased ME laminates.

Moreover, finite element simulation was undertaken to show the differences of the magnetic field strength around the magnet-biased and self-biased laminates. The perturbation to ambient B field from the self-biased ME laminate was significantly smaller in comparison to the magnet-biased one. When decreasing the distance to 2.5 mm between two self-biased ME laminates, the value of ME coefficient remained at > 75%. Thus, in arrays of ME laminates, the area of the cross section of the sensor unit could be reduced significantly.

CHAPTER 6.

CONVERSE AND NONLINEAR ME EFFECTS

6.1 Introduction

The converse magnetoelectric (CME) effect, which is defined as the induction of magnetization by an applied electric field, has been widely investigated in recent years.[1-7] Laminates with large CME effects hold promise for many applications, such as in sensors, actuators, and magnetic heads. Laminate composites of $Pb(Mg_{1/3}Nb_{2/3})O_3$-$PbTiO_3$ (PMN-PT) and Terfenol-D, or PMN-PT and Metglas have been reported to exhibit large CME effects at low frequency under a small DC magnetic bias (H_{bias}).[48-50] In contrast, these studies did not consider the effect of the thickness of the magnetostrictive phase, which is known to remarkably affect ME properties.[51,52] Moreover, these prior studies targeted laminates that were longitudinally magnetized and transversely poled: termed as an L-T mode. It is important to note that the ME effects in longitudinally magnetized and longitudinally poled, or (L-L) mode, laminates are notably larger than the L-T ones. This finding is principally due to the fact that the longitudinally piezoelectric coefficients ($^{p}d_{33}$) of PMN-PT or $Pb(Zr,Ti)O_3$ (PZT) are larger than the transverse ones ($^{p}d_{31}$).[21,23,43,92] However, few reports have been made concerning the CME effect.

When ME laminates were motivated by passive magnetic sensor applications, a linear response of the ME composites to a weak AC magnetic field H_{AC} was shown.[34] A DC magnetic bias field was applied to obtain the maximum piezomagnetic coefficient $d_{33,m}$, yielding the highest induced ME voltage (V_{ME}) to H_{AC}. ME laminate composites can also be used in an active mode to sense small DC magnetic fields or weak AC

magnetic fields, via a frequency modulation technique.[53,54] Such an approach has been utilized to reduce the environmental vibrational noise and 1/*f* noise in the low frequency range. In a magnetically unshielded environment, the sensitivity to small changes in H_{AC} can be enhanced by at least two orders magnitude compared to passive magnetic sensors.[54] However, to date, all investigations of the nonlinear ME coefficient, which is the physical basis of the frequency modulation method, have been reported using the same laminate structure as that used in the passive mode.[93] Due to a dependence of the different orders of nonlinearity on the magnetostrictive material, the structure resulting in a maximum nonlinear ME coefficient may not be the same as for the linear ME effect used in the passive mode. However, any investigations of the ME laminate structure that optimize the mode have not yet been undertaken.

As described in this chapter, I investigated the converse ME effect and nonlinear ME effect for multi-push-pull mode Metglas/PZT/Metglas laminates. To achieve high values of converse and nonlinear ME effect in Metglas/PZT laminates, the structure differences were examined and are discussed herein. Additionally, materials with different properties and stress effects were studied.

6.2 Converse ME Effect

This investigation considered the multi-push-pull mode Metglas/PZT/Metglas sandwich structure in the (2,3) plane. We assumed that the polarization of the piezo-fibers was uniformly arranged along the longitudinal direction (3-axis). Thus, the multi-push-pull configuration can be considered as a multi-L-L mode, as illustrated in Figure 6.1. Furthermore, we only considered the stresses in the 3-direction.

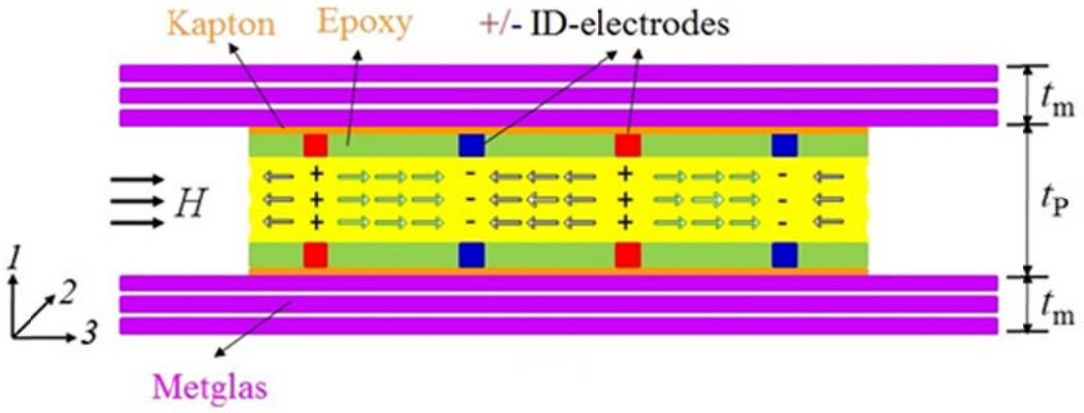

Figure 6.1. Schematic diagram of simplified Metglas/PZT/Metglas multi-L-L structure laminate consisting of a Kapton/piezofiber core composite and *N* layers Metglas on the bottom and top of the core composite, where the polarization of piezofibers was idealized to be arranged in the longitudinal direction.

An averaging method is used for deriving the effective material parameters of the composite. The piezoelectric constitutive equations can be written as:

$$\begin{aligned} {}^{p}S_3 &= {}^{p}s_{33}\,{}^{p}T_3 + {}^{p}d_{33}E_3 \\ D_3 &= {}^{p}d_{33}\,{}^{p}T_3 + {}^{p}\varepsilon_{33}E_3; \end{aligned} \tag{6.1}$$

where ${}^{p}S_3$ and ${}^{p}T_3$ are the strain and stress tensor components of the piezoelectric phase along the length direction, E_3 and D_3 are the vector components of the electric field and electric displacement, ${}^{p}s_{33}$ and ${}^{p}d_{33}$ are the compliance and piezoelectric coefficients, and ${}^{p}\varepsilon_{33}$ is the dielectric permittivity. The magnetostrictive phase can be described by the following equations:

$$\begin{aligned} {}^{m}S_3 &= {}^{m}s_{33}\,{}^{m}T_3 + {}^{m}q_{33}H_3 \\ B_3 &= {}^{m}q_{33}\,{}^{m}T_3 + {}^{m}\mu_{33}H_3; \end{aligned} \tag{6.2}$$

where ${}^{m}S_3$ and ${}^{m}T_3$ are the strain and stress tensor components of the piezomagnetic phase along the length direction, H_3 and B_3 are the vector components of the magnetic field and magnetic flux induction, ${}^{m}s_{33}$ and ${}^{m}q_{33}$ are the compliance and piezomagnetic coefficients, and ${}^{m}\mu_{33}$ is the magnetic permittivity. Equations (6.1)-(6.2) were then solved under the following boundary conditions:

$${}^{m}S_3 = {}^{p}S_3, \tag{6.3}$$

$$v\,{}^{p}T_3 = -(1-v)\,{}^{m}T_3; \tag{6.4}$$

where $v = \dfrac{t_p}{t_p + 2t_m}$ denotes the thickness fraction of the piezoelectric phase.

Using open circuit conditions $(H_3 = 0)$, the following relationship for α_B can be obtained:

$$\alpha_B = \left|\frac{dB_3}{dV_3}\right| = \frac{1}{t_p}\left|\frac{v\,{}^{p}d_{33}\,{}^{m}q_{33}}{(1-v)\,{}^{p}s_{33} + v\,{}^{m}s_{33}}\right|. \tag{6.5}$$

From Equation (6.5), the value of α_B can be calculated as a function of v for a Metglas/PZT/Metglas in a multi-push-pull configuration, as shown in Figure 6.2. The

following parameters were used in the calculations: ${}^{p}d_{33}$ = 440×10^{-12} C/N, ${}^{m}q_{33}$ = 50.3×10^{-9} m/A, ${}^{p}s_{33}$ = 17.3×10^{-12} m^2/N and ${}^{m}s_{33}$ = 10×10^{-12} m^2/N. In this figure, it can be seen that the predicted values of α_B for the multi-push-pull mode are much higher than those for the L-T one. Furthermore, the predicted values of α_B for Terfenol-D/PMN-PT, or other material couples, L-T mode laminates are quite low: which agrees well with previously reported experimental values. Accordingly, the CME effect in laminates having a multi-push-pull configuration should be experimentally investigated.

To confirm this prediction, a Metglas/PZT/Metglas multi-push-pull mode laminate was fabricated. A 40 mm × 10 mm PZT bundle served as the core of the laminates, which consisted of five 40 mm × 2 mm PZT-5A fibers (Smart Material Corp., Sarasota, FL) that were oriented along the length direction of the laminates. Two interdigitated Kapton electrodes were bonded to the top and bottom surfaces of the piezoelectric bundle with epoxy resin (Stycast 1264, USA). *N* layers of 80 mm × 10 mm $Fe_{74.4}Co_{21.6}Si_{0.5}B_{3.3}Mn_{0.1}C_{0.1}$ Metglas foils (Vitrovac 7600F, Hanau, German) were then laminated to both the top and bottom surfaces of the interdigitated electrode/PZT core composite, with a different epoxy resin (West System 105/206, USA). Laminates with different numbers *N* of Metglas layers bonded to both sides of the PZT core composite were fabricated for *N* = 2 to 7.

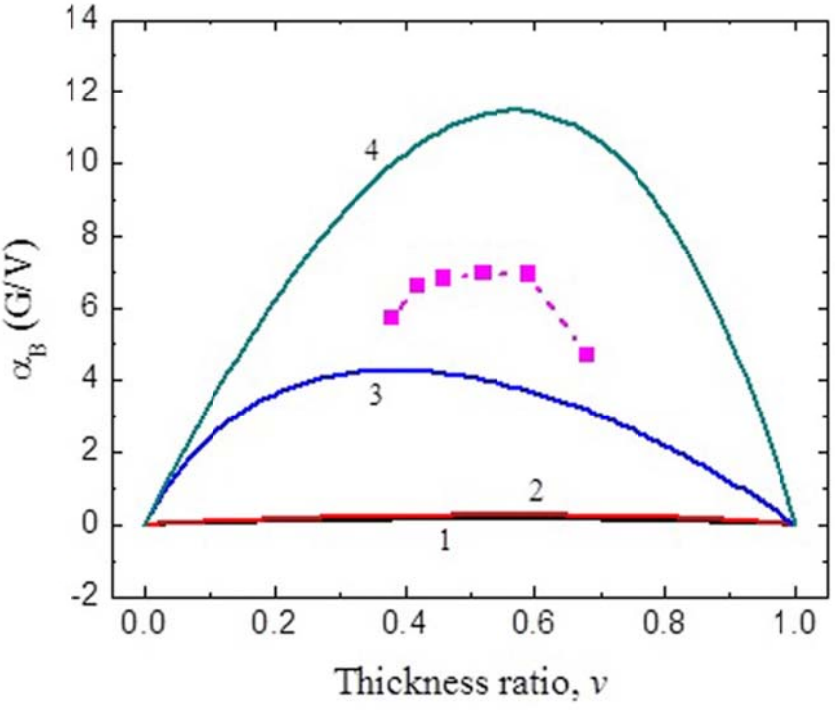

Figure 6.2. α_B as a function of the thickness ratio v. Lines 1, 2 and 3 represent the calculations for Terfenol-D/PMN-PT, Metglas/PMN-PT and Metglas/PZT L-T mode laminates using Ref. 10 and 12, with the data in these paper respectively. Lines 4 are calculations for Metglas/PZT/Metglas multi-push-pull mode laminates using Equation 6.5. Dots are the experimental data.

To measure the magnetic induction (B_3), a search coil was wrapped around the laminate. A signal from a lock-in amplifier (SR-850) was amplified by a high voltage amplifier, which was then applied as a voltage (V_3) across the PZT fibers. A change of the magnetic flux in the Metglas resulted, which was measured as an induced voltage in the search coils that was then subsequently measured by the lock-in amplifier. Figure 6.3 shows the value of α_B as a function of H_{dc} for laminates with different numbers of layers

epoxied to both sides of the core composite (f = 1 kHz). It can be seen that α_B increased as H_{dc} was increased, reached a maximum value, and subsequently decreased as H_{dc} was further increased. Furthermore, it can be seen that the maximum value of α_B increased with increasing number of Metglas layers N, and then decreased with further increase in N. The maximum value of α_B was 6.94 G/V under H_{dc} = 11 Oe for N = 4 (v = 0.52). The dependence of the values of α_B on N can be attributed to the differences of effective strain on the Metglas layers. Using an optimum v, the effective strain transferred from PZT fibers to Metglas is larger. Thus, the larger change in the induced magnetization leads to higher values of α_B, giving rise to a maximum CME response for N = 4.

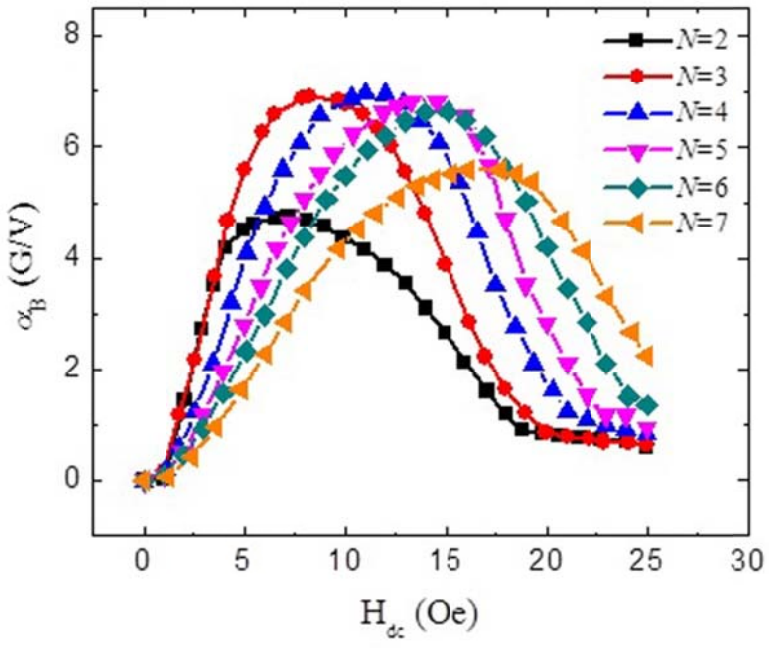

Figure 6.3. The value of α_B as a function of H_{dc} for Metglas/PZT/Metglas laminates with different N at an applied ac voltage of 50 V at the frequency of 1 kHz.

The maximum values for α_B are shown in Figure 6.2, as a function of the thickness ratio v, calculated from N. The experimental values of α_B exhibited similar trends to the predicted ones. However, due to a non-ideal interfacial bonding (i.e. coupling factor $0 < k < 1$) between the piezoelectric and magnetostrictive phases,[28] the experimental values were only 60% of the theoretical ones. This outcome strongly suggests that there remains notable potential to enhance the value of α_B by improving the interfacial bonding conditions. The frequency dependence of α_B for the laminate with $N = 4$ is given in Figure 6.4, for $H_{dc} = 11$ Oe. The maximum value of α_B was 79.5 G/V at an electromechanical resonance (EMR) frequency of 29.6 kHz. Such giant values of α_B at EMR are >25× higher than those previously reported for other modes.

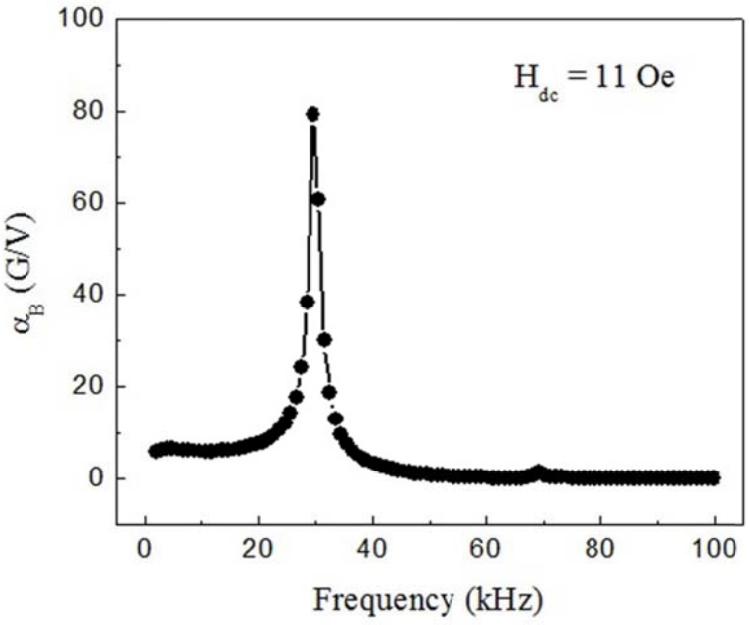

Figure 6.4. The frequency response of α_B at an applied ac voltage of 50 V and a H_{dc} of 11 Oe.

(Reprinted with permission from Ref. 94, Copyright © 2012 AIP Publishing LLC)

6.3 Nonlinear ME Effect

6.3.1 Structural dependence of magnetostrictive materials

Dr. Zhuang and Dr. Dolabdjian introduced a nonlinear modulation technique to transfer low-frequency signals to higher frequencies. Such techniques showed the advantages that the low-frequency signals were not suffered from low-frequency interferences, such as noise vibrations.[53]

When a relatively small magnetic field is applied, the magnetostriction of Metglas foils can be described with Livingston's model of coherent rotation of the magnetization.[30] The strain in Metglas is given by

$$\lambda = \frac{3\lambda_s}{2H_A^2} H^2; \tag{6.6}$$

where H is the applied magnetic field, λ_s is the saturation magnetostriction, H_A is the magnetic anisotropy field equal to M_s/χ_0, χ_0 is the magnetic susceptibility, and M_s is saturation magnetization.

When a modulation field H_{mod} and a small signal field H_{ac} are applied to Metglas/PZT laminates ($H = H_{mod} + H_{ac}$), the magnetostrictive response of the Metglas layers is given by

$$\lambda = \frac{3\lambda_s}{2H_A^2}(H_{mod}^2 + 2H_{mod}H_{ac} + H_{ac}^2). \tag{6.7}$$

The amplitude of the ME voltage V_{ME} at the sideband frequency of $f_{mod} \pm f_{ac}$ is proportional to the magnetostriction of Metglas at the same frequency, which could be expressed as[95]

$$\lambda_{f_{\mathrm{mod}} \pm f_{ac}} = \frac{3\lambda_s \chi_0^2}{M_s^2} H_{\mathrm{mod}} H_{ac}. \tag{6.8}$$

λ_s and M_s are constants in our Metglas materials with fixed dimensions. Thus, the amplitude of V_{ME} will be mainly determined by χ_0.

In the case of multiple layers of Metglas bonded together by epoxy layers, the magnetization of Metglas will be restricted due to the constraint from the epoxy layers. [51,96] To study this epoxy-based constraint effect, I examined a multilayer structure consisting of N layers of Metglas and N-1 layers of epoxy. If only considering the stress and strain along the longitudinal direction (3-direction) of the Metglas foil, when a magnetic field H_3 is applied, the constitutive equation of Metglas will be as follows:

$$\begin{aligned} {}^{m}S_3 &= {}^{m}s_{33}\,{}^{m}T_3 + q_{33}H_3 \\ B_3 &= q_{33}\,{}^{m}T_3 + \mu_{33}H_3; \end{aligned} \tag{6.9}$$

where ${}^{m}S_3$ is the strain along 3 direction, and q_{33} is the piezomagnetic coefficient and ${}^{m}s_{33}$ is the elastic constant. Using the boundary condition:

$${}^{m}S_3 = {}^{e}S_3; \tag{6.10}$$

$$\text{and } {}^{m}T_3 N t_m + {}^{e}T_3 (N-1) t_e = 0; \tag{6.11}$$

the stress in Metglas layers could be identified by the following equation:

$${}^{m}T_3 = -\frac{\lambda (N-1) t_e}{{}^{m}s_{33}(N-1)t_e + {}^{e}s_{33} N t_m}, \tag{6.12}$$

where t_e and t_m are the thickness of each epoxy and Metglas layers. According to Livingston's model[30], under stress σ, the initial susceptibility of Metglas χ_0 is:

$$\chi_0 = \left(\frac{\partial M}{\partial H}\right)_\sigma = \frac{\mu_0 M_s^2}{2K_u - 3\lambda_s \sigma}. \tag{6.13}$$

In the above multilayer structure, the compressive stress on the Metglas σ is equal to ${}^{m}T_3$. Thus, the relationship of χ_0 and N could be given as:

$$\chi_0 = \frac{\mu_0 M_s^2}{2K_u + \frac{3\lambda_s \lambda (N-1)\,t_e}{{}^{m}s_{33}(N-1)t_e + {}^{e}s_{33}Nt_m}}. \tag{6.14}$$

Using M_s = 1.0 T, λ_s = 40 ppm, t_e = 8 μm, t_m = 20 μm, K_u = 2 J/m^3 [31], ${}^{m}s_{33}$ = 10e-12 m^2/N, and ${}^{m}s_{33}$ = 400e-12 m^2/N, the value of χ_0 at various N can be calculated. Figure 6.5 shows the calculated χ_0 verses N. With increasing values of N, the value of χ_0 decreases, implying for N = 1 that V_{ME} is the highest. These results illustrate that the optimum structure of a Metglas/PZT/Metglas laminate for the active mode is different in comparison to one intended to be used in the passive mode.

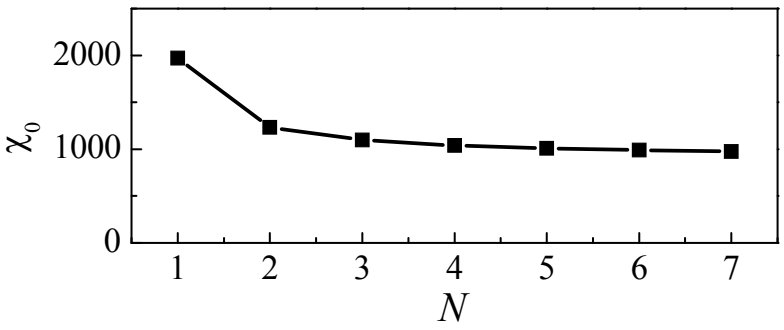

Figure 6.5. Calculated χ_0 as function of N, calculated by Equation (6.14).

I then measured *M-H* hysteresis loops by a vibrating sample magnetometer (VSM) for various values of N, as shown in Figure 6.6(a). The value of the initial magnetic susceptibility χ_0 was then calculated as dM/dH, where M is the magnetization. In Figure 6.6(b), the value of χ_0 can be seen to be maximum for N = 1, and but then

decreases as N increases. Our experimental results show a similar trend as my calculated results for χ_0, but the values were smaller than the calculated ones. This is mainly due to the additional stress applied to the Metglas layers during the measurement. In VSM measurement, the samples were firmly bonded on the holder by double sided tapes. This adhesive tape applied constraint stress to Metglas layer, which shows similar effect as the adhesive epoxy layers on χ_0. Thus, the measured values of χ_0 were smaller than the calculated ones. If the magnetization of Metglas was measured by non-contact methods, such as SQUID or magneto-optical Kerr effect, the results would be closer to the calculated values.

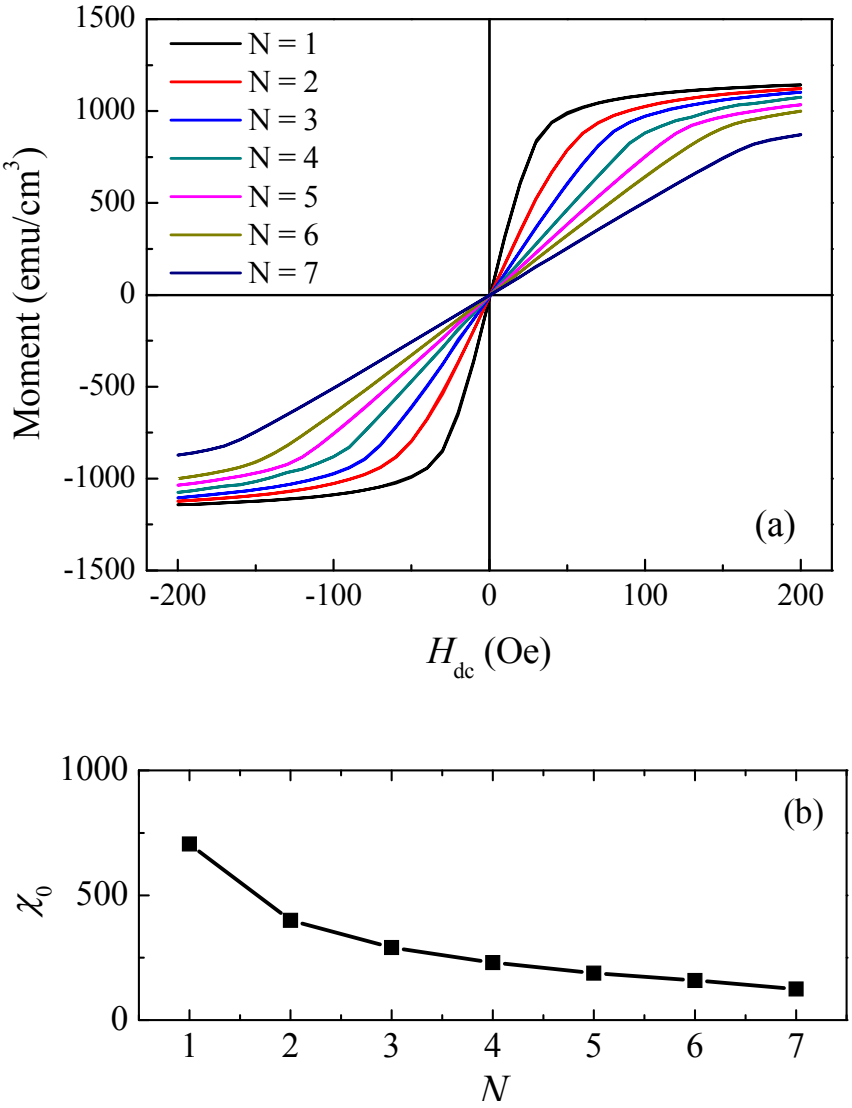

Figure 6.6. (a) *M-H* hysteresis loops and (b) χ_0 for various values of *N*.

From the above analysis it could be seen that, to obtain the highest value for the output signal, the structure that yields the maximum value of χ_0 should be chosen, which is $N = 1$. Several Metglas/PZT/Metglas laminates with varying numbers of Metglas layers were fabricated.[66] A 40 mm × 10 mm PZT bundle served as the core, which consisted of five 40 mm × 2 mm PZT-5A fibers (Smart Materials, Sarasota, FL) oriented along the length direction of the laminates. Different numbers N of Metglas layers (Vitrovac 7600F, Hanau, German) of dimensions 80 mm× 10 mm were bonded to both sides of the PZT core composite for $N = 1$ to 7.

An incident magnetic field of H_{mod} = 1 Oe at f_{mod} = 1 kHz was applied using a Helmholtz coil and an AC field of B_{ac} = 70 nT at a f_{ac} = 1 Hz using a drive coil. The modulation field H_{mod} was then measured using a SR-785 dynamic signal analyzer (Stanford Research Systems). Figure 6.7(a) shows the measured modulation spectrum in the frequency range between 998.5 Hz and 1001.5 Hz for various N. As shown in Figure 6.7(b), for N = 1, the ME output voltage V_{ME} at $f_{\text{mod}} - f_{AC}$ was maximum; and subsequently decreased with increasing N. At $f = f_{\text{mod}} - f_{AC}$, the voltage noise V_{noise} for B_{AC} = 0 at the value of each N was also measured as shown on the right axis of Figure 6.7(b). With increasing N, the V_{noise} also increased slightly due to an increased value of α_{ME} at low fields (i.e. $H_{\text{dc}} < 1$ Oe). The magnetic field sensitivity can be estimated as $B_{\text{ac}}*V_{\text{noise}}/V_{\text{ME}}$, as shown in Figure 6.7(c). With increasing N, the active sensor displayed enhanced magnetic field sensitivity. Specifically, the magnetic field sensitivity was 0.66 nT/Hz$^{0.5}$ for $N = 1$, which was 4.2 times larger than for $N = 7$ and 3.1 times larger than for N = 5. Clearly, the optimum structure for the ME active mode structure (N = 1) is different in comparison to the passive one ($N = 5$).

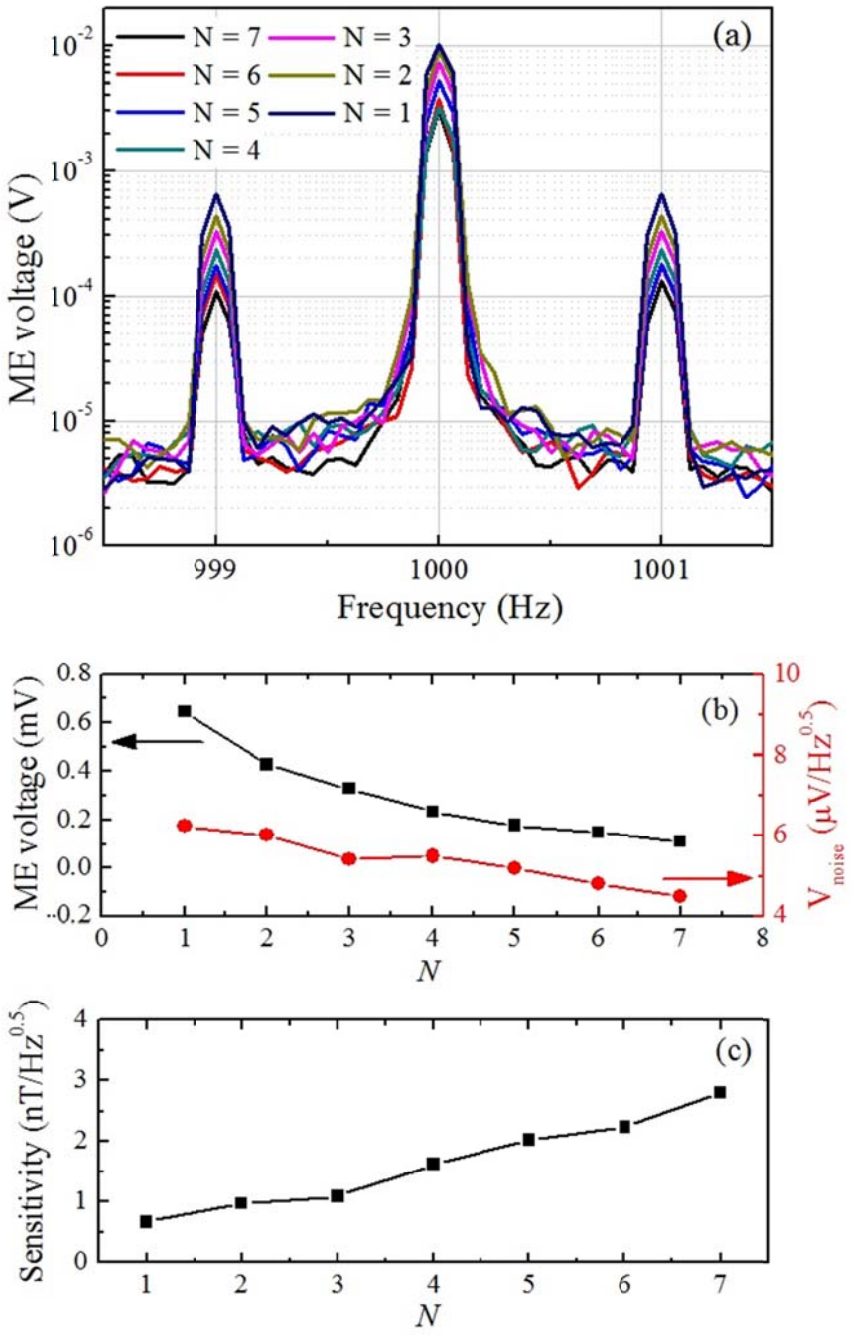

Figure 6.7. (a) Measured modulation spectrum taken over the frequency of 998.5 Hz to 1001.5 Hz for various values of N; (b) V_{ME} and V_{noise} at $f = f_{mod} - f_{ac}$; and (c) magnetic field sensitivity as a function of N.

(Reprinted with permission from Ref. 97, Copyright © 2013 AIP Publishing LLC)

6.3.2 Pre-stress effect on nonlinear ME effect

A simple model of the domain structure of Metglas was presented by Livingston.[30] In the absence of an external bias field, the domains remain along the transverse direction, and are perpendicular to the direction of the applied magnetic field H, which is an ideal condition. However, after a longitudinal magnetic field H is applied, the domain will rotate to the direction of H. When applying a longitudinal stress σ to the Metglas foil, the longitudinal strain could be expressed by the following equation:

$$\lambda = \frac{\sigma}{E_M} + \frac{3\lambda_s}{2}\left(\frac{H^2}{H_A^2} - \frac{1}{3}\right); \tag{6.15}$$

where H_A is the anisotropy field and $H_A = \frac{2K_u - 3\lambda_s\sigma}{M_s}$, K_u is the energy constant, λ_s is the saturation magnetostriction, and E_M is the Young's modulus. According to this model and Equation (6.13), when applying a longitudinal stress, the susceptibility χ_0 will be increased. As discussed in Section 6.3.1, when the χ_0 level is high, the nonlinear coefficient of a Metglas/PZT laminate will also be higher. From modeling studies, one could predict that a self-stressed ME laminate will possess a higher nonlinear coefficient than a non-stressed one.

I also measured the $\alpha_{ME} - H_{dc}$ curves for pre-stressed and non-stressed ME laminates at 1 kHz. Both ME laminate samples consisted of five PZT fibers and one layer of Metglas. When bonding the Metglas layer to the PZT core composite, a 5 Oe DC bias magnetic field was applied. After the epoxy was cured, pre-stress was induced between the Metglas and PZT layers. As shown in Figure 6.8, the pre-stressed Metglas/PZT laminate displayed a higher peak value of α_{ME}, which agrees well my results (see Section 3.4).

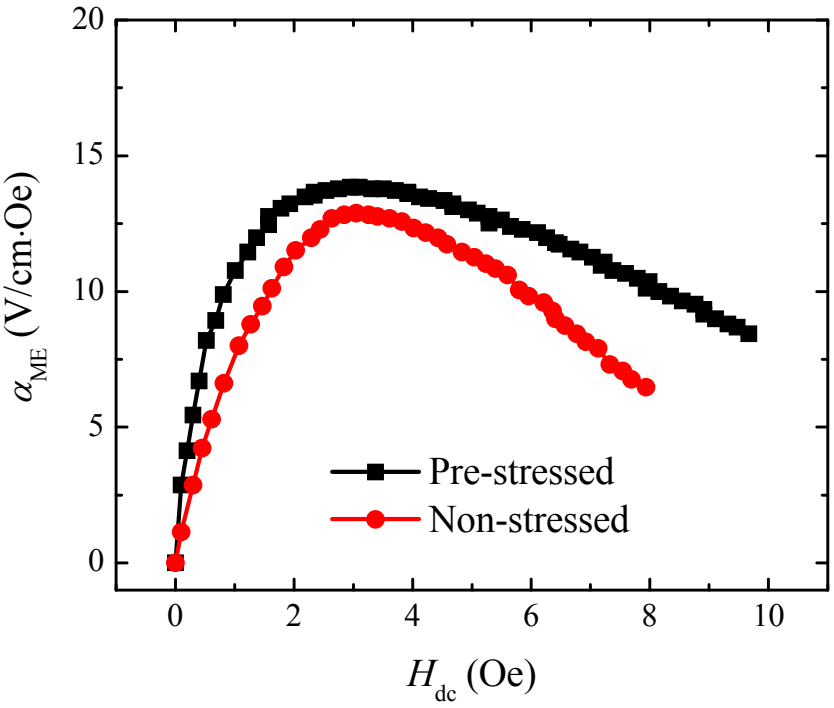

Figure 6.8. $\alpha_{ME} - H_{dc}$ curves for pre-stressed and non-stressed Metglas/PZT laminates at f = 1 kHz.

The relative value of χ_0 for pre-stressed and non-stressed Metglas layers can be calculated by Equation (6.13). The stress in a pre-stressed laminate fabricated under a 5 Oe DC bias field was about 0.12 MPa, according to the results displayed in Figure 3.16. As such, the ratio of calculated χ_0 for pre-stressed to non-stressed Metglas layers is about 1.35, while the amplitude of V_{ME} is proportional to χ_0^2. Thus, the amplitude of V_{ME} for pre-stressed Metgls/PZT laminate could be enhanced by a factor of ×1.82, compared to non-stressed one.

The modulated ME output voltage results for the pre-stressed and non-stressed ME laminates are shown in Figure 6.9. The modulation signal was 0.1 Oe at 1 kHz, and

the small ac magnetic signal was 70 nT at 1 Hz. The amplitude of the cross-modulation peak V_{ME} at 999 Hz for the pre-stressed Metglas/PZT laminate was 1.27×10^{-3} V, which is higher by a factor of ~1.5× compared to 8.44×10^{-4} V for the non-stressed one. This ratio is close to the calculated ratio of χ_0^2, indicating that our experimental results agree well with calculated predictions. Considering that the noise level for both types of sensors was approximately 4.0×10^{-6} V, the magnetic field sensitivity of the pre-stressed Metglas/PZT sensor was shown to be higher than the non-stressed one by a factor of 1.5×.

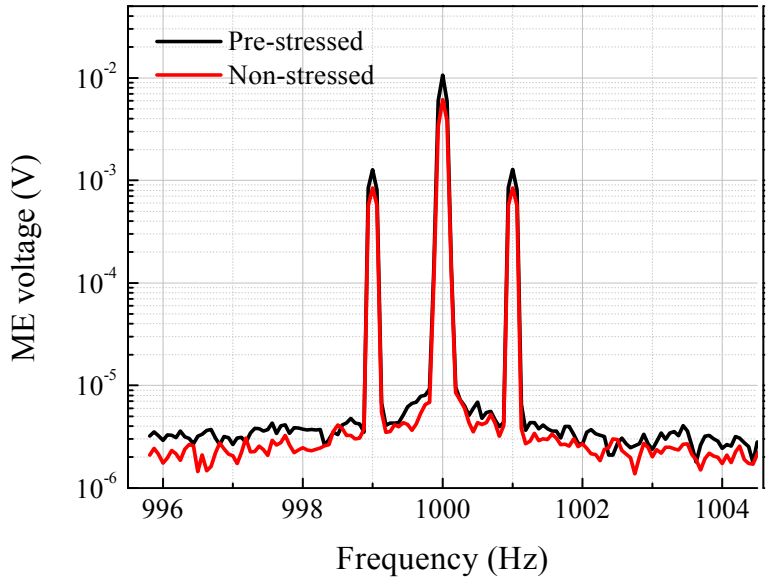

Figure 6.9. Test voltage output signals of pre-stressed and non-stressed Metglas/PZT sensor the using a modulation scheme under AC magnetic field at a modulation frequency of 1 kHz.

6.3.3 Dependence of piezoelectric materials

The modulation-demodulation technique is based on the nonlinear ME effect, which can be expressed as:

$$V_{\mathrm{ME}}\big|_{f_{\mathrm{mod}}\pm f_{AC}} = \frac{\partial V}{\partial \lambda}\cdot\frac{A_1}{2}\cdot H_{AC}; \tag{6.16}$$

where f_{mod} and f_{ac} are the frequency for H_{mod} and H_{ac} respectively; and the parameter $A_1 = a_1 H_{\mathrm{mod}} + \frac{3}{4}a_3 H_{\mathrm{mod}}^3 + \frac{5}{8}a_5 H_{\mathrm{mod}}^5$ is the magnetostriction (λ) which is determined by the amplitude of H_{mod} and the Fourier coefficients a_{i} that can be obtained by fitting the curve of λ in H, as studied in the above section.

From Equation (6.16), it can be seen that the amplitude of the ME voltage at the sideband frequency $f_{\mathrm{mod}} \pm f_{ac}$ is determined by the elasto-electric properties of the piezoelectric layer, the applied modulation field H_{mod}, and the Fourier coefficients. Piezoelectric single crystals of PMN-PT and Mn-doped PMN-PT displayed higher piezoelectric properties and lower dielectric losses than PZT, as summarized in Table 6.1[98,99]. ME laminates based on such single crystals in a multi-push-pull configuration could have higher nonlinear ME effects.

Table 6.1. Property parameters for PMN-PT, Mn-doped PMN-PT and PZT piezoelectric ceramics.

Piezoelectric ceramics	$\varepsilon_{33}/\varepsilon_0$	tanδ	d_{33} (10^{-12}C/N)	g_{33} (10^{-3}Vm/N)	Q
PMN-PT [a)]	7000	0.005	2000	32.3	100
Mn-doped PMN-PT [b)]	5400	0.002	1750	36.6	530
PZT [a)]	1850	0.012	440	25.5	80

a) Cited from Ceracomp Co., Ltd.

b) Measured

High-quality PMN-PT and Mn-doped PMN-PT single crystals were grown directly from a melt using a modified Bridgman technique[100]. As-grown single crystals were oriented along <001>-directions, and diced to prepare fibers with dimensions of 40×2×0.2 mm^3. Five such PMN-PT, Mn-doped PMN-PT and PZT fibers were then overlaid by a pair of interdigitated (ID)-electrodes with a spacing of 1.5 mm to form the core composites. The core composites were then attached and bonded with three-layers of Metglas on both the top and bottom. A modulated AC field H_{mod} at a frequency of f_{mod} (using a drive coil), as well as an AC magnetic field H_{ac} at a frequency of f_{AC} (using a Helmholtz coil), were applied. Subsequently, the cross-modulation signals with a frequency of ($f_{\text{mod}} \pm f_{ac}$) were then measured using a dynamic signal analyzer (SR 785, CA).

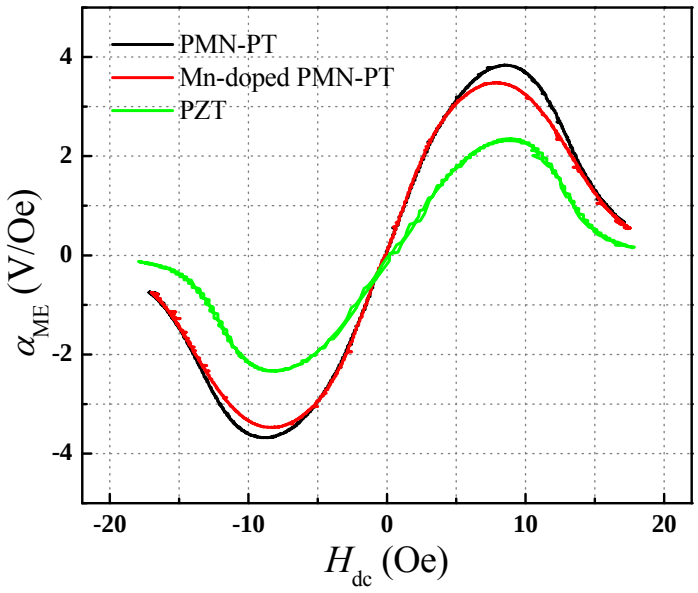

Figure 6.10. Linear ME coefficients α_{ME} of the Metglas/PMN-PT, Metglas/Mn-doped PMN-PT and Metglas/PZT heterostructures as a function of DC magnetic bias field H_{DC} at 1 kHz.

First, the linear ME coefficient α_{ME} for both PMN-PT and Mn-doped PMN-PT sensors was measured as a function of H_{DC} in response to a H_{AC} = 0.1 Oe at a frequency of f = 1 kHz, as shown in Figure 6.10. The functional form of the variation of α_{ME} with H_{DC} was similar to that previously reported[98,101]. Please note that the laminates with PMN-PT fibers had a slightly higher maximum value of α_V than ones with Mn-doped PMN-PT (i.e., 3.8 V/Oe relative to 3.5 V/Oe) at an optimal bias of H_{DC} = 8 Oe This finding is associated with the similar piezoelectric properties (d_{33} and g_{33}) of the two single crystals (see Table 6.1). The maximum α_{ME} value for the Metglas/PZT laminate was 2.4 V/Oe, which is due to the much lower d_{33} value of the piezo-fibers.

Figure 6.11 shows α_{ME} as a function of frequency under bias fields near H_{dc} = 8 Oe. The effective mechanical quality factor Q_m of the laminates is also provided in this figure. For $f \leq 20$ kHz, the value of α_{ME} was nearly independent of f for all types of laminates. A significant enhancement of α_{ME} was found at the EMR, but the laminate with Mn-doped PMN-PT fibers had a larger and sharper ME resonance peak by a factor of ~1.3 to the PMN-PT one (i.e., 195 V/Oe to 152 V/Oe), and ~2.9 to the PZT one (i.e., 195 V/Oe to 68 V/Oe). Please note that the effective values of Q_m for laminates with Mn-doped PMN-PT fibers were also higher, which can be attributed to a higher Q_m value for the individual fibers.

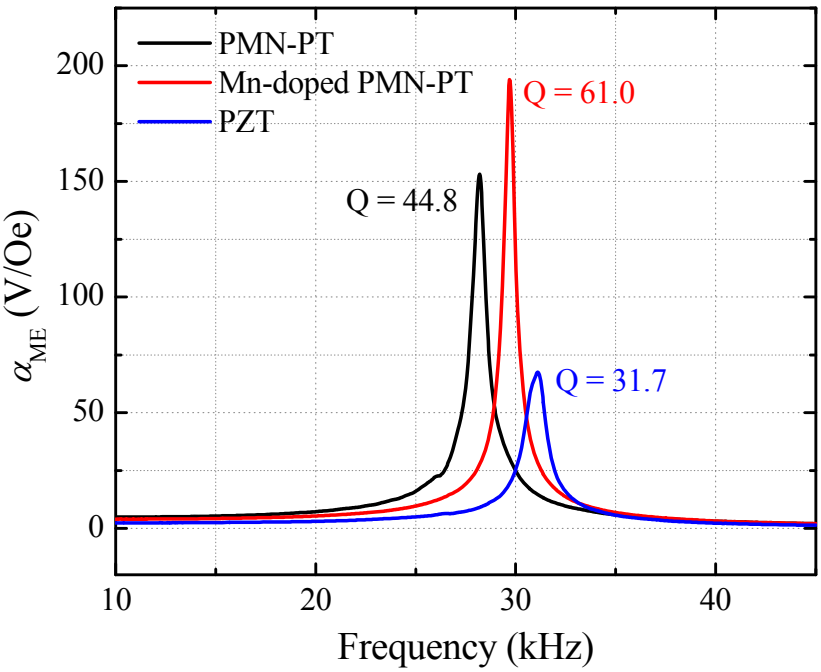

Figure 6.11. Linear ME coefficient α_{ME} of the three piezoelectric fiber/Metglas sensors as a function of frequency f over the range of 0.1 kHz < f <100 kHz under DC magnetic field of H_{dc} = 8 Oe.

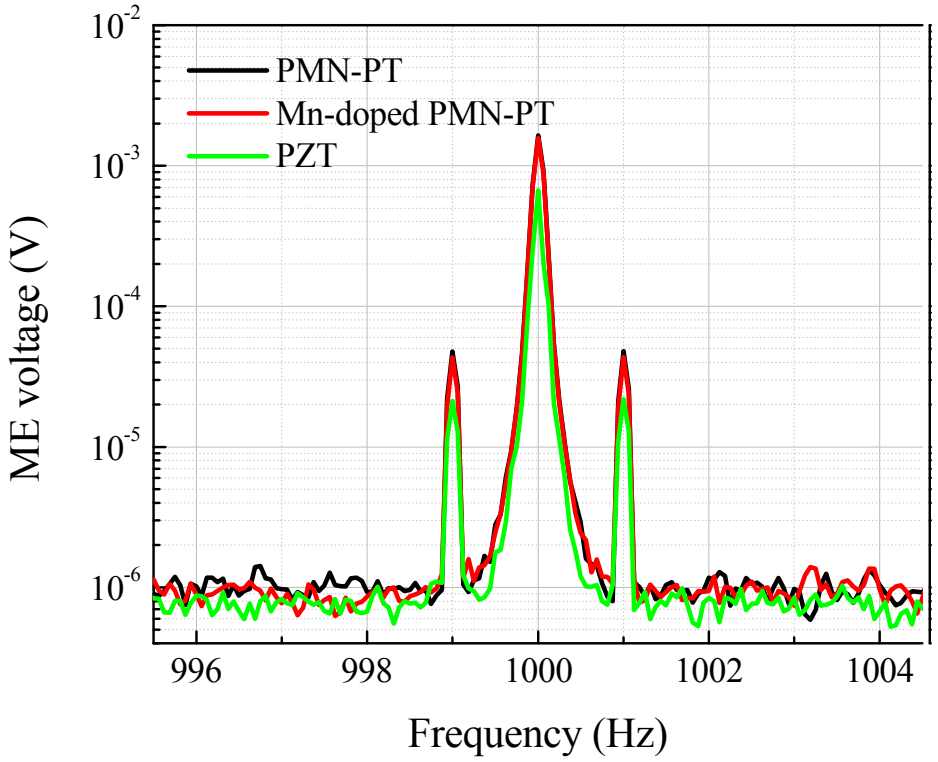

Figure 6.12. Test voltage output signals of the Metglas/PMN-PT, Metglas/Mn-doped PMN-PT and Metglas/PZT sensors using cross-modulation scheme under AC magnetic field of $H_{dc} = 0$ Oe at modulation frequency of 1 kHz.

Figure 6.12 illustrates the results for our modulation measurements, where $H_{ac} =$ 0.0007 Oe at $f = 1$ Hz, and $H_{mod} = 0.1$ Oe at $f_{mod} = 1$ kHz. In this figure, the output signals can be seen to contain cross-modulation peaks at frequencies of 999 Hz and 1001 Hz. The amplitude of the cross-modulation peaks for laminates with pure and Mn-doped PMN-PT fibers were similar—namely, they were both higher than the analogous PZT fiber laminate by a factor of ~2.0. This similarity for laminates with pure and Mn-doped

PMN-PT fibers is associated with the fact that the values of $\partial V / \partial \lambda$ (see Eq.(6.9)) at frequencies of f = 999 Hz and 1001 Hz were equal—i.e., the elasto-electrical conversion efficiency is dominated by the piezoelectric properties.

Figure 6.13 shows the results for the modulation measurements and noise level at EMR. Two output voltage peaks can be seen at modulation frequencies of f = 28659 Hz and 28661 Hz (laminate with PMN-PT fibers), f = 29809 Hz and 29811 Hz (laminate with Mn-doped PMN-PT fibers), and f = 30839 Hz and 30841 Hz (laminate with PZT fibers). The amplitude of the modulation peak V_{ME} for laminates having Mn-doped PMN-PT fibers was 4.2×10^{-4} V, which is higher by a factor of ~1.8× compared to 2.3×10^{-4} V for PMN-PT ones, and ~4.2× compared to 1.01×10^{-4} V for PZT ones. The higher value of V_{ME} for laminates with Mn-doped PMN-PT fibers is due to the elasto-electrical conversion efficiency of the EMR, as determined not only by the piezoelectric properties, but also by the effective Q_{m}.

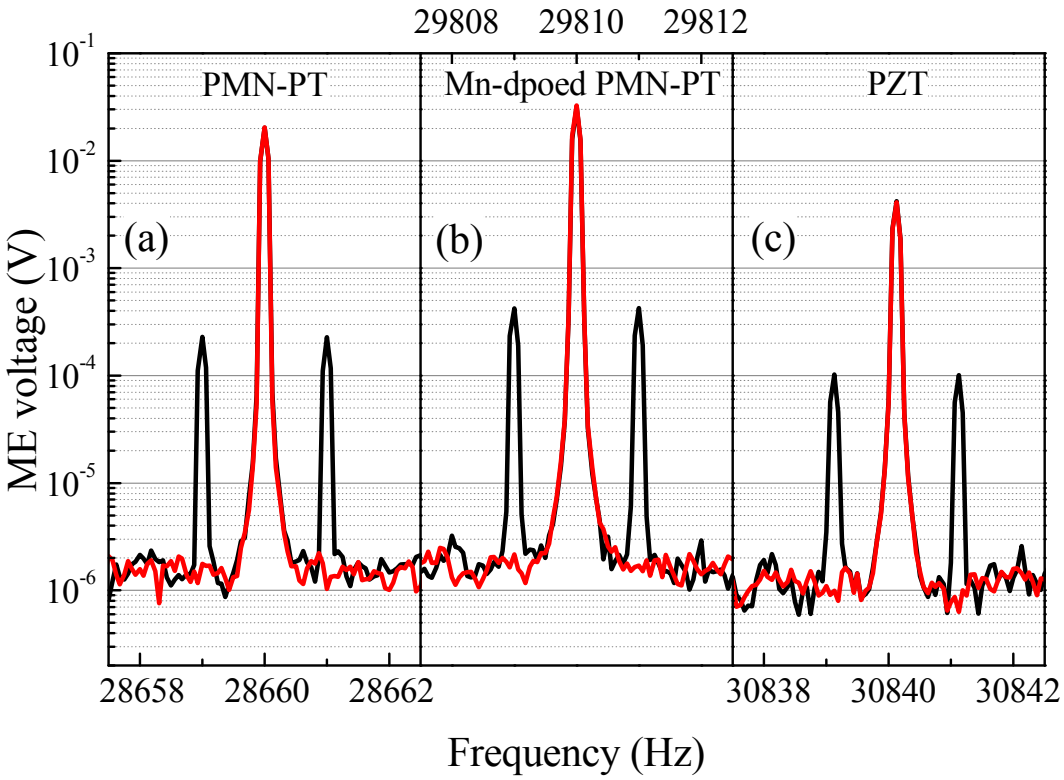

Figure 6.13. Test voltage output signals (black line) and noise level (red line) of the (a) Metglas/PMN-PT, (b) Metglas/Mn-doped PMN-PT and (c) Metglas/PZT sensors using modulation scheme under AC magnetic field of H_{dc} = 0 Oe at modulation frequency of EMR.

The modulated ME voltage was then demodulated using a lock-in amplifier (SR 850), after which it was recorded by the signal analyzer SR 785. Figure 6.14(a) shows the demodulated spectrum of the ME voltage over a frequency range of 0.0625 Hz and 50 Hz for ME laminates with different piezo-fibers. Given that the value of V_{ME} was 1 Hz, the transfer function of each ME laminate could be calculated as follows: 4.25 kV/T, 2.69

kV/T and 1.15 kV/T for ME laminates with Mn-doped PMT-PT, PMN-PT and PZT fibers, respectively. Therefore, the demodulated equivalent magnetic noise was determined to be the voltage noise divided by the transfer function, as shown in Figure 6.14(b). The equivalent magnetic noise of Metglas/Mn-doped PMN-PT, Metglas/PMN-PT and Metglas/PZT laminates was identified as 197.2 $pT/Hz^{0.5}$, 300.6 $pT/Hz^{0.5}$, and 840.1 $pT/Hz^{0.5}$, respectively.

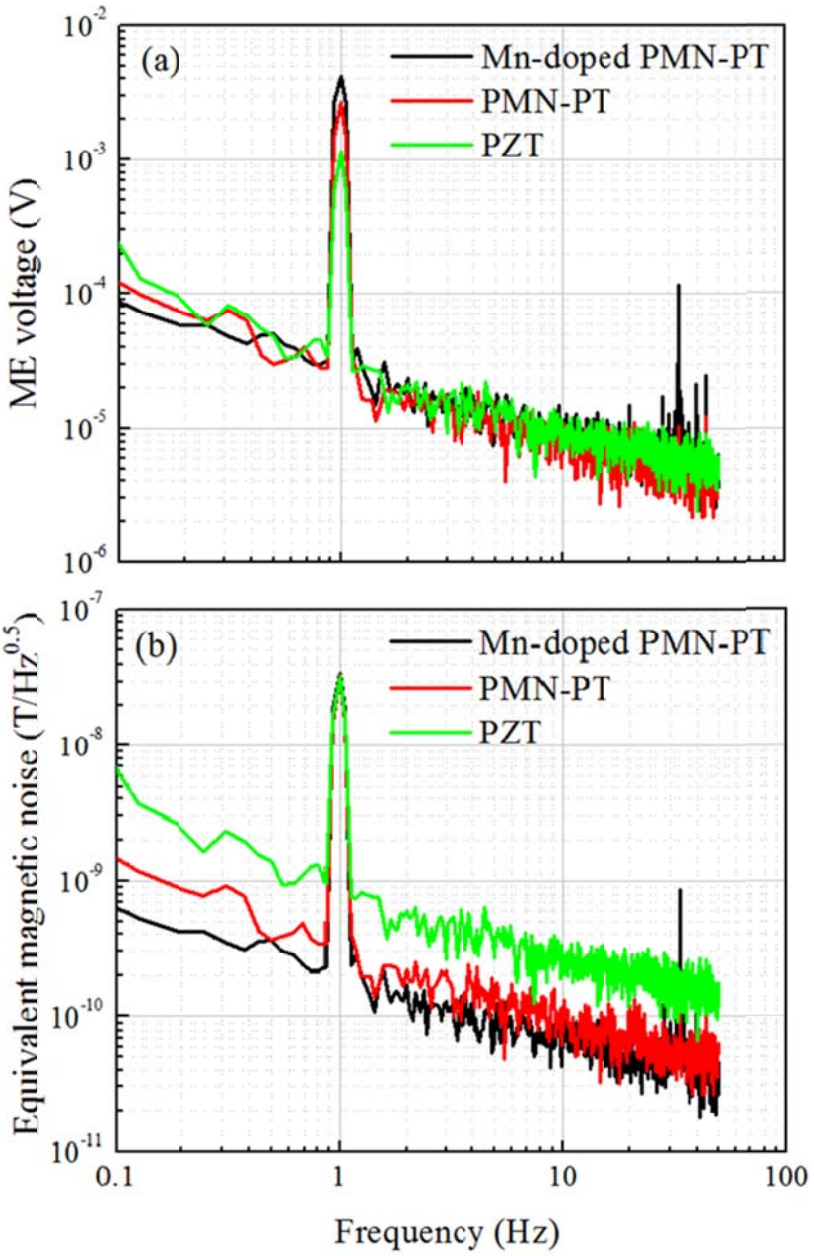

Figure 6.14. Demodulated spectrum of (a) ME voltage and (b) equivalent magnetic noise of ME laminates with different piezo-fibers using cross-modulation scheme over the frequency range of 0.0625 Hz and 50 Hz.

6.4 Section Summary

We investigated various CME effects for multi-push-pull mode Metglas/PZT/Metglas laminates. A theoretical model was presented that predicted large CME coefficients (α_B); experimental results revealed good agreement with predicted values. In particular, by utilizing an optimum thickness ratio, we were able to identify giant CME effects, which exhibit a further enhancement at the resonance frequency.

The nonlinear ME effect was studied in three aspects. Firstly, we revealed the structure differences between ME laminates for sensor applications in passive versus active modes. In the active mode, the calculated and measured value of the magnetic susceptibility χ_0 indicated that the ME output voltage was highest for $N = 1$. Experimental results agree well with this prediction. Thus, magnetic field sensitivity can be enhanced by optimizing structure.

Secondly, utilizing the pre-stressed effect was proven to enhance the nonlinear ME effect in Metglas/PZT laminates. When applying a longitudinal tensile stress, the susceptibility χ_0 of Metglas was increased. My experimental results confirmed that pre-stressed Metglas/PZT laminates had higher magnetic field sensitivities in comparison to non-stressed laminates.

Thirdly, the nonlinear ME effect was studied in ME laminates with various piezo-fibers. This study determined that laminates having Mn-doped PMN-PT crystal fibers had similar values of α_{ME} at $f \leq 1$kHz as those with pure PMN-PT; however, much higher values of α_V were found near the EMR due to a higher mechanical quality factor. Correspondingly, the nonlinear ME effect was similar for laminates having pure and Mn-doped PMN-PT fibers when modulated at $f = 1$ kHz. In contrast, Mn-doped PMN-PT

resulted in a notably higher ME output voltage V_{ME} when modulated at the EMR. After demodulation, laminates with Mn-doped PMN-PT fibers showed higher magnetic field sensitivities compared to laminates with PZT and pure PMN-PT fibers.

CHAPTER 7.

FUTURE WORK

Large ME effect has been achieved in Metglas/piezo-fiber laminates. Based on such ME laminate, the equivalent magnetic noise of ME sensor could be as low as 5.0 pT/Hz$^{0.5}$ at 1 Hz. A demo of 2×2 sensor arrays was built to show the ability to further decrease the noise level. To make the equivalent magnetic noise lower than 1.0 pT/Hz$^{0.5}$, an arrays of 10×10 ME sensors should be constructed. The configuration of this array needs to be studied to decrease the mutual effect from neighboring sensors. The test results for small magnetic signals need to be analyzed by signal processing. There will also be many issues need to be solved to make the array a good sensing system, such as the charge amplifier in each sensor unit, and the collection and steerage of the signals from sensors.

The ME effect in self-biased ME laminates was not as large as the magnet-biased one, which was mainly due to the constrain effect from annealed Metglas layers. Thinner layer of hard ferromagnetic material could be a better choice to replace these annealed Metglas layers. Thick film of NdFeB or SmCo layers could be deposited on surface Metglas layers to provide the magnetic anisotropy field. Because these layers were directly deposited on Metglas layers, the constraint effect to magnetostriction would be much smaller. The value of α_{ME} at zero bias field should be as large as the peak value of α_{ME} in magnet-biased ME laminates. This could further decrease the equivalent magnetic noise of self-biased ME laminate, so that the space resolution of arrays of such laminates could be enhanced compared to magnet-biased ones.

In the detection of magnetic field by frequency modulation techniques, the sensitivity was not as high as passive ME sensors. The undesired noise near the modulation

frequencies limited the SNR. The sources of this noise need to be analyzed. By decreasing this noise near the modulation frequencies, the SNR of ME sensor by this frequency modulation technique could be further decreased by 2-3 orders. This will make this detection method more promising in applications, because of its advantages of not sensitive to low-frequencies vibrational noise and high SNR.

In this thesis, the ME laminates are bulk size. It would be interesting to develop ME composite sensor in nano-scale. Nano-scale thin films could be deposited on a substrate. However, the strain would be restricted by the substrate, because the thickness of the substrate is much thicker than that of films. This might dramatically decrease ME coefficient of the thin film composite. The substrate could be removed to solve this problem. If large ME effect could be achieved in nano-scale thin films, it will broader the applications of ME thin films, such as magnetic head and magntostrictive random-access memory.

REFERENCES

1 N. A. Spaldin and M. Fiebig, Science **309,** 391 (2005).
2 W. Eerenstein, N. D. Mathur, and J. F. Scott, Nature **442,** 759 (2006).
3 R. Ramesh and N. A. Spaldin, Nature Materials **6,** 21 (2007).
4 I. E. Dzyaloshinskii, Sov. Phys. **10,** 628 (1959).
5 D. N. Astrov, Sov. Phys. **11,** 708 (1960).
6 D. N. Astrov, Sov. Phys. **13,** 729 (1961).
7 G. A. Gehring, Ferroelectrics **161,** 275 (1994).
8 M. I. Bichurin, V. M. Petrov, and G. Srinivasan, Journal of Applied Physics **92,** 7681 (2002).
9 J. B. N. J. Wang, H. Zheng, V. Nagarajan, S. B. Ogale, B. Liu, D. Viehland, V. Vaithyanathan, D. G. Schlom, U. V. Waghmare, N. A. Spaldin, K. M. Rabe, M.Wuttig and R. Ramesh, Science, **299,** 1719 (2003).
10 J. W. H. Zheng, S. E. Lofland, Z. Ma, L. Mohaddes-Ardabili, T. Zhao, L. Salamanca-Riba, S. R. Shinde, S. B. Ogale, F. Bai, D. Viehland, Y. Jia, D. G. Schlom, M. Wuttig, A. Roytburd and R. Ramesh, Science **303,** 661 (2004).
11 C.-W. N. Zhan Shi, J.M. Liu, D. A. Filippov and M. I. Bichurin, Phys. Rev. B **70,** 134417 (2004).
12 N. P. U. Laletsin, G. Srinivasan and C. P. Devreugd, Appl. Phys. A-Mater. Sci. Process. **78,** 33 (2004).
13 J. F. L. a. D. V. S. X. Dong, , , Appl. Phys. Lett. **83,** 2265 (2003).
14 R. H. G. Srinivasan, C. P. DeVreugd, V. M. Laletsin and N. Paddubnaya, Appl. Phys. A-Mater. Sci. Process. **80,** 891 (2005).
15 E. T. R. G. Srinivasan, J. Gallegos, R. Srinivasan, Y. I. Bokhan and V. M. Laletin, Phys. Rev. B **64,** 214408 (2001).
16 C.-S. Park and S. Priya, Journal of the American Ceramic Society **94,** 1087 (2011).
17 Y. Yan, Y. Zhou, and S. Priya, Applied Physics Letters **102,** 052907 (2013).
18 S. Dong, J. F. Li, D. Viehland, J. Cheng, and L. E. Cross, Applied Physics Letters **85,** 3534 (2004).
19 S. Dong, J. Zhai, N. Wang, F. Bai, J. Li, D. Viehland, and T. A. Lograsso, Applied Physics Letters **87,** 222504 (2005).
20 J. Zhai, S. Dong, Z. Xing, J. Li, and D. Viehland, Applied Physics Letters **89,** 083507 (2006).
21 S. Dong, J. Zhai, J. Li, and D. Viehland, Applied Physics Letters **89,** 252904 (2006).
22 J. Gao, D. Gray, Y. Shen, J. Li, and D. Viehland, Applied Physics Letters **99,** 153502 (2011).
23 J. Zhai, Z. Xing, S. Dong, J. Li, and D. Viehland, Journal of the American Ceramic Society **91,** 351 (2008).
24 J. L. S.X. Dong, and D.Viehland, IEEE transactions on ultrasonics, ferroelectrics, and frequency control **51,** 7 (2004).
25 S. Dong, J. Zhai, F. Bai, J.-F. Li, and D. Viehland, Applied Physics Letters **87,** 062502 (2005).
26 J. P. D. G. Harshe, and R. E. Newnham, Mathematics in Smart Structures **1919,** 224 (1993).
27 M. A. a. G. Harshe, J. Intell. Mater. Syst. Struct. **5,** 501 (1994).
28 M. Bichurin, V. Petrov, and G. Srinivasan, Physical Review B **68,** 054402 (2003).
29 D. C. MORRIS, Acta Materialia **29** (1981).
30 J. D. LIVINGSTON, phys. stat. sol. **70** (1982).

[31] A. P. T. a. M. R. J. Gibbs, Journal of Magnetism and Magnetic Materials **103,** 14 (1992).
[32] M. H. H. Bartehelmess, B. Schiefenhovel, E. Heim, M. Schilling, and R. Zimmermann, IEEE Trans. Appl. Supercond. **11,** 657 (2001).
[33] J. M. B. M. N. Baibich, A. Fert, F. N. Van Dau, F. Petroff, P. Eitenne, G. Creuzet, A. Friederich, and J. Chazelas, Phys. Rev. Lett. **21,** 2472 (1988).
[34] S. Dong, J. Zhai, Z. Xing, J.-F. Li, and D. Viehland, Applied Physics Letters **86,** 102901 (2005).
[35] J. Zhai, Z. Xing, S. Dong, J. Li, and D. Viehland, Applied Physics Letters **88,** 062510 (2006).
[36] Z. Xing, J. Zhai, J. Li, and D. Viehland, Journal of Applied Physics **106,** 024512 (2009).
[37] J. Gao, J. Das, Z. Xing, J. Li, and D. Viehland, Journal of Applied Physics **108,** 084509 (2010).
[38] S. Dong, J. Zhai, J. Li, and D. Viehland, Applied Physics Letters **88,** 082907 (2006).
[39] J. Gao, L. Shen, Y. Wang, D. Gray, J. Li, and D. Viehland, Journal of Applied Physics **109,** 074507 (2011).
[40] W. O. Henry, *Noise reduction Techniques in Electronic Systems* (John Wiley & Sons, New York, 1988).
[41] M. I. Montrose, *Emc and the Printed Circuit Board: Design, Theory, and Layout Made Simple* (Wiley-IEEE Press, New York, 1998).
[42] Keithley, *Low Level Measurement Handbook_Precision DC current, Voltage, and Resistance Measurements (6th Edition)* (Keithley, Cleveland, 2004).
[43] Y. Wang, D. Gray, D. Berry, J. Gao, M. Li, J. Li, and D. Viehland, Advanced Materials **23,** 4111 (2011).
[44] E. Lage, C. Kirchhof, V. Hrkac, L. Kienle, R. Jahns, R. Knochel, E. Quandt, and D. Meyners, Nat Mater **11,** 523 (2012).
[45] S. K. Mandal, G. Sreenivasulu, V. M. Petrov, and G. Srinivasan, Physical Review B **84** (2011).
[46] T. R. Clem, Nav. Res. Rev. **3,** 29 (1997).
[47] M. Diaz-Michelena, Sensors (Basel) **9,** 2271 (2009).
[48] Y. Jia, S. W. Or, H. L. W. Chan, X. Zhao, and H. Luo, Applied Physics Letters **88,** 242902 (2006).
[49] Y. Wang, F. Wang, S. W. Or, H. L. W. Chan, X. Zhao, and H. Luo, Applied Physics Letters **93,** 113503 (2008).
[50] H. C. Xuan, L. Y. Wang, S. C. Ma, Y. X. Zheng, Q. Q. Cao, D. H. Wang, and Y. W. Du, Applied Physics Letters **98,** 052505 (2011).
[51] F. Fang, C. Zhao, and W. Yang, Science China Physics, Mechanics and Astronomy **54,** 581 (2011).
[52] J. Das, J. Gao, Z. Xing, J. F. Li, and D. Viehland, Applied Physics Letters **95,** 092501 (2009).
[53] M. L. C. S. Xin Zhuang, Christophe Cordier, Sébastien Saez, Christophe Dolabdjian, Liangguo Shen, Jie Fang Li, Menghui Li, and Dwight Viehland, IEEE SENSORS JOURNAL **11,** 2266 (2011).
[54] J. Petrie, D. Gray, D. Viehland, G. Sreenivasulu, G. Srinivasan, S. Mandal, and A. S. Edelstein, Journal of Applied Physics **111,** 07C714 (2012).
[55] Y. Wang, D. Gray, D. Berry, J. Gao, M. Li, J. Li, and D. Viehland, Adv Mater **23,** 4111 (2011).
[56] R. B. Williams, Journal of Reinforced Plastics and Composites **23,** 1741 (2004).
[57] A. A. Bent and N. W. Hagood, Journal of Intelligent Material Systems and Structures **8,** 903 (1997).
[58] J. W. H. a. W. K. Wilkie, Nasa Technical Reports **NASA/TM-2003-212427,** ARL (2003).

[59] M. H. Li, D. Berry, J. Das, D. Gray, J. F. Li, and D. Viehland, Journal of the American Ceramic Society **94,** 3738 (2011).
[60] D. Hasanyan, Y. Wang, J. Gao, M. Li, Y. Shen, J. Li, and D. Viehland, Journal of Applied Physics **112,** 064109 (2012).
[61] D. Hasanyan, J. Gao, Y. Wang, R. Viswan, M. Li, Y. Shen, J. Li, and D. Viehland, Journal of Applied Physics **112,** 013908 (2012).
[62] C. R. Bowen, L. J. Nelson, R. Stevens, M. G. Cain, and M. Stewart, Journal of Electroceramics **16,** 263 (2006).
[63] M. I. B. a. D. Viehland, *Magnetoelectricity in Composites* (Pan Stanford Publishing, Singapore, 2010).
[64] C.-W. N. G. Liu, N. Cai, and Y. Lin, J. Appl. Phys. **95,** 2660 (2004).
[65] G. L. C.-W. Nan, and Y. Lin, Appl. Phys. Lett. **83,** 4366 (2003).
[66] M. Li, D. Berry, J. Das, D. Gray, J. Li, and D. Viehland, Journal of the American Ceramic Society **94,** 3738 (2011).
[67] A. E. Clark, J. P. Teter, and O. D. McMasters, Journal of Applied Physics **63,** 3910 (1988).
[68] D. Viehland, Journal of the American Ceramic Society **89,** 775 (2006).
[69] S. Dong, J. Zhai, J.-F. Li, D. Viehland, and E. Summers, Journal of Applied Physics **101,** 124102 (2007).
[70] K. H. Lam, C. Y. Lo, J. Y. Dai, H. L. W. Chan, and H. S. Luo, Journal of Applied Physics **109,** 024505 (2011).
[71] Y. K. Fetisov, L. Y. Fetisov, and G. Srinivasan, Applied Physics Letters **94,** 132507 (2009).
[72] T. Wu, T.-K. Chung, C.-M. Chang, S. Keller, and G. Carman, Journal of Applied Physics **106,** 054114 (2009).
[73] M. Li, Y. Wang, J. Gao, J. Li, and D. Viehland, Applied Physics Letters **101,** 022908 (2012).
[74] S. U. Pillai, *Array signal processing* (Springer-Verlag, New York 1989).
[75] T. D. David R. Walt, Joel White, John Kauer, Stephen Johnson, Heidi Engelhardt, Jon Sutter, Peter Jurs, Biosensors & bioelectronics **13,** 3 (1998).
[76] J. N. J.D.TarDos, P.M. Newman, J.J. Leonard, The International Journal of Robotics Research **21** (2002).
[77] J. M. M. Richard P. Welty, IEEE TRANSACTIONS ON MAGNETICS **27** (1991).
[78] Y. Abulafia, D. Giller, Y. Wolfus, A. Shaulov, Y. Yeshurun, D. Majer, E. Zeldov, J. L. Peng, and R. L. Greene, Journal of Applied Physics **81,** 4944 (1997).
[79] Z. Xing, J. Zhai, J. Gao, J. Li, and D. Viehland, IEEE ELECTRON DEVICE LETTERS **30,** 445 (2009).
[80] Z. Xing, J. Li, and D. Viehland, Applied Physics Letters **91,** 142905 (2007).
[81] M. Li, Y. Wang, J. Gao, D. Gray, J. Li, and D. Viehland, Journal of Applied Physics **111,** 033923 (2012).
[82] Z. Xing, J. Li, and D. Viehland, Applied Physics Letters **91,** 182902 (2007).
[83] M. Li, J. Gao, Y. Wang, D. Gray, J. Li, and D. Viehland, Journal of Applied Physics **111,** 104504 (2012).
[84] Z. P. Xing, J. Y. Zhai, S. X. Dong, J. F. Li, D. Viehland, and W. G. Odendaal, Measurement Science and Technology **19,** 015206 (2008).
[85] S.-C. Yang, C.-S. Park, K.-H. Cho, and S. Priya, Journal of Applied Physics **108,** 093706 (2010).
[86] M. Rivas, J. A. García, M. Tejedor, E. Bertrán, and J. G. Céspedes, Journal of Applied Physics **97,** 023903 (2005).
[87] J. He, L. Zhou, D. L. Zhao, and X. L. Wang, Journal of Materials Research **24,** 1607 (2009).

[88] L. Zhou, J. He, X. Li, B. Li, D. L. Zhao, and X. L. Wang, Journal of Physics D: Applied Physics **42,** 195001 (2009).
[89] M. Rivas, J. A. García, M. A. Cerdeira, and J. C. Martínez-García, Journal of Non-Crystalline Solids **358,** 310 (2012).
[90] J. Torrejón, L. Kraus, K. R. Pirota, G. Badini, and M. Vázquez, Journal of Applied Physics **101,** 09N105 (2007).
[91] M. Li, Z. Wang, Y. Wang, J. Li, and D. Viehland, Applied Physics Letters **102,** 082404 (2013).
[92] J. Ma, J. Hu, Z. Li, and C. W. Nan, Adv Mater **23,** 1062 (2011).
[93] L. Shen, M. Li, J. Gao, Y. Shen, J. F. Li, D. Viehland, X. Zhuang, M. Lam Chok Sing, C. Cordier, S. Saez, and C. Dolabdjian, Journal of Applied Physics **110,** 114510 (2011).
[94] M. Li, Y. Wang, D. Hasanyan, J. Li, and D. Viehland, Applied Physics Letters **100,** 132904 (2012).
[95] S. M. G. A. L. G. D. G. D. V. C. V. V. G. Harris, IEEE MAGNETICS LETTERS **2** (2011).
[96] X. J. Zheng and X. E. Liu, Journal of Applied Physics **97,** 053901 (2005).
[97] M. Li, Y. Wang, Y. Shen, J. Gao, J. Li, and D. Viehland, Journal of Applied Physics **114,** 144501 (2013).
[98] Y. J. Wang, D. Gray, D. Berry, J. Q. Gao, M. H. Li, J. F. Li, and Viehland.D., Adv. Mater. **23,** 4111 (2011).
[99] Y. Wang, J. Gao, M. Li, D. Hasanyan, Y. Shen, J. Li, D. Viehland, and H. Luo, Appl. Phys. Lett. **101** (2012).
[100] H. S. Luo, G. S. Xu, H. Q. Xu, P. C. Wang, and Z. W. Yin, Japanese Journal of Applied Physics Part 1-Regular Papers Short Notes & Review Papers **39,** 5581 (2000).
[101] S. X. Dong, J. Y. Zhai, J. F. Li, and D. Viehland, Appl. Phys. Lett. **89,** 252904 (2006).

Appendix A

Coefficient of A_i, B_i (i = 1 to 4) in equation (3.7)

$$A_1 = \frac{2Nt_m({}^{p}s_{13}\,{}^{m}s_{12} - {}^{p}s_{11}\,{}^{m}s_{33})}{{}^{m}s_{12}\,{}^{m}s_{12} - {}^{m}s_{33}\,{}^{m}s_{11}} + \frac{2(N+1)t_g({}^{p}s_{13}\,{}^{g}s_{12} - {}^{p}s_{11}\,{}^{g}s_{33})}{{}^{g}s_{12}\,{}^{g}s_{12} - {}^{g}s_{33}\,{}^{g}s_{11}} + \frac{2t_c({}^{p}s_{13}\,{}^{c}s_{12} - {}^{p}s_{11}\,{}^{c}s_{33})}{{}^{c}s_{12}\,{}^{c}s_{12} - {}^{c}s_{33}\,{}^{c}s_{11}} + t_p;$$

$$A_2 = \frac{2Nt_m({}^{p}s_{33}\,{}^{m}s_{12} - {}^{p}s_{13}\,{}^{m}s_{33})}{{}^{m}s_{12}\,{}^{m}s_{12} - {}^{m}s_{33}\,{}^{m}s_{11}} + \frac{2(N+1)t_g({}^{p}s_{33}\,{}^{g}s_{12} - {}^{p}s_{13}\,{}^{g}s_{33})}{{}^{g}s_{12}\,{}^{g}s_{12} - {}^{g}s_{33}\,{}^{g}s_{11}} + \frac{2t_c({}^{p}s_{33}\,{}^{c}s_{12} - {}^{p}s_{13}\,{}^{c}s_{33})}{{}^{c}s_{12}\,{}^{c}s_{12} - {}^{c}s_{33}\,{}^{c}s_{11}};$$

$$A_3 = \frac{2Nt_m({}^{p}s_{11}\,{}^{m}s_{12} - {}^{p}s_{13}\,{}^{m}s_{11})}{{}^{m}s_{12}\,{}^{m}s_{12} - {}^{m}s_{33}\,{}^{m}s_{11}} + \frac{2(N+1)t_g({}^{p}s_{11}\,{}^{g}s_{12} - {}^{p}s_{13}\,{}^{g}s_{11})}{{}^{g}s_{12}\,{}^{g}s_{12} - {}^{g}s_{33}\,{}^{g}s_{11}} + \frac{2t_c({}^{p}s_{11}\,{}^{c}s_{12} - {}^{p}s_{13}\,{}^{c}s_{11})}{{}^{c}s_{12}\,{}^{c}s_{12} - {}^{c}s_{33}\,{}^{c}s_{11}};$$

$$A_4 = \frac{2Nt_m({}^{p}s_{13}\,{}^{m}s_{12} - {}^{p}s_{33}\,{}^{m}s_{11})}{{}^{m}s_{12}\,{}^{m}s_{12} - {}^{m}s_{33}\,{}^{m}s_{11}} + \frac{2(N+1)t_g({}^{p}s_{13}\,{}^{g}s_{12} - {}^{p}s_{33}\,{}^{g}s_{11})}{{}^{g}s_{12}\,{}^{g}s_{12} - {}^{g}s_{33}\,{}^{g}s_{11}} + \frac{2t_c({}^{p}s_{13}\,{}^{c}s_{12} - {}^{p}s_{33}\,{}^{c}s_{11})}{{}^{c}s_{12}\,{}^{c}s_{12} - {}^{c}s_{33}\,{}^{c}s_{11}} + t_p;$$

$$B_1 = \frac{2Nt_m({}^{p}d_{33}\,{}^{m}s_{12} - {}^{p}d_{31}\,{}^{m}s_{33})}{{}^{m}s_{12}\,{}^{m}s_{12} - {}^{m}s_{33}\,{}^{m}s_{11}} + \frac{2(N+1)t_g({}^{p}d_{33}\,{}^{g}s_{12} - {}^{p}d_{31}\,{}^{g}s_{33})}{{}^{g}s_{12}\,{}^{g}s_{12} - {}^{g}s_{33}\,{}^{g}s_{11}} + \frac{2t_c({}^{p}d_{33}\,{}^{c}s_{12} - {}^{p}d_{31}\,{}^{c}s_{33})}{{}^{c}s_{12}\,{}^{c}s_{12} - {}^{c}s_{33}\,{}^{c}s_{11}};$$

$$B_2 = \frac{2N_2t_m({}^{m}d_{33}\,{}^{m}s_{12} - {}^{m}d_{31}\,{}^{m}s_{33})}{{}^{m}s_{12}\,{}^{m}s_{12} - {}^{m}s_{33}\,{}^{m}s_{11}};$$

$$B_3 = \frac{2Nt_m({}^{p}d_{31}\,{}^{m}s_{12} - {}^{p}d_{33}\,{}^{m}s_{11})}{{}^{m}s_{12}\,{}^{m}s_{12} - {}^{m}s_{33}\,{}^{m}s_{11}} + \frac{2(N+1)t_g({}^{p}s_{13}\,{}^{g}s_{12} - {}^{p}s_{33}\,{}^{g}s_{11})}{{}^{g}s_{12}\,{}^{g}s_{12} - {}^{g}s_{33}\,{}^{g}s_{11}} + \frac{2t_c({}^{p}d_{31}\,{}^{c}s_{12} - {}^{p}d_{33}\,{}^{c}s_{11})}{{}^{c}s_{12}\,{}^{c}s_{12} - {}^{c}s_{33}\,{}^{c}s_{11}};$$

and $B_4 = \frac{2Nt_m({}^{m}d_{31}\,{}^{m}s_{12} - {}^{m}d_{33}\,{}^{m}s_{11})}{{}^{m}s_{12}\,{}^{m}s_{12} - {}^{m}s_{33}\,{}^{m}s_{11}}.$